



**FACULTY
OF MECHANICAL
ENGINEERING
CTU IN PRAGUE**

Department of Designing and Machine Components

**Design of a Tilting Mechanism of CBM
experiment Beam Pipe**

**Návrh naklápění iontovodu pro
experiment CBM**

DIPLOMA THESIS

2021

Jan KOLLARCZYK

Study programme: (NDTT) Automotive, Railway and
Transportation Engineering
Specialization: (N071TTTE) Transportation Engineering
Supervisor: Ing. Martin Janda

I. OSOBNÍ A STUDIJNÍ ÚDAJE

Příjmení: **Kollarczyk** Jméno: **Jan** Osobní číslo: **466478**
Fakulta/ústav: **Fakulta strojní**
Zadávací katedra/ústav: **Ústav konstruování a částí strojů**
Studijní program: **Dopravní a transportní technika**
Specializace: **Transportní technika**

II. ÚDAJE K DIPLOMOVÉ PRÁCI

Název diplomové práce:

Návrh naklápění iontovodu pro experiment CBM

Název diplomové práce anglicky:

Design of a Tilting Mechanism of CBM experiment Beam Pipe

Pokyny pro vypracování:

Navrhněte vhodné konstrukční řešení mechanismu naklápění kompozitového iontovodu pro experiment CBM urychlovače FAIR v GSI Darmstadt v Německu. Mechanismus je umístěn mezi pevným kuželovým iontovodem detektoru RICH/MUCH a 12metrovou naklápěcí kompozitovou sekcí, která vede svazek do absorberu. Iontovod je naklápěn ve vodorovné rovině v rozsahu $\pm 2.5^\circ$. Navrhněte několik vhodných variant pro plynulé naklápění v celém rozsahu s ohledem na co nejmenší množství materiálu. Střed rotace naklápění je ve vzdálenosti 3.7m od mechanismu. Navrhněte pohon pro naklápění mechanismu. Vytvořte MKP model mechanismu s vlnovci, který bude popisovat jeho tvar po vychýlení do krajní pozice a navrhněte experiment pro jeho validaci.

Seznam doporučené literatury:

Jméno a pracoviště vedoucí(ho) diplomové práce:

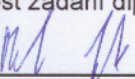
Ing. Martin Janda, ústav konstruování a částí strojů FS

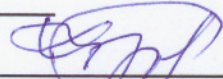
Jméno a pracoviště druhé(ho) vedoucí(ho) nebo konzultanta(ky) diplomové práce:

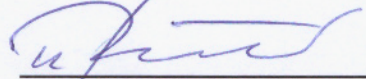
Datum zadání diplomové práce: **12.04.2021**

Termín odevzdání diplomové práce: **04.06.2021**

Platnost zadání diplomové práce: _____


Ing. Martin Janda
podpis vedoucí(ho) práce


Ing. František Lopot, Ph.D.
podpis vedoucí(ho) ústavu/katedry

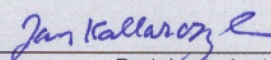

prof. Ing. Michael Valášek, DrSc.
podpis děkana(ky)

III. PŘEVZETÍ ZADÁNÍ

Diplomant bere na vědomí, že je povinen vypracovat diplomovou práci samostatně, bez cizí pomoci, s výjimkou poskytnutých konzultací. Seznam použité literatury, jiných pramenů a jmen konzultantů je třeba uvést v diplomové práci.

30.4.2021

Datum převzetí zadání



Podpis studenta

INSTRUCTIONS FOR DIPLOMA THESIS

Design the tilting mechanism of the composite beam pipe for the CBM experiment of the FAIR accelerator at GSI Darmstadt in Germany. The mechanism is located between the fixed conical beam pipe of the RICH / MUCH detector and the 12-meter tilting composite section that leads the beam to the absorber. The ion guide is tilted in the horizontal plane in the range of $\pm 2,5^\circ$. Design several suitable variants for smooth tilting in the entire range with regard to the smallest possible amount of material. The centre of rotation of the tilt is at a distance of 3.7m from the mechanism. Design a drive for tilting the mechanism. Create an FEM model of the mechanism with bellows that will describe its shape after deflection to the extreme position and design an experiment for its validation.

ANNOUNCEMENT

I declare, I worked out the diploma thesis on the topic “Design of a Tilting Mechanism of CBM experiment Beam Pipe“ alone under the leadership of Ing. Martin Janda. There are introduced all of used information sources in the end of the thesis. The citation of literature follows the standard ISO 690.

In Prague 30. July 2021

Jan Kollarczyk

I would particularly like to express my gratitude to Ing. Martin Janda for an excellent leadership of my thesis even during the distant education period. Many thanks to Ing. František Lopot, Ph.D., who let me participate in such an interesting project based on the collaboration with the foreign research institute GSI Helmholtzzentrum für Schwerionenforschung. I would dearly like to propose a vote of thanks to Ing. Marek Rachač and Ing. Martin Dub, Ph.D for their time dedicated to our technical consultations as well as for much advice and patience. I should like to thank Ing. Jiří Král and Ing. Petr Chudoba, Ph.D for their design review. I appreciate the time of the technical deputies of the Mewasa AG company for developing and consulting the design solutions regarding metal bellows applications. Last but not least, thousands thanks to my family, which supported me permanently during writing this thesis and in my studies.

ANNOTATION LIST

Name of author: *Jan KOLLARCZYK*

Title in English: *Design of a Tilting Mechanism of CBM experiment Beam Pipe*

Title in Czech: *Návrh naklápění iontovodu pro experiment CBM*

Year: *2021*

Field of study: *(N071TTTE) Transportation Engineering*

Department: *Department of designing and machine elements*

Supervisor: *Ing. Martin JANDA*

Tutor: *Ing. Marek RACHAČ*

Bibliographic information: number of sites 101
number of figures 85
number of tables 5
number of attachments 35

Keywords in English: beam pipe, bellow, compressed baryonic matter, flange, spheric surface

Keywords in Czech: iontovod, vlnovec, stlačená baryonová hmota, příruba, sférická plocha

Abstract in English:

This thesis is focused on the construction design of an adjustable connection between two mating sections of the beam pipe for the CBM experiment. The thesis contains a few possible design implementations for ensuring any required position of horizontally deflected parts of the beam pipe. There were created CAD models supported by technical drawing, analytical calculations and finite element method analysis.

Abstract in Czech:

Tato diplomová práce je zaměřena na konstrukční návrh nastavitelného spojení mezi dvěma přiléhajícími částmi iontovodu pro experiment CBM. Diplomová práce obsahuje několik možných designových provedení pro zajištění libovolné požadované pozice horizontálně vychylovaných částí iontovodu. Byly vytvořeny CAD modely doplněné technickou dokumentací, analytickými výpočty a analýzou metodou konečných prvků.

Table of contents

1. Introduction.....	1
1.1. CBM experiment.....	1
1.2. Starting point of tilting joint design with the background of experimental assembly	3
2. Metal bellows.....	9
2.1. Seamless hydroformed bellows.....	12
2.1.1. Pros and cons.....	14
2.1.2. Materials.....	14
2.1.3. Producers.....	16
2.1.4. Application.....	17
2.2. Roll-formed bellows	18
2.2.1. Pros and cons.....	19
2.2.2. Materials.....	19
2.2.3. Producers.....	20
2.2.4. Application.....	20
2.3. Edge-welded bellows	21
2.3.1. Pros and cons.....	24
2.3.2. Materials.....	25
2.3.3. Producers.....	26
2.3.4. Application.....	26
2.4. Electro-formed bellows	27
2.4.1. Pros and cons.....	29
2.4.2. Materials.....	30
2.4.3. Producers.....	30
2.4.4. Application.....	30
2.5. Other applications.....	31
2.6. Tip for design of tilting mechanism of CBM experiment beam pipe.....	31
3. Design of tilting mechanism.....	32
3.1. Design of mechanism with metal spheric workpieces.....	32
3.1.1. O-ring sealing.....	35
3.2. Design of the mechanism with composite spheric workpieces.....	37
3.3. Design of weldment with two bellows and intermediate tube.....	39
3.3.1. Bellows weldment with slender struts.....	39
3.3.2. Bellows weldment with rolling system	43
3.4. Design of the weldment with one bellow (and eccentric flange)	48
4. Design of the drive for the tilting mechanism	52
4.1. Handle drive (wheel).....	52
4.2. Electric drive	53
4.3. Hydraulic cylinder	62
4.4. Passive tilting of bellow joint	64
5. FEM analysis of bellows deformation	67
6. Experiment with bellow	73
6.1. Design of experiment	73
6.2. Bellow struts	76

6.2.1. Analytical calculations.....	76
6.2.2. Finite element method	80
6.2.3. RFEM analysis	83
7. Conclusion	84
LITERATURE	85
LIST OF FIGURES.....	93
LIST OF TABLES	95
LIST OF ATTACHMENTS.....	96
LIST OF ABBREVIATIONS AND SYMBOLS.....	97

1. Introduction

The aim of this thesis is to contribute with some technical design outlines to the construction of the CBM experiment infrastructure. The whole assembly of devices and support systems of the CBM experiment is being designed by the mechanical engineers and physical experts from different countries and institutes under the auspices of the German research organisation *GSI Helmholtzzentrum für Schwerionenforschung*. This project is based on the international collaboration of different research organizations and it might be realized in the near future.

Such a contribution might be performed via design of a tilting mechanism of the CBM experiment beam pipe, that is expected to allow setting of any position of the beam pipe within the horizontal plane in a defined range of angle deflections. The tilting joint is supposed to connect the fixed conical section and the adjustable downstream section of the beam pipe, which represents an element for the accelerated heavy ion beam conduction. The design of the tilting joint may be supported by the FEM analysis, which is expected to simulate the shape of the tilting mechanism after its deflection.

1.1. CBM experiment

Nowadays, the scientists from different parts of the whole world are applying to convey piece of knowledge about cosmic matters in order to get know more about the phenomena regarding the origin of stars or planets, explore the area of elementary particle physics or even research medical issues. When talking about the compressed baryonic matter (CBM) experiment, the researchers might be able for example to simulate the conditions just after the *Big Bang* during the formation of our solar system in a short period. During the last years the project of building new international accelerator facilities in Darmstadt in Germany has been developed in terms of the Facility for Antiproton and Ion Research (FAIR), which includes a wide range of experiments such as the CBM experiment. [1]

The following figure shows actual as well as planned facilities of the FAIR complex, which already comprises smaller heavy ion synchrotron SIS 18 and linear Accelerator UNILAC with ion sources, storage ring or a fragment separator. [2]

All new planned infrastructure, accelerators and storage rings are highlighted red in the figure 1. The currently designed experimental facilities are depicted in green colour. Except for the CBM experiment, there are constructed rooms for Atomic, Plasma Physics and Applications (APPA), NUclear STructure,

Astrophysics, and Reactions (NUSTAR) and antiProton ANnihilation in Darmstadt (PANDA) experiments or Superconducting FRagment Separator (Super-FRS) and a few storage rings, particularly High Energy Storage Ring (HESR), Collector Ring (CR), the accumulator / decelerator Storage Ring (RESR) and New Experimental Storage Ring (NESR). These systems will use the accelerated beams of particles from round accelerator SIS 100 with the circumference 1084 m and later from the accelerator SIS 300. [1] [3] [4]

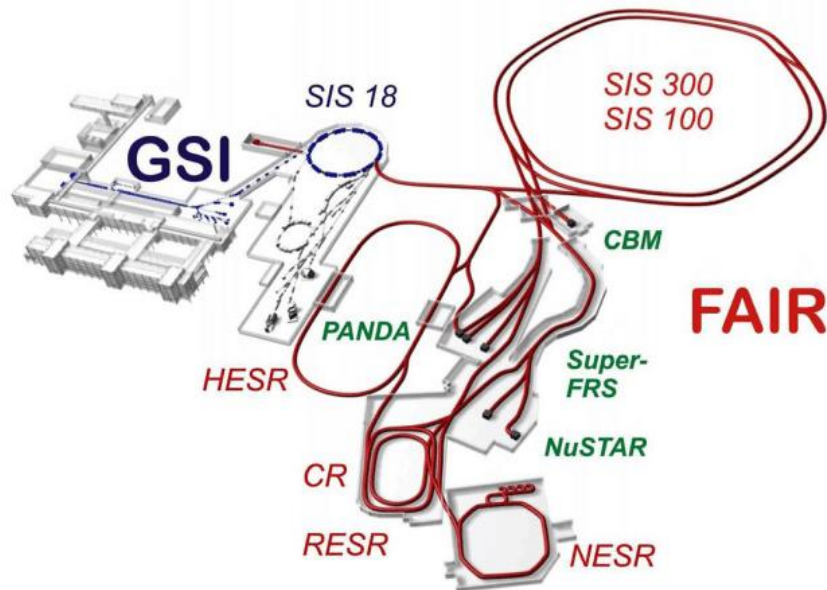


Fig. 1: Scheme of accelerator facilities in Darmstadt (FAIR, The PANDA Collaboration: Technical Design Report) [5]

The cave for CBM experiment will comprise not only devices for one experiment, but also High Acceptance DiElectron Spectrometer (HADES), which will be used for the research of dense baryonic matter as well. These 2 experimental systems are expected to work separately in different times under different constellations. The setup of HADES experiment is situated in front of the CBM experimental complex according to the figure below. When operating just the HADES experiment, so called beam dump will be installed in front of the target of the CBM experiment to disperse the ion beam right behind the HADES. [1] [6]

The research performed within the CBM experiment is related to the physical issues regarding the nuclear atomic or hadron branch and nuclear astrophysics. The aim of the CBM experiment is to observe heavy ion collisions and related phenomena such as the matter emerging from the ion interactions. Further objectives include the research of photons, collective hadron flow, mesons, electrons or dynamical fluctuations of particles etc. [7] Nonetheless, the results

might have an exceeding influence on other fields of science such as material engineering, plasma or radiation physics research and even on the medicine in terms of development of diseases treatment. [8]

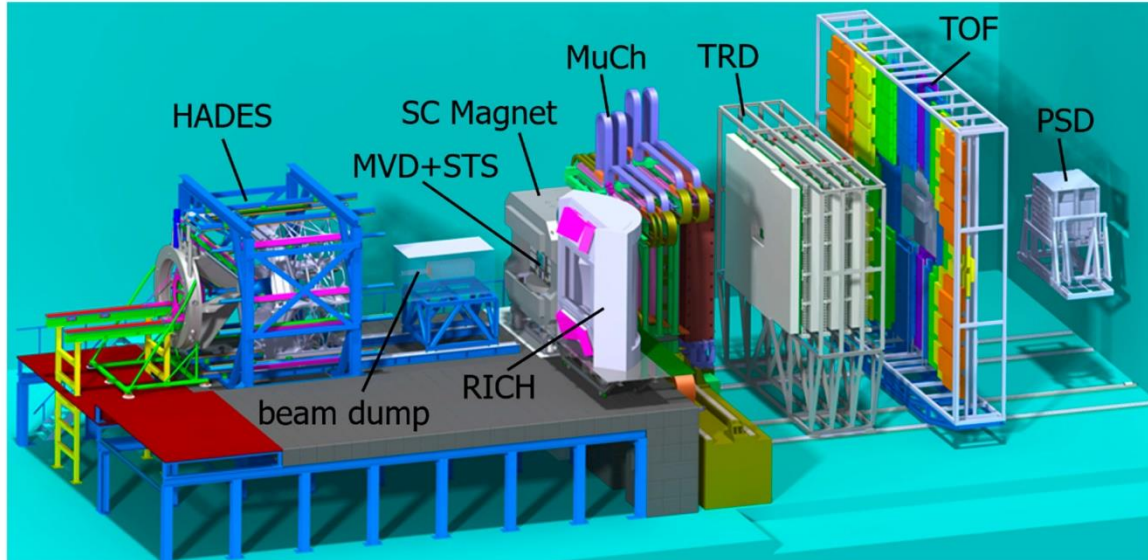


Fig. 2: The HADES detector (left) with the assembly for CBM experiment (right) (Peter Senger) [8]

1.2. Starting point of tilting joint design with the background of experimental assembly

The facility for CBM experiment will use accelerated beams of ions at different energy states from the new round particle accelerator SIS 100 in Darmstadt. The whole process will run under extreme physical conditions, which means that the mechanical components must be good adapted, for example, to resist the forces caused by inner vacuum. [1] [9] [10]

Taking into account the physical characteristics of the experiment, which handles mainly with the Au particles from the proton or nucleus collisions, there are high requirements on all components not to devalue the experimental data. Because of the high level of the measurement sensibility, it is necessary to install electronical systems for a high-speed data processing, working with fast algorithms, or radiation hard detectors for smooth and precise data acquisition from the experiment. The mechanical components and detectors are expected to meet such requirements as well, which means that they should be designed with as low material budget as possible in order to prevent the experimental results from their devaluation through the interactions of the particles inside the apparatus with the surrounding objects. Especially high demands are placed on the infrastructure including the beam pipe and its connecting parts. It is the reason, why thin-wall components are preferable

for the installation in the areas directly afflicted by the ion beams. All in all, the equipment for the CBM experiment might ensure the quality of physical measurements. [11]

The setup of CBM experiment consists of some detectors interconnected through the infrastructure elements including the beam pipe taking 16 meters in its longitudinal dimension. Individual devices and components are described through their abbreviations in the scheme below.

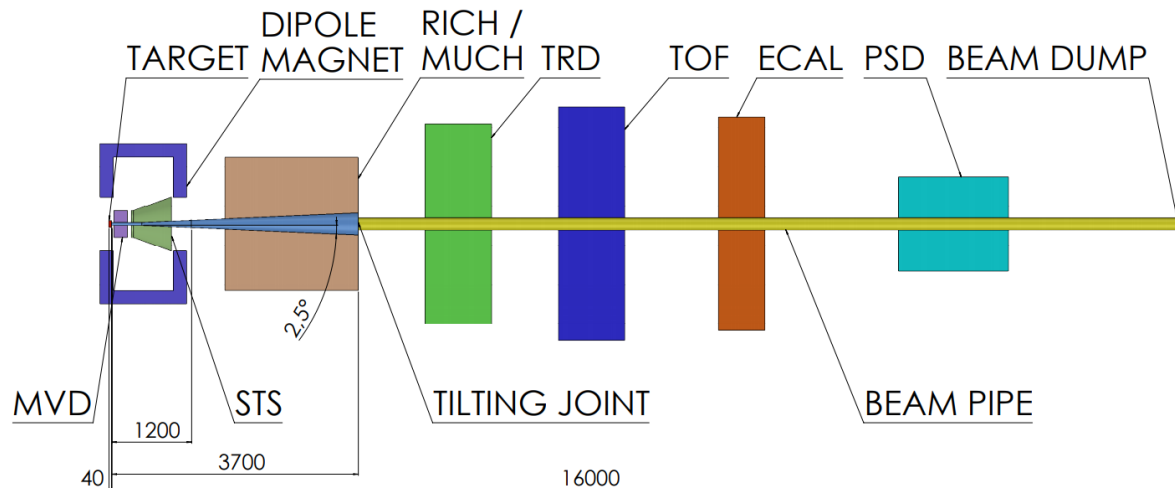


Fig. 3: Scheme of the CBM experiment

When beginning from the left side of the picture, the first functional object is represented by a target. This element determines type of a heavy-ion experiment under the condition that there are commonly distinguished two alternatives of a collider experiment and a fixed target experiment. A collider experiment operates with the collisions of two particle or nuclear beams. In this case, the CBM experiment is specific for the solution of the fixed target, which is based on interactions of accelerated beams from the accelerator SIS 100 with this fixed target. The target comprises a fixed thin foil of a heavy metal suited for the application in the CBM experiment (f. e. Au, Ag, Ni). [6] [7] [12]

The superconducting dipole magnet serves for the beam inclination. Its magnetic field has strong intensity enough to determine the direction of the flight of particles. [13]

Inside the hole of the magnet are located Micro-Vertex Detector (MVD) and Silicon Tracking System (STS). The MVD the detector is placed in the immediate proximity to the target. Silicon detectors of STS are situated at distances between 300 mm and 1000 mm from the target in the downstream direction. Both detection

systems STS as well as MVD are designed with very small material budget in order not to scatter the particles and devalue the experimental outputs. [7] [12]

Behind the dipole magnet follow some detectors in adjustable configuration. It goes around Ring-Imaging Cherenkov Detector (RICH) and Muon Chambers (MUCH). The RICH detector consists of mirrors with a radius of curvature corresponding with the detector position related to the target, which is about 1.6 m upstream of the RICH, and photodetectors. The option of the Muon Detection System includes 6 hadron absorber layers and about 18 gaseous tracking chambers. [6] [12]

An additional electron and positron detection system is presented by the Transition Radiation Detector (TRD), which consists of 9 detector layers in 3 layers. The assembly of TRD is placed behind the last hadronic absorber and the layers are located progressively 5m, 7,2 m and 7,5 m downstream the target. [6] [12]

The Time-of-Flight Detector (TOF) is operated approximately 6 m downstream the target behind TRD. The detector consists of an array of multi-gap resistive plate chambers made from glass. [6] [12]

Furthermore, there will be installed two calorimeters downstream the TOF detector, namely the Electromagnetic calorimeter (ECAL) and the Projectile Spectator Detector (PSD) in a subsequent order. The ECAL is formed by the modules involving 140 lead layers and scintillator plates inserted in the gaps between them. The location of ECAL might be variable. The second calorimeter PSD consists of the lead layers and scintillator sheets as the ECAL. The position of PSD will be adjustable in the range of 10 – 15 m downstream the target. The frame of PSD allows horizontal as well as vertical displacement and the rotational tilting around the vertical axis in order to set the position of the detector as exact as possible with the beam axis. [1] [6] [7] [12] [14]

The next crucial group is the infrastructure comprising all mechanical components such as frame assemblies, roller systems, and last but not least the most important beam pipe setup with its demountable joints and deflection mechanisms. There is a number of frame constructions needed for the support of detectors as shown in the figure 2. Several detectors are placed on rail systems (TRD, TOF, PSD), which enables their movement in axial direction of the beam pipe. The precision of detector positioning for the measurement standby is 0,1 mm depending on the drive mechanics. The value of the toleration for the system

positioning in horizontal and vertical direction could be less than 0,5 mm in relation to the rails assembling. The interface between the rail system and other devices is formed by connection plates. Besides that, the plates serve for drive mechanism mounting. [14]

The vacuum beam pipe itself is divided into the conical and straight section. The conical section roots in the area v dipole magnet and goes through the STS and RICH / MUCH detector. The conical-shape pipe is not expected to change its position. Nevertheless, behind RICH / MUCH is being designed a tilting joint, which might ensure any deflection of the straight pipe section in the range of $\langle -2,5^\circ; 2,5^\circ \rangle$. The tilting mechanism situated 3 700 mm downstream the target, which represents the centre of rotation of the tilting joint, is supposed to connect both the conical and the straight section of the 16 m long beam pipe, which further consists of shorter segments connected through special square-shaped flanges. If the pipe continued in a conical shape, it would not fit into the downstream detector inner holes, and so there is a shape change of the beam pipe behind the tilting joint and the pipe continues in the cylindrical-shape in the downstream direction. As the material of the beam pipe has been appointed carbon-fibre composite because of its convenient resilient properties at low material budget, and thus saving pipe wall thicknesses. [1] [12]

The figure 4 depicts two design options of the straight section of the beam pipe. Both designs operate with the connections with bellow system behind RICH / MUCH detector. Such a technical node is being solved in practical part of this thesis and, moreover, there are raised even other alternatives to bellows. Back to the pipe options, there are differences in the beam pipe diameter of the straight section between the tilting joint and PSD detector. The first possibility is to set the pipe diameter to 323,2 mm, which corresponds to the diameter of the end of the conical section of the beam pipe. In this case, the reduction of the pipe diameter on 190 mm would be performed approximately 9 m downstream the target, because the hole through the PSD is not adapted for bigger diameter. The second attitude is based on the diameter reduction just immediately behind the tilting joint. The beam pipe could have the same diameter along its whole straight section. Both alternatives are expected to preserve the beam of particles in the centre of the beam pipe in each position after tilting the cylindrical section as much as possible. According to the decisions within the CBM collaboration, it has been appointed, that the second

option will be used further and that the design will contain the beam pipe of the diameter 180 mm with the wall thickness of 1 mm. [12]

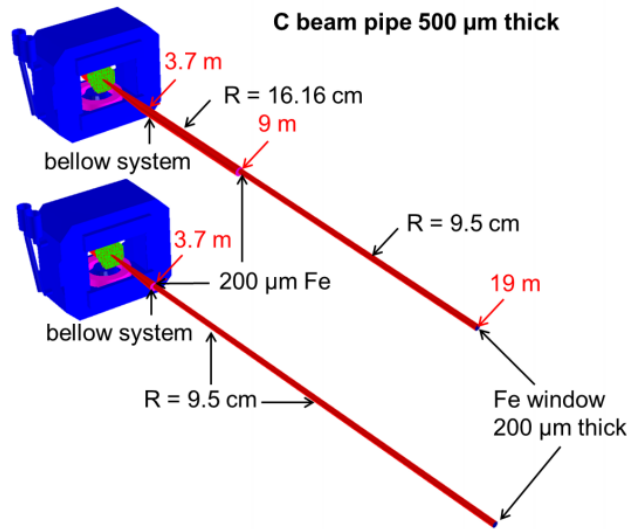


Fig. 4: Beam pipe versions (CBM progress report 2018, Design simulations of beam pipe and radiation studies for the CBM experiment, A. Senger and the CBM collaboration) [12]

Recently, there occurred some ideas to apply an eccentrically mounted straight section of the beam pipe, which means, that the ion beam need not be confined necessarily in the centre of the beam pipe, but it is possible to count with some acceptable distance between the beam centre and the inner surface of the pipe. In the figure 5 from the CBM progress report are depicted functions of the beam energies at the distance 3 700 mm downstream the target. Evidently, the density of scattered Au ions sharply falls in distant areas related to the centre of the beam, where is expected the highest intensity of the particle concentration. The beam pipe has been sketched as the blue rectangle in the diagram in order to show an eccentric mounting possibility of the straight part of the beam pipe. [12]

The design of an eccentric tilting mechanism with bellow will be introduced in the practical part of the thesis as well.

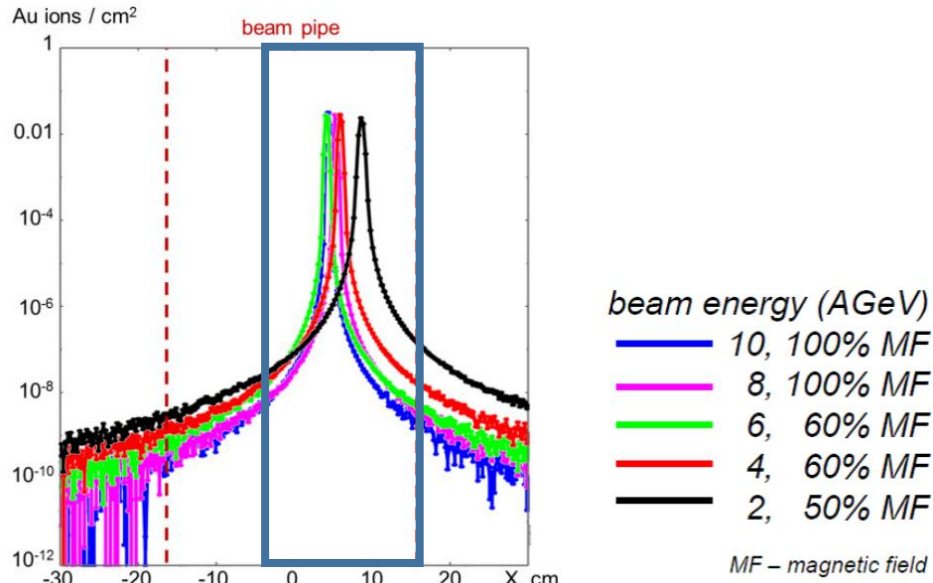


Fig. 5: Horizontal profiles of Au beams in the beam pipe deflected by a magnetic field (Design simulations of beam pipe and radiation studies for the CBM experiment, A. Senger and the CBM collaboration) [12]

The end of the beam pipe as well as the beam shut down is realized through the beam dump formed by the iron core packed in a radiation shielding. The dump is designed to be able to bear the high-intensity ion beams, especially the radiation from the backscattering particles. One of the tasks of the beam dump is to reduce the radiation in the CBM experiment cave. [12]

2. Metal bellows

Metal bellows play the main role in the design of a tilting mechanism. Therefore, this whole chapter is being dedicated to their recherche. The aim is to provide the information about different types of metal bellows, their manufacturing, materials, applications, potential producers, or other relevant knowledge.

The metal bellows represent suitable thin-walled components for compensation of angular, axial, and lateral displacements of any opposite mating pipes. Very common issues regard the combination of, above mentioned, elastic deformations. A metal bellow is a highly flexible as well as resistant part, which consists of number of convolutions, that allow to ensure the transformation into a required final deformed shape of this spring-like component in order to achieve any mechanical connection of deflected pipework and maintain such a transition between separated elements under the conditions of mechanical, temperature or pressure conversions. [15] [16] [17]

When designing a construction with metal bellows, the biggest emphasis is put on the proper definition of geometrical attributes as well as operating physical conditions.

Between the most characteristic properties of bellows belongs the mean effective area (MEA), which counts with inner diameter (ID) and outer diameter (OD) of a bellow: [18]

$$MEA = \frac{\pi}{12} \cdot (OD^2 + OD \cdot ID + ID^2) \quad (1)$$

The mean effective area is the crucial parameter for determination of a relation between the pressure changes and the force effecting bellows walls. [18]

Except for diameters, other characteristics of bellows are, for example, the free length, which is the length of an undeformed bellow, number and shape of convolutions, that results in maximal allowed stroke, wall-thickness having an impact on the spring rate of a bellow etc. [19]

The following tables include the key design parameters of bellows, which could be taken into account and that the most crucial of them might be presented to the bellows producer depending on their application, because different areas of bellows implementation regard different physical conditions as well as their priority. So, the first table tackles the geometrical attributes and basic physical conditions of bellows operation.

Key Dimensional Requirements	
Bellows OD, max / min.	This is the bellows acceptable outside diameter range for the application. This helps to define the acceptable size envelope for the bellows. It is critical for tool selection to optimize performance.
Bellows ID, max. / min.	This is the bellows acceptable inside diameter range for the application. This helps to define the acceptable size envelope for the bellows.
Effective area	This is the equivalent piston surface area of the bellows, as defined by the bellows OD and ID.
Bellows free length	This is the “as manufactured” length of the bellows convolutions, with the bellows at a neutral “at rest” position with no applied forces acting on it.
Assembly required	This lets the design engineer know if assembly of the bellows to end pieces is required.
Media / Environment	This is the type of environment or substances (gas, liquids, and materials) that the bellows would be exposed to in the application.
Bellows material	This is the bellows material required for the application, if known.
Temperature, max. / min.	This is the potential range of temperatures that the bellows or bellows assemblies might be exposed to in the application.
Operating temperature	This is the temperature that the bellows or bellows assembly will experience during normal operation.

Tab: 1 Dimensional attributes of bellows (MW Components catalogue) [17]

Meanwhile, the second table involves required deflections, operating pressures, lifecycles, bellows properties related to sealing capabilities such as leak rate and mechanical parameters such as spring rate. All of these factors, especially the pressure conversions, operating temperature and the spring rate, effect on the wall-thickness and type of material. [20]

Back to the most characteristic attributes of bellows. The already mentioned spring rate (SR) reflects a force needed for bellows compression or extension by a given stroke. In other words, the spring rate express the relation between the axial load and achieved deflection. [18] [19]

$$SR = \frac{\text{Axial load}}{\text{Deflection}} \quad (2)$$

The leak rate (LR) represents a relation of the volume of internal space V and the difference between the external and internal pressure (Δp) per the time (Δt). It expresses the amount of gas, that leaks through material per the time on the basis of pressure difference between outer and inner space relate to the volume of a container [21]

$$LR = V \cdot \frac{\Delta p}{\Delta t} \quad (3)$$

Key Performance Requirements	
Pressure Responsive	What is the desired response with pressure changes?
Leak Rate	If the bellows or bellows assembly must be leak rate will vary as a function of the bellows material.
Operating Pressure	This is the differential pressure the bellows will be subjected to in the application. It is important to specify what pressures will be applied internally and externally to the bellows.
Total Stroke	This represents the total of the axial deflections of the bellows, from its nominal at-rest length, in both compression and extension.
Lateral Offset	This the distance between the centerlines of the ends of the bellows that are parallel but not on the same line.
Angular Offsset	This is the angle between the centerlines of the ends of the bellows.
Spring Rate	If known or required for performance, this the spring rate (force per linear deflection), of the bellows.
Lifecycle	This is the expected number of flexures the bellows will be expected to endure before failure or maintenance.
Cycle Rate	This is the rate or speed (cycles per unit time) that the bellows will experience in the application.

Tab: 2 Performance attributes of bellows (MW Components catalogue) [17]

The bellows characteristics may be divided into the area of linear behaviour and the area of permanent deformation depending on the size of deflection. The limit of the linear are is called the elastic limit. As shown in the diagram below, the hysteresis seems to be pretty small for metal bellows on the basis of their similarity to springs in terms of mechanical properties. It means, that a new state of

deformation is not supposed to be very afflicted by a previous state of deformation. Especially, in the case that the elastic limit was not crossed, there would not be any changes in bellows behaviour. [18]

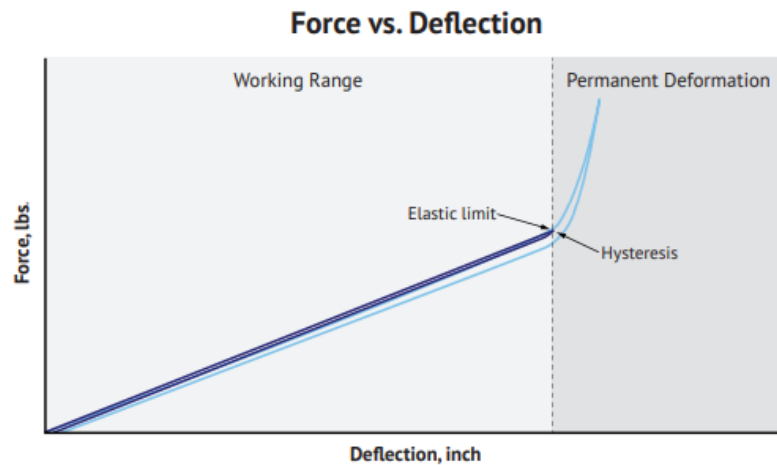


Fig. 6: The diagram of relation between force and deflection of bellow (Sigma-Netics catalogue) [18]

The types of metal bellows differ in principle in the way of its manufacturing. The process of fabrication and the choice of bellows material have a direct impact on the mechanical properties of a bellow, and therefore on different possibilities of their application. The two crucial groups are represented by formed and welded bellows. The aim is to compare different types of bellows to select the most convenient one for the implementation to the design of a tilting mechanism of the beam pipe for CBM experiment. [18]

2.1. Seamless hydroformed bellows

Firstly, let's focus on the seamless hydroformed type of bellows, which represent one of the most economical solution for high volume production of bellows.

The production of seamless hydroformed bellows consists of several steps, which do not include any welding. The process of the bellow shape development is in this case characterised by deep drawing of metal strips and followingly by hydroforming to the final product. [22]

Firstly, a suitable material type is selected as a semi-product. The piece of sheet or metal strip is further sheared and prepared for drawing process, which involves degreasing, heat treatment, chemical neutralization and lubrication [23]

The procedure of multi-step deep drawing is carried out on presses, where are metal round plates transformed into an intermediate product, which reminds of cups. [24]

After getting an intermediate product from drawing operations and cleaning preparations, the process of hydroforming follows. The tubes are in this case formed in special closing tools, where is brought an active pressure medium, the most often a water-oil emulsion. The deformation of tubes is performed under high inner pressures up to 250 bar in dependence on the wall-thicknesses, composition of material or local dimensions such as a radius of edge fillets. Due to a parallel compression of the whole tool, the convolutions of a bellow are formed. [25] [26]

During the final operations, the bellows are eventually degreased, heat treated cleaned and dried in terms of the finishing operations before being ready for an expedition. [23]

The hydroforming is performed on hydraulic-based machines. The maximal possible diameter of a bellow is limited by the die plate dimension. [27]

The figure below depicts two kinds of hydroformed ripple shape. The left scheme shows the sinus profile and on the right side is captured the omega profile. The sinus profile is typical for roll-formed bellows as well. [15]

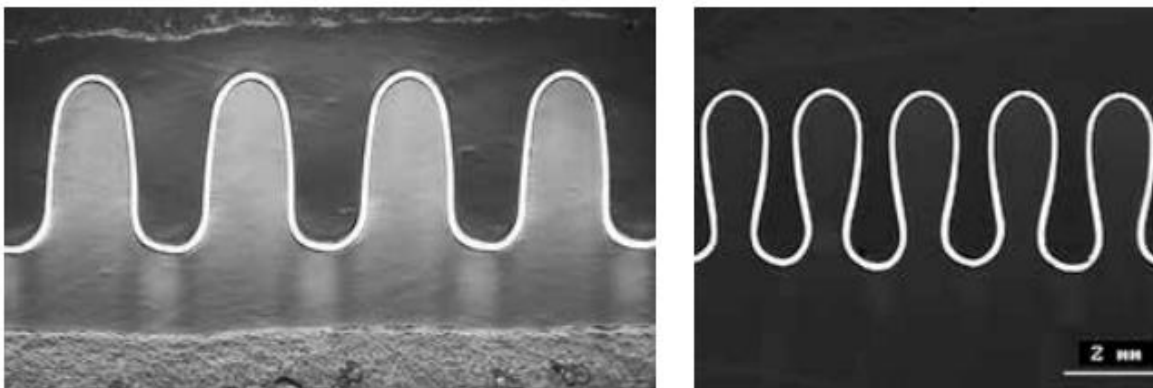


Fig. 7: From left: sinus and omega convolution profiles of formed bellows (Witzenmann catalogue) [15]

Occasionally, it is possible to substitute the first step of the deep drawing operation with another option, which is based on plate rolling and welding, nevertheless, such a method is evidently no more seamless. For example, the Fulton Bellows offers company seamless as well as seam-welded hydroformed bellows, but commonly are used drawn tubes for hydroforming. [28]

2.1.1. Pros and cons

Disadvantages of hydroformed bellows for the use in the experimental technique are bigger wall-thickness dimensions. The great advantage of such a manufacturing method is the possibility to reach consistent dimensional tolerances and to develop complicated shapes of complex parts. In comparison to the welded bellows, the seamless hydroformed bellows do not suffer from internal stresses caused by heat effects from welding. [18] [25] [29]

In another point of view, the method of bellow manufacturing profoundly influences the range of allowed bellow stroke in both cases of compression and extension. Typically, the hydroformed bellows are allowed to be compressed by 15% of their free length and extended by 10% of their free length. In comparison to other types of bellows, they resist smaller pressure differences. Their tooling costs are lower than for the welded bellows, nevertheless, higher number of produced pieces in production series should cover such cost differences. It depends on the material, but generally hydroformed bellows can be operated under lower temperatures than welded bellows and higher than electrodeposited ones. [30]

2.1.2. Materials

The seamless hydroformed bellows are commonly fabricated from different metallic alloy combinations, especially from those forming stainless steels, nickel alloys, bronze or brass.

For example, the Mera Bellows company offers within its catalogue non-ferrous alloys such as Brass (e. g. CuZn20) and Bronze (e. g. CuSn6) mainly for the purpose of application in control and measuring technologies primarily focused on temperature as well as pressure sensing devices. Brass belongs to the one of the most traditional materials used for metal bellows. In comparison to brass, bronze alloys are considered to perform better corrosion resistance and they can withstand little bit higher tensile stresses. Usually, both materials are soft soldered to endpieces. The advantages of brass and bronze materials are low manufacturing costs. [22] [28] [31] [32]

Further possibilities are represented by beryllium-copper (CuBe2) metallic alloys with 0,4–2% of beryllium. As it goes around a material with good electric conductivity, it is commonly used in electrical devices and systems in terms of activation, alarm systems. Their elastic properties and high tensile strength cause that they are convenient for applications of mechanical pressure sensor. With a

great lifecycle duration, the beryllium-copper bellows appear in aerospace engineering. It is supported by heat treatment after their assembly. It is suitable for brazing as well. [22] [28] [31] [32]



Fig. 8: Seamless hydroformed bellows of (from left) brass, beryllium-copper and bronze (Mera Bellows) [32]

The significant group of bellows materials are nickel alloys. There is a wide range of alloy version, where belong for example nickel-copper alloys such as Monel (e.g. Monel 400 - NiCu30Fe) comprising 65-70% nickel, 20-30% copper, 5% magnesium and iron and other elements like sulphur, carbon or silicon. Monel belongs to that type of material, which shows great chemical properties, in the first place, the corrosion resistance, and so its use is broadened within the chemical industry, where is needed to manipulate with salt water, steams, acid or alkaline fluids. The material is brazing, arc or laser welding – friendly. Another nickel-based alloy is Inconel with minimal content of 72% nickel and with the second main element 17% chromium plus additive elements. The material is suitable for welding and shows very good properties in terms of corrosion resistance or thermal stress changes. Another material option is covered by Hastelloy (e.g. Hastelloy C276), a representative nickel molybdenum (15-17%) chromium (14,5-16,5%) superalloy with an important additional element of 3-4,5% tungsten, which shows the best properties compared with above mentioned nickel alloys. An outstanding alloy is also Ni-Span C Alloy 902, which comprises nickel, iron and chromium with additions of aluminium and titanium. It is specific for its constant thermo-elastic coefficient within the range of temperatures $-45^{\circ}\text{C} - 65^{\circ}\text{C}$. [22] [28] [31] [33] [34] [35]



Fig. 9: Seamless hydroformed bellows of Monel (Sigma-Netics) [31]

The next significant group of seamless bellow materials is stainless steel. There is a wide range of metal compounds, that belong to this class, for example (according to the terms of the American Iron and Steel Institute): AISI 304, AISI 309S, AISI 310S, AISI 321, AISI 316, AISI 316L, AISI 316Ti, AISI 347, A 286 etc. This kind of material stands out for its great tensile as well as compression strength and corrosion resistance. Therefore, the bellows of stainless steel are rather allowed to adopt to larger strokes than bellows of other materials. They can be designed to be operated under extreme conditions of high pressure differences and high temperatures, what leads to their convenient application in terms of vacuum technologies. Because of the anticorrosion properties of the stainless steel with suitable surface treatment, it can resist aggressive chemical fluids as well. The materials may withstand brazing, soldering and welding as well. [17] [22] [28] [30] [31]



Fig. 10: Seamless hydroformed bellows of stainless steel (Mera Bellows) [32]

2.1.3. Producers

The Polish Mera bellows company has been already mentioned in the previous chapter. Its productions is directly focused on the seamless hydroformed bellows within different variants. Except for the material selection, there are offered open-ended or closed-ended bellows and special two-ply bellows, which consist of two

inserted tubes with precise diameter dimensions, that are hydroformed to create convolutions. [32]

The Sigma Netics company from USA is oriented in the field of pressure technique as well as bellow manufacturing through all – hydroforming, edge-welding and electroforming technologies. Their products are used in the area of temperature sensing devices, aerospace technologies or isolation systems. [31]

The Beijing Bellowman Technology company in China uses also for the fabrication of metal bellows the seamless hydroforming method. Except for steel or bronze bellows, it offers metal expansion joints, hoses and pipes. [23]

The American Fulton Bellows company produces bellows via hydroforming as well as mechanical roll-forming method in a wide range of material types. For the standard hydroforming procedure can be used either seamless drawn tube or seam-welded metal tubing. This process of seam-welded forming is described in the chapter 2.2. The company offers single-ply bellows as well as multi-ply bellows [28]

2.1.4. Application

The areas of hydroformed application are related to aerospace, astronautics, petrochemistry, metallurgy, electric power, solar and nuclear powerplants, medical devices, heating and power transmission systems, ship and automobile industry. The Bellows are often used as a sealing component, pressure gauges or as a part of industrial controls and regulators able to be operated under vacuum conditions. [15] [23] [25] [36]

For example, the already mentioned Fulton Bellows company constructs packless valves with hydroformed or roll-formed bellows. Nevertheless, such an application might meet edge-welded bellows as well. Furthermore, it offers leakless expansion joints, which are able to absorb thermal changes or vibrations and, therefore, ensure a reliable flexible connection of two opposite mating components. Moreover, the bellows could be installed as liquid reservoirs or chambers, that are able to withstand pressure as well as temperature differences. The bellows are expected to compensate the movement of vibrating parts of motors or it can be used as a shaft sealing or seal in vacuum pumps and vacuum interrupters or more precisely electric circuit interrupters. [22] [36]

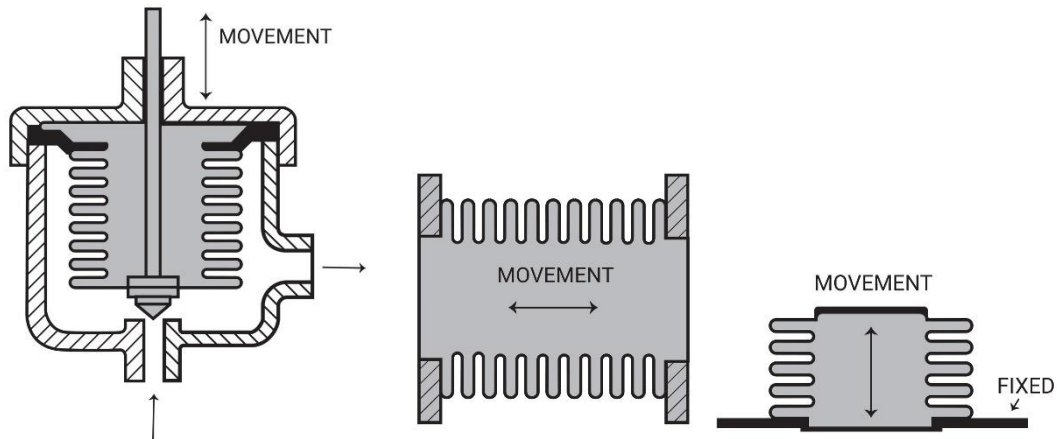


Fig. 11: From left: packless valve, expansion joint, expansion chamber (Fulton Bellows company) [36]

2.2. Roll-formed bellows

Another way of bellow manufacturing is represented by rolling technology. Actually, we could differ 2 types of roll-formed bellows depending on the intermediate product, which is determined for the milling of new convolutions. For such a forming procedure can be utilized either seam welded tubing or seamless drawn tubes. According to these intermediate products and their technical fabrication might be presented 2 groups of rolled bellows. In particular, it goes around seam-welded roll-formed bellows and seamless roll-formed bellows. [28]

The seam welded formed bellows are manufactured from thin metal plates, which are rolled and after that welded in longitudinal direction, and therefore, there emerges a seam. There is an option to make not only a single-ply bellow but also a multi-ply bellow through inserting two or more close fitting tubes in each other. [28] [37] [38]

The following operations in terms of mechanical roll-forming are based on deformation of tubes and shape transformation into bellows convolutions. The mechanical forming is realized along the tube intermediate product and the requested dimensions of diameters as well as lengths are step by step created. Such a mechanical method seems to be convenient especially for huge bellows or multiply bellows, but, of course, the way of the bellow fabrication is determined primarily by its application. [28] [37] [38]

Originally, the principle of this bellow forming method has been invented in the USA. According to the patent "*Bellows forming method and apparatus*" from 1976 was developed the first machine using rolling for corrugation forming. [39]

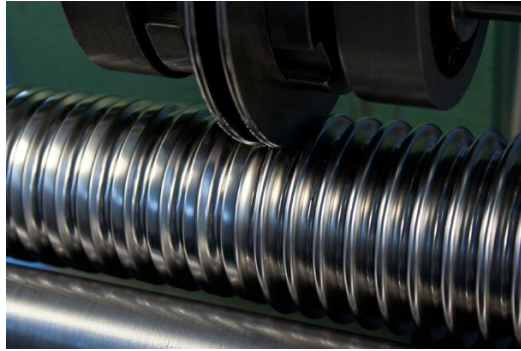


Fig. 12: Roll forming tool (Spiroflex) [37]

Nowadays, the CNC machines have already substituted the conventional manually operated types. For example, the Nutberry Limited company offers low cost metal bellows created on the CNC controlled roll forming machines. [38]

2.2.1. Pros and cons

When considering the comparison of the roll-formed bellows with seamless hydroformed bellows, the advantages such as cost saving due to lower tooling costs and wide size range of seam-welded roll-formed bellows come out. The deep drawing method is unfortunately limited by sizes of bellow diameters regarding die patterns and working area dimensions of a press. Therefore, the seam-welding technology represents a convenient way for manufacturing of huge metal bellows, which involves plate rolling and longitudinal seam welding. The seam welding does not set any limits for length limitations of a bellow as well. It is the reason, why seam-welded rolled bellows might be applied as expansion joints or flexible connections of mating pipes. [18]

On the other hand, when is needed to put emphasis on the bellow spring rate accuracy, the right choice represents the group of seamless hydroformed bellows, as their wall-thickness tolerance much more better than the tolerance achieved by fabrication of seam-welded rolled bellows. This fact leads to more precise spring rate, stroke as well as pressure characteristics of seamless bellows. The seam-welded type is also used for lower number of stroke cycles and the conditions for its material choice are welding-friendly properties, which means that the scale of applicable materials is smaller than in the case of hydroformed bellows. [18]

2.2.2. Materials

Fundamentally, the range of materials is similar to the list introduced in the chapter 2.1.3 of hydroformed bellows, especially regarding stainless steels or nickel alloys. [37] [38]

2.2.3. Producers

This section will introduce in brief some producers of roll-formed bellows.

As above mentioned, the British Nutberry Limited company is deeply focused on production of seam-welded formed bellows, which includes plate cutting, rolling and welding and then CNC roll-forming. The company also offers gas springs as thermodynamic elements, where are implemented bellow convolutions as well. [38]

Except for already introduced the Fulton Bellows company, just another producer the Croatian Spiroflex company is involved in production of roll-formed metal bellows through automatic seam-welding technique of different methods such as TIG welding, plasma welding, MIG-MAG welding or resistance spot-welding. [37] [40]

2.2.4. Application

Roll-formed bellows find the broadest application within the chemical, petrochemical, electrical or transportation industry. Bellows serve as expansion joints in terms of pipelines for fluids or vapours, heat exchangers, exhaust conductors in motor systems. It can be applied in vacuum technology and they may be built up within valves as hydroformed bellows. [28] [37]

For instance, the products of the Spiroflex company may be applied as axial expansion joints within pipeline systems, which balance the axial movements of mating components via bellows extension or compression. In the case of lateral and angular deformations, the bellows systems are designed as restrained expansion joints, for example, within the “L” or “U” shape pipelines. Moreover, the Spiroflex company offers solutions for the pressure balanced expansion joints. Bellows used for pressure compensation are designed with twice bigger effective area as shown in the right picture below, where the balancing bellow is situated in the centre of the compensation assembly and the flow bellows are neighbouring on both sides. The axial thrust forces caused by pressure changes are absorbed by the slender struts mounted to the bellows end flanges. The size of the bellow pressure forces is directly influenced by the spring rates of each bellows within the compensation unit. [37] [40]



Fig. 13: Application of pressure balanced expansion joints at turbine pipeline (left) and as an axial in-line compensator (right) (Spiroflex) [37]

2.3. Edge-welded bellows

Taking into account special applications, related low material budget, high number of lifecycles, huge strokes and precise dimension requirements, the edge welding bellows represent the ideal choice, even if it is considered to be one of the most expensive solutions. The reason of higher costs of an edge-welded bellow piece is more technology as well as time-demanding manufacturing, which includes stamping with the following edge-welding. Therefore, this type of bellows is not produced in high volumes, but it is rather used in non-standard technical areas such as aircraft engines, semiconductor devices or medical and high-vacuum technologies. [18]

The edge-welded bellows have got a very specific profile. It consists of welded pairs of pressed diaphragm rings. The shape of metal rings reminds of spline curves as depicted in the schematic picture with added detail of a metallographic profile cut below. [15]

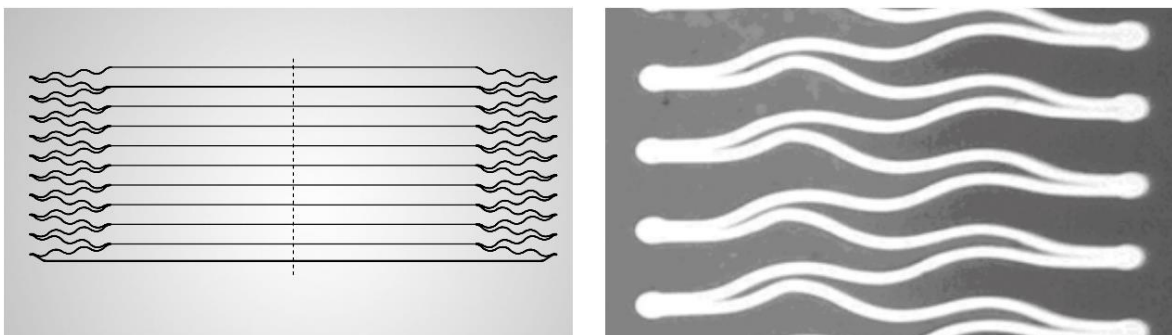


Fig. 14: Diaphragm profile of an edge-welded bellow (Witzenmann catalogue) [15]

The shape of the punched convolutions as well as the edge-welded joints represent the crucial factors of the bellows properties and performance. The number of convolutions and their material attributes might be adopted to required spring

rates and expected strokes. The ductility of the bellow material has a great impact on both the allowed number of convolutions and shape of its corrugation. The quality and precision of diaphragm manufacturing and its welding is reflected in the lifespan of a bellow. [20] [41]

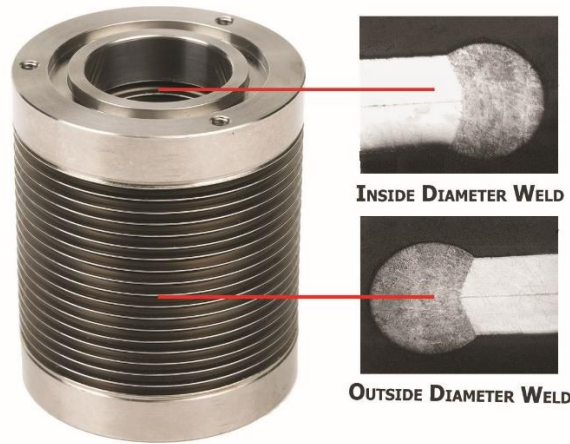


Fig. 15: Edge welded bellow with end flanges, detail of welded joints (Bellowstech) [20]

The transformation of the initial product into the final products starts with automatized stamping process. The metal strips are cut and punched on presses with proper patterns in dies. There are patterns for both the female and male types of diaphragms, which are then prepared as convolution pairs for welding procedure. Due to the stamping technology, it is possible to achieve very precious the dimensions of the bellows diameters and preserve tight tolerances of the diaphragm shapes. For example, the company Comvat produces stamped edge-welded bellows in the range of minimal inner diameter of 2,7 mm to maximal outer diameter of 810 mm. Before shifting to welding operations, the metal stamped rings are cleaned and degreased. [18] [20] [42]



Fig. 16: Stamping tools mounted on the machine (Comvat AG) [42]

The subsequent operations are related to edge-welding. The diaphragms are welded along their inner and outer diameter. First of all, the diaphragms are prepared on special round-shape stands in pairs of one male and one female type of a diaphragm. [18]

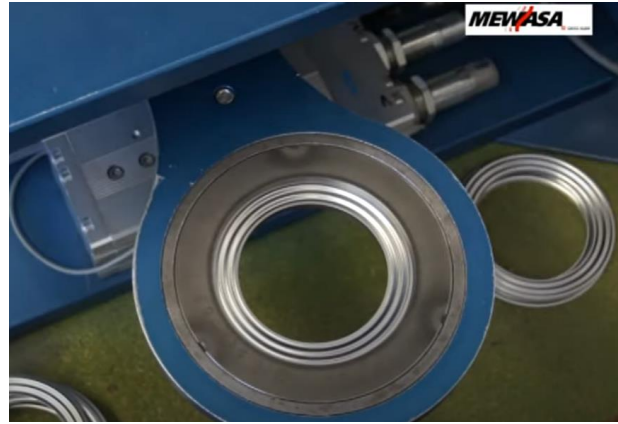


Fig. 17: Stamped metal diaphragm on a stand prepared for welding (Mewasa AG) [43]

Then can be performed welds on the inner diameter of the pair of metal rings. The result of this step are the single convolutions, which are finally welded on their outer diameter with each other to create the hole piece of bellow. At the same time, the convolutions are supported by chill rings in order to ensure smooth welding procedure and to enable joining of multiple pieces together. Another contribution of these chill rings is related to the part cooling, what helps to put clean and precise weld seams. After installation of chill rings, the convolutions are accumulated on an arbour, which serves for rings alignment before outer welding. Except for common fuse welding methods such as TIG welding, other technologies like arc welding, plasma welding, electron beam welding or laser fusion are used as well. The automatized laser welding technology is rather determined for higher volume production. On the other hand, the manual microplasma or laser welding is suitable for single piece production. [17] [20] [42] [44]



Fig. 18: Edge-welding of inner diameter of two diaphragms (Mewasa AG) [43]

After making welds on outer diameters, a bellow is ready for final procedure, during which are welded end pieces on outer bellows diameter (OD) such as standard end rings or end rings with a prolonged neck. Eventually may be implemented ISO K as well as ISO KF flanges or any flanges, that are similar to them, especially in terms of the thickness when considering vacuum technique. In such a case, the flanges could be equipped with a groove for vacuum sealing. [20]

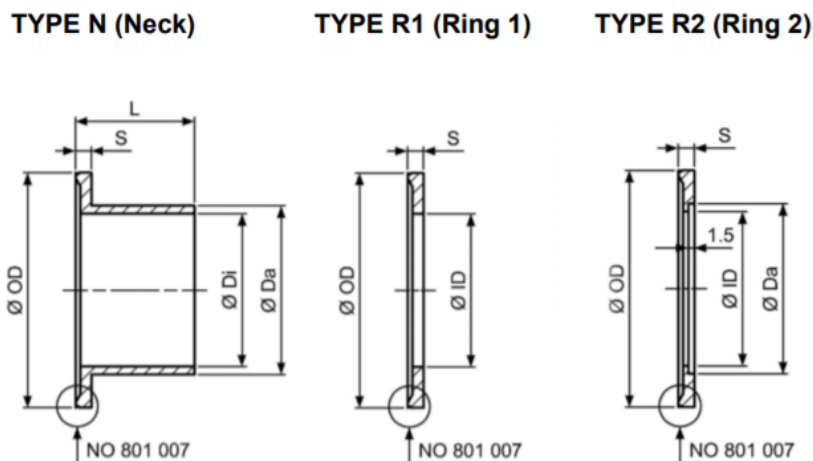


Fig. 19: Standard end pieces for bellows (Mewasa AG) [45]

2.3.1. Pros and cons

There are many advantages of edge-welded bellows, especially regarding the application in vacuum technologies such as a tilting mechanism of this thesis. The best benefits lie in huge stroke possibilities, fine flexibility and relatively small material budget considering the wall-thickness of convolutions. For example, it is stated, that the maximal stroke might achieve up to 80% of the bellow free length in compression and approximately 25% in extension. Taking into account the material thickness, the MW Components company offers the smallest bellows with the thickness of 0,051 mm or the Mewasa company produces edge-welded bellows with

small diameter in the thickness value of 0,076 mm. [45] Compared with hydroformed bellows, the edge-welded type may be offered in wider range of materials as the welding technology allows to operate with different metals. [15] [30] [41]

Back to the flexibility. Even if the spring rate, which has a direct impact on the sensitivity of a bellow, is influenced by the type of bellows material, wall-thickness as well as the size and number of convolutions, by edge welding can be achieved really low values of this physical parameter firstly due to the possibility of optimal stamped plate design, and so the edge-welded bellows might belong to one of the best deformable types of such flexible compensators. Furthermore, the shape of bellows ripples with three sweeps is developed enough to minimize the notch stresses in critical areas such as weld seams. [19] [30]

Another point of view are the costs for manufacturing. The tooling costs of edge-welded bellows are considered to be the highest among the production methods. According to MW Components company catalogue, the tooling costs for a new set of bellows may range between \$ 4 500 to \$ 8 000, what reflects the final price for a customer. Nevertheless, the advantages might be worth it as, for example, the edge-welding bellows are widely used within vacuum technique, because the welded convolutions can withstand considerable pressure differences. The bellows could resist aggressive acidic environments and they can be operated in pretty wide range of temperatures between -250°C to 815°C as well depending on the material properties and its corrosion resistance. [30] [19]

2.3.2. Materials

The range of applicable materials for edge-welded bellows machining is considered to be wider than the range for other manufacturing methods. First of all, the choice of material is determined by its weldability, mechanical attributes such as tensile strength, elastic modulus etc and last but not least the field of application of a bellow. [41]

Beginning with the most significant group, which are stainless steels. The single types of steel are the same as introduced by hydroformed bellows added for example by AM 350 or Titanium Gr 2. Furthermore, edge-welded bellows are produced with the material of nickel alloys, which are listed in the chapter 2.1.3. Aluminium alloys play its role within the edge-welded bellows production as well. [30]

2.3.3. Producers

This chapter will briefly introduce several producers of edge-welded metal bellows.

To begin with already named the Swiss Mewasa company, which is highly specialized in production just of edge-welded bellows in round-shape as well as non-circular shape and further complex devices such as manipulators, accumulators, pillow seals or ultra high vacuum chambers. [45]



Fig. 20: Edge-welded bellow with flanges in deflected position (Mewasa AG) [46]

The next representant is the German Vacom company, which is involved primarily in vacuum technology including vacuum optics, pressure measurement, valves etc. The edge-welded bellows are designed as feedthroughs from vacuum chambers, compensators of thermal changes and mounting strokes or vibration absorbers. [47]

Other producers are the Witzenmann company and the MW Components company. The both are focused on different manufacturing methods including forming, welding or even electrodeposition, which is described shortly in the chapter 2.4. [15] [30]

2.3.4. Application

Edge-welded bellows find very wide field of applications and one of the most significant areas is the sealing technology and compensation devices. Such an element plays a big role within the oil, gas and chemical industries due to the fact, that it serves as a good compensator of length as well as angular deflection caused by high temperatures or pressures. Then the bellows can serve as flexible coupling and form a part of gas lines, valves, leak detectors etc. The bellows have the similar purpose in semiconductor technology within beam lines. [19] [41]

The next important group is the aerospace, where the edge-welded bellows can find its use within reservoirs for fluid processing or cooling systems, hydraulic accumulators, seals for pumps, fuel drain pipelines, damper assemblies etc. [41]

Necessary to mention are the medical technologies, where are edge-welded bellows often installed to blood pumps, control devices, endoscopes, vacuum pumps, oxygen pumps etc. [41]

To be more concrete, the following figure shows the assembly of a “port aligner” with pivot mounts offered by the Ferrovac GmbH company. It consists of an edge-welded bellow joined through neck-type end fittings to DN40CF flanges and three hexagonal slender struts fixed by left-hand and right-hand threaded hexagonal nuts. The vertical screws are fixed to the flanges on one end and on the other side, the screws are bolted to the flange just through pivot mounts, that are formed by radial spherical plain bearings inserted in rod ends. Its material is the stainless steel 1.4404 (AISI 316L). The assembly allows an alignment: ± 5 mm in both the lateral and the axial direction as well as the angle deflection of $\pm 5^\circ$. [48]



Fig. 21: Edge welded bellow with pivot mounts as an aligner [48]

2.4. Electro-formed bellows

Electroforming represents very specific way of bellows production. The main process of electrodeposition is based either on putting thin metal layers onto a manufactured mandrel and following elimination of this mandrel via chemical reactions, if it is not possible to separate the new electroform from the mandrel mechanically. The final electroformed product remains after mandrel dissolving. As the most common material for electrochemical deposition are used nickel alloys, which are laid on aluminium mandrel. [17] [18] [49] [50]

The process of bellows manufacturing via electrochemical deposition could be divided into a few technological procedures.

The first one is related to the mandrel preparation. Bellows-shaped mandrels can be either permanent, respectively reusable, or expendable, which are dissolved after finishing the metal deposition of an electroform. The permanent mandrels are usually made from stainless steel, nickel alloys brass or copper. The expendable mandrels are often manufactured from aluminium alloys. Actually, mandrels form a model of a geometrical pattern of electroformed bellows, what leads to very precise following of inner dimensional tolerances. Mandrels can be machined in larger lengths than defined length of bellows, because the material may be trimmed after electrodeposition. [50] [51] [52]



Fig. 22: Metallic mandrels for electroforming (NiCoForm) [51]

The next step is the own bellows machining. It can be realized on CNC machines, what contributes to develop the automatized process of electroform creation. Due to numerical control systems can be produced bellows of very small sizes, for example the diameter less than 0,5 mm and wall thickness 0,008 mm as the Servometer company presents in its catalogue. [51]

The leading procedure of the hole manufacturing is plating, which is based on chemical electrolysis. Actually, electroforming is just similar as electroplating, which is considered as “ionic relocation.” The process involves electrolyte deposition of metallic ions extracted from anode, for example positive ions of nickel, onto the cathode, which is formed by the mandrel. Such a phenomenon occurs under the operation of the electric current between both electrodes through conductive electrolyte containing metallic salts, e.g. the nickel sulphate solution. The composition of electrolyte may strongly influence the properties of the final product. During the electrolysis, the scattered metallic ions are converted into atoms on the

surface of cathode and they create step by step new layers, which represent an electroform. The metal deposit copies the shape of the mandrel. The time for chemical deposition as well as the current density influence the wall-thickness of an electroform. The whole process might be monitored to get a precise product. [50] [51] [53]

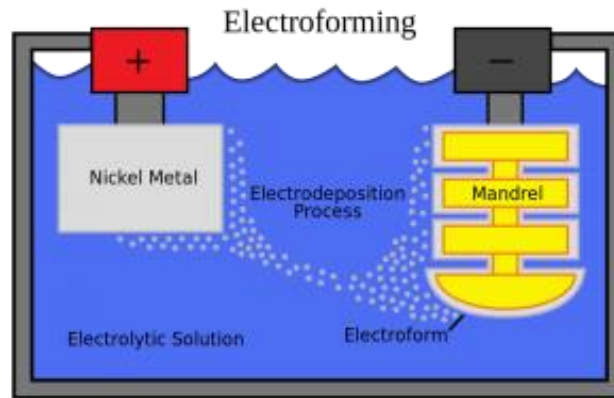


Fig. 23: Scheme of electroforming [54]

After accomplishing the electrodeposition procedure, the ends of an electroform, which stick out, are trimmed and the mandrel is either dissolved in a caustic soda or mechanically removed. It is possible to perform surface finishing procedures on a new bellows to develop corrosion resistance of the product. [17] [50]

2.4.1. Pros and cons

One of the most significant advantages of electroformed bellows is the fact, that their geometry is not limited and that by using this method may be achieved precise dimensions in terms of tolerances including managing thin wall-thicknesses as well as control over ripple shape. For example, the smallest wall-thickness may achieve 5 μm . Moreover, electroformed bellows are manufactured with very low material budget and they are able to perform large deformations and react with a small force response as edge-welded bellows do. [17] [18] [52]

Electrodeposited bellows do not allow as high strokes as edge welded bellows, but they are less expensive, even if not as cheap as hydroformed bellows. It is the reason, why electroformed bellows are produced in lower volumes and they are applied in performance-demanding areas, e. g. aerospace. One more time compared with edge-welded bellows, the electroformed bellows have lower tensile strength and rather narrow temperature range of their operation. Nevertheless, the quality of material is still a matter of development and for example, the NiCoForm company introduces high strength nickel – cobalt alloy called NiColoy, which is

comparable with the properties of a better steel. Electrodeposited bellows are usually not expected to be welded or brazed. [18] [30] [52]

2.4.2. Materials

The most spread materials for electroforming are used nickel and copper alloys, silver, gold or a combination of these metallic elements. For instance, the cobalt-nickel alloys, such as FlexNickel of the Servometer company or already mentioned NiColoy of the NiCoForm company, nowadays belong to the most convenient materials for its high tensile strength, elasticity and purity. It can be superficially treated by silver, gold, copper etc. [17] [49] [52]

2.4.3. Producers

The American NiCoForm company is deeply focused on diverse production via electroforming technology. Except for seamless electrodeposited bellows based on nickel-cobalt alloys, it produces different structural electroforms and optical components. [52]

The next U.S. electroformed bellows producer is the Servometer company. It offers bellows of different shapes and it is focused on the production of edge-welded bellows, shaft couplings and electrical contacts as well. [49]

Other producers, e.g. the Sigma-Netics company, have been already introduced.

2.4.4. Application

Electroformed bellows are due to their good developed properties often used within aerospace and medicine industry. For instance, they can be implemented in oxygen systems, aneroids for fuel mixing chambers or other sensing devices such as temperature or pressure sensing. In the case of medicine, electroforms could be applied as a part of implants or other special devices. [55]

2.5. Other applications

The intention of this chapter is to highlight some interesting ideas, which could serve as an inspiration for the design of a tilting mechanism. The following assemblies may be theoretically equipped with any kind of bellows. Therefore, these products are introduced separately.

The first one is the single hinged expansion joint. This assembly includes one metal bellow with welded end flanges, of which shape is adopted to hinge connection. Due to flat hinges joined with a pin might be the bellow deformed just angularly in the horizontal plane. [56]

On the other hand, the same company has developed pretty smart solution for multi plane angular deflection of a bellow. The gimbal expansion joint including four hinges is presented on the right side of the picture below. [57]

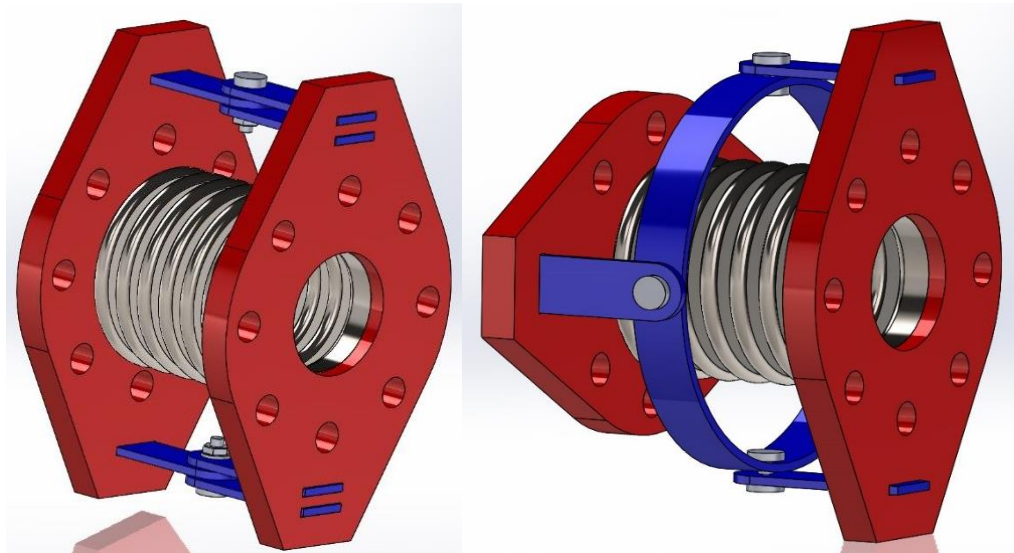


Fig. 24: From left: Single hinged and gimbal expansion joints (ArcFlex) [56] Chyba! N enalezen zdroj odkazů.

2.6. Tip for design of tilting mechanism of CBM experiment beam pipe

Summing up all of the remarks concerning advantages of different types of bellows, the choice for the application in CBM experiment beam pipe may fall on edge-welded bellows as they represent the most suitable solution in relation to the material budget as well as mechanical properties. Between the most important pros belongs their deformation flexibility, which allows them to adopt to high displacements of mating components. Of course, it goes around verified product in vacuum technologies, what meets the experimental demands. Further information was introduced within the chapter 2.3.1.

3. Design of tilting mechanism

The tilting joint for the infrastructure of the CBM experiment is specific for its geometrical as well as physical conditions. The flexible connection is expected to set any required position in the range of $\pm 2,5^\circ$ in the horizontal plane with the centre of rotation in area of the dipole magnet, which is 3 700 mm distant upstream from the end of the RICH / MUCH. The equipment of the tilting joint must fit to the rectangular hole between parts of detectors and absorbers. So, the width is about 1 010 mm and the height should not exceed 570 mm. The experiment expects high intensity of radiation. The measurements of the experiment will be operated under ultra-high vacuum conditions. The matter of the research is supposed to be heavy accelerated ions at high energy levels.

During the design development occurred two crucial ideas, how to ensure the tilting joint of the beam pipe. The first one is based on the mutual sliding of two opposite spherical surfaces. The other variant operates with metal bellows. Both of these ways have been worked out. Each of them includes more design options, of which STEP files with CAD models are attached to the thesis.

3.1. Design of mechanism with metal spheric workpieces

In the early phase of this project the focus was on the development of the tilting joint based on the mutual sliding movement of two parts with spheric surfaces. The key element of the assembly is a deflective weldment, which consists of a milled workpiece, a tube connected to the kinematic mechanism and a flange fixed to the downstream section of the beam pipe. This weldment with a concave spheric surface fits tightly to the intermediate workpiece with a convex surface. Such a middle part is then joined to the end flange from the RICH / MUCH section. The upper and lower linear bended pieces of bars serve for manual fixation of the sliding elements in required setting due to a linear row of screws.

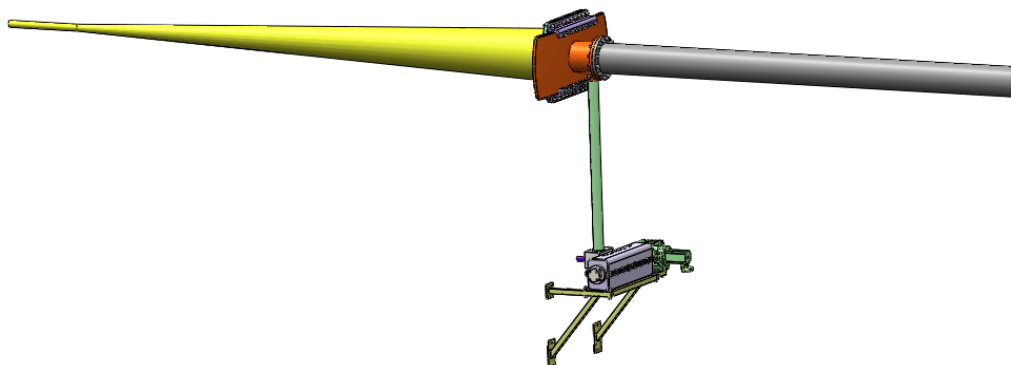


Fig. 25: Design of tilting mechanism with spheric-shaped workpieces

The weldment of the tilting element (brown) is joined through screws to a long vertical shaft, that already forms a part of the kinematic mechanism described in the chapter with the design of the drive. The displacement of moving parts is limited by the arc-shape groove in the upper and bottom bar. The value of its radius is corresponding with the distance from the target, where is the middle of the rotation.

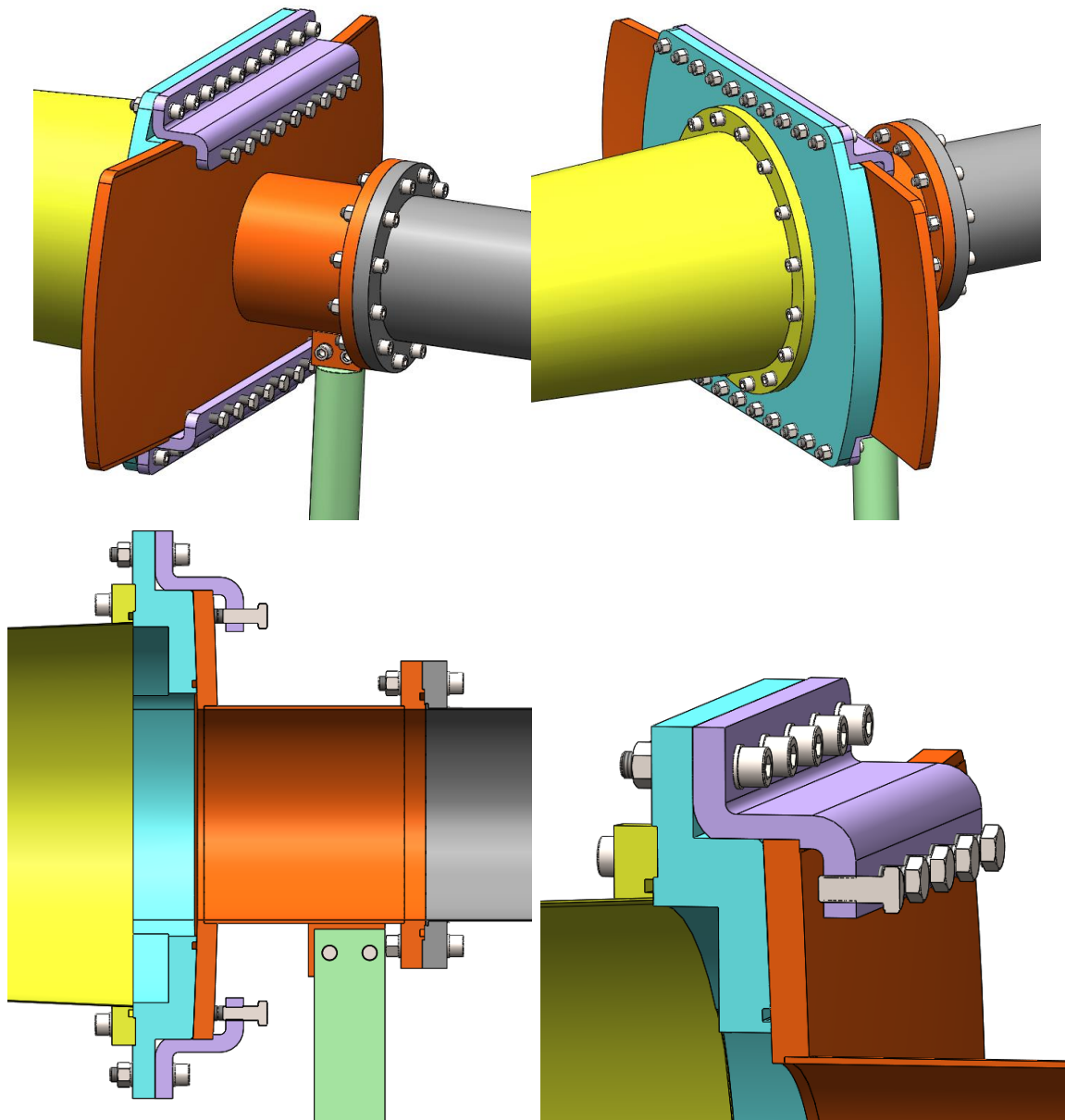


Fig. 26: Different views of the design of spheric connection

The figure below highlights the clearance between the arc groove in the bar and the outer spheric surface of the welded workpiece. Such a mutual positioning allows the movement of the weldment, when the tightening screws are loosened.

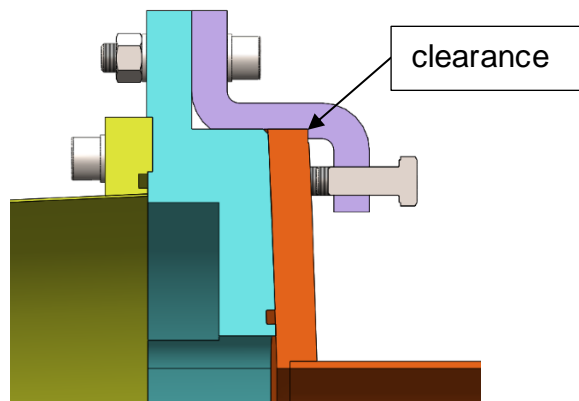


Fig. 27: Cut view of spheric tilting joint with highlighted clearance

The intermediate spheric flange is manufactured primarily by milling and drilling. The workpiece includes spherical sliding surface for the contact with the opposite weldment. On the surface is machined a groove for O-ring, which might ensure the sealing of inner vacuum. It means, that the roughness and geometrical tolerances of the sealing surface are expected to be designed and fabricated at the corresponding quality to meet those sealing requirements. The cutting of the workpiece sketch is presented as an example in the figure bellow. The functional elements of the part are tolerated to ensure the right assembly. The highest emphasis is laid on the machining of the spheric sealing surface with the profile tolerances of shape and orientation, which is related to the base E. Further information is contained in the attachment 14.

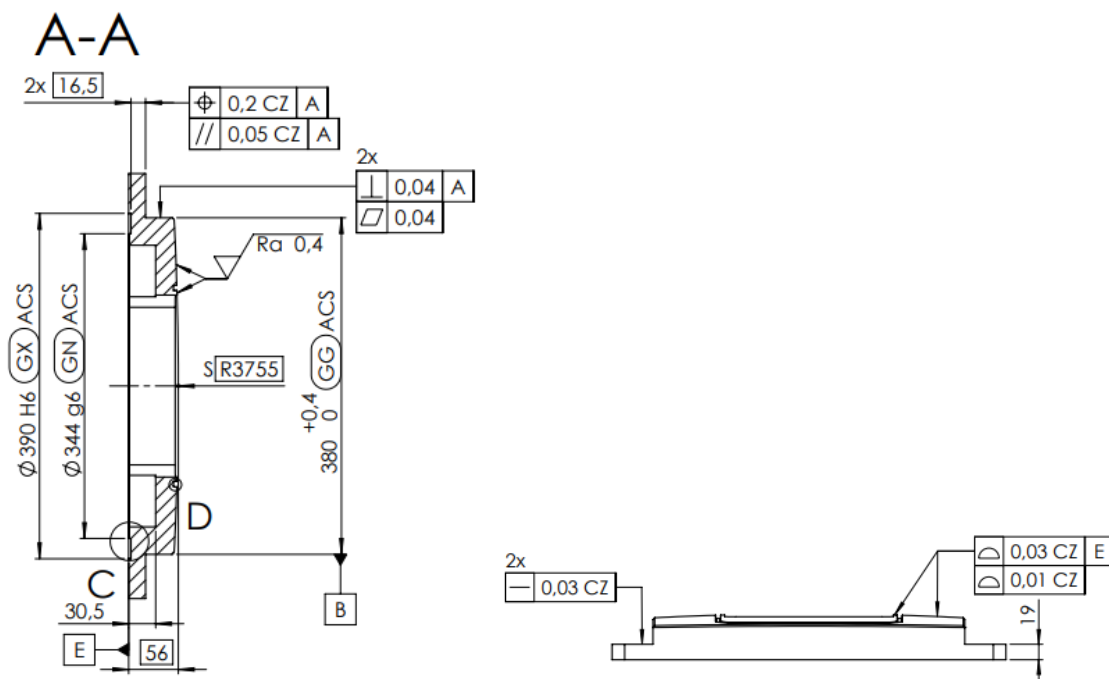


Fig. 28: Example of drawing views of spheric workpiece (attachment 14)

The materials of the components of the tilting joint are in this case supposed to be stainless steels, for instance the steel 1.4301 or any stainless material, that could propose the customer. Considering the physical requirements of the ion research, the aluminium alloys might be suitable for such an application as well.

The picture below introduces some drawing cuttings from the attachment 13, which includes the information about welds that connect the single parts of the tilting weldment.

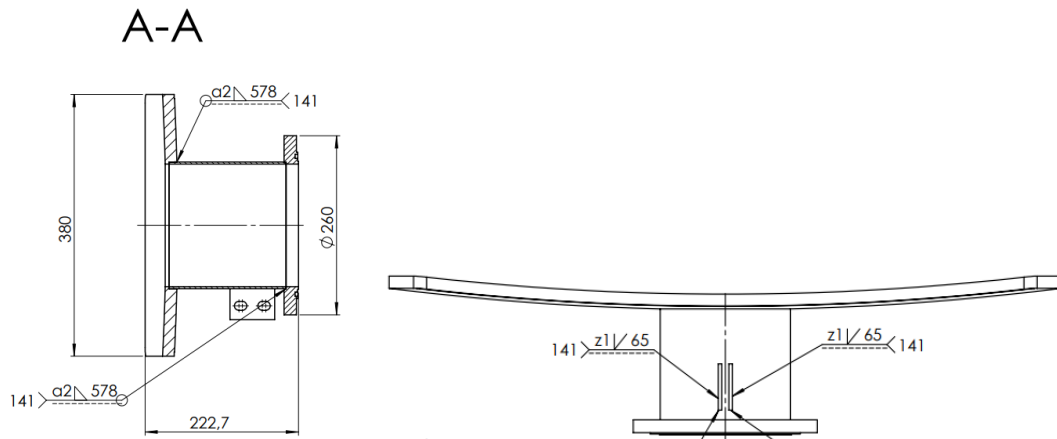


Fig. 29: Views of drawing with welds (attachment 13)

3.1.1. O-ring sealing

The O-ring from Viton¹ material represents ideal solution for sealing the components of the tilting joint of any metallic material and keep inner vacuum. The choice of each O-ring for the designs of this thesis follows the recommendations of the Dimer company, that are specified in its catalogue. Here is an example of the O-ring dimension calculation and the product classification. [58]

The flange from the conical section of the beam pipe has got a groove for O-ring with the smaller diameter $d_3 = 330 \text{ mm}$. According to the Dimer catalogue the inner diameter d_1 of the O-ring should range between 0,98% and 0,99% of the diameter d_3 . It is valid just for inner vacuum sealing. So, the diameter d_1 might range:

$$d_{1min} = d_3 \cdot 0,98 = 330 \cdot 0,98 = 323,4 \text{ mm} \quad (4)$$

$$d_{1max} = d_3 \cdot 0,99 = 330 \cdot 0,99 = 326,7 \text{ mm} \quad (5)$$

I choose the O-ring with $d_1 = 325 \text{ mm}$ and $d_2 = 7 \text{ mm}$ from the catalogue. [58]

¹ Viton is a fluoroelastomer material often used for sealing production such as O-rings. It is outstanding for its chemical fluid and heat resistance. [59]

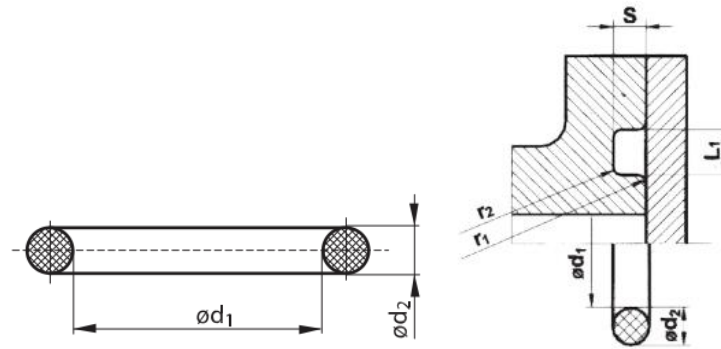


Fig. 30: Characteristic diameters of O-ring and groove dimensions (Dimer catalogue) [58]

It is recommended to choose as big diameter d_2 as possible to fill the flange groove as much as possible and to provide better vacuum sealing properties of the assembly. Other dimensions correspond with the catalogue values. After pumping of the gas from the inner areas of the vacuum sealed assembly, the O-ring shrinks to the smaller diameter of the groove and fills the gap between flanges. The sealing surface of the part must meet the roughness requirements. FPM is the Viton material. The ring hardness is 80 Shore. [58]

The final indication of the Dimer O-ring is: OK FPM 80 325x7.

All of the O-rings within this thesis are chosen in the same way.

The two pictures below show the deflection of $2,5^\circ$ in the extreme position of the tilting weldment, that joins the downstream beam pipe. The right picture demonstrates the reason, why must be the intermediate flange so wide. The sealing is supposed to work in every position ranging $\pm 2,5^\circ$. Therefore, the sealing groove of the O-ring might be wide enough in order to ensure its function.

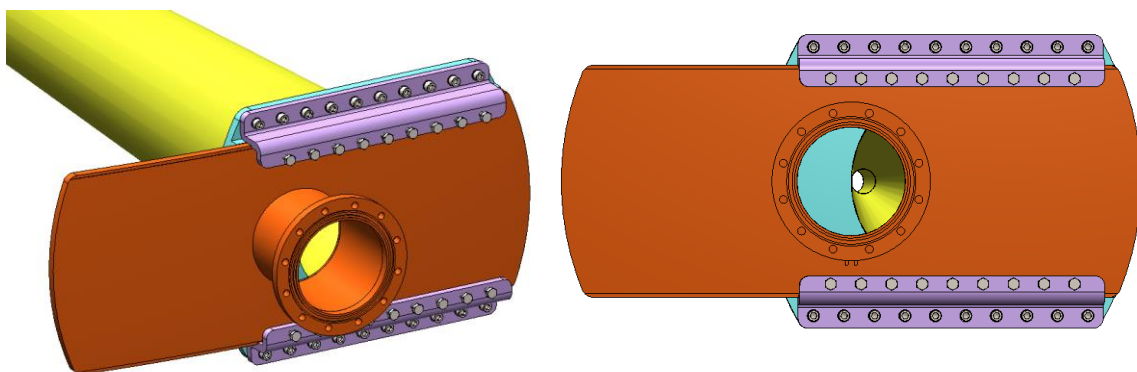


Fig. 31: Position of $2,5^\circ$ of the tilting weldment

3.2. Design of the mechanism with composite spheric workpieces

Another option looks like very similar to the previous solution. Nevertheless, all of the parts are adapted with their shapes for the application of carbon-fibre composite materials. The fabrication of the parts might include hand lamination and vacuum hardening. The parts are finally glued together to substitute the weldments of the previous solution. For example, the Loctite company develops the chemical epoxide glues for different applications regarding carbon composite joints. [60]

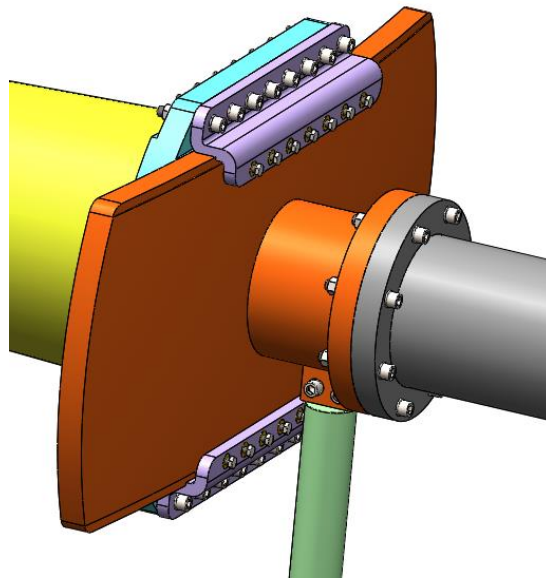


Fig. 32: Composite version of the tilting mechanism with spherical parts

The thread inserts for screws are inspired by the product Trisert-3® of the Tappex Thread Inserts company. They are manufactured with female threads and they are glued to the hole in the carbon-fibre composite. The thread inserts are applied in the connection of the flange from the conical section and in the linear row of tightening screws, that push on the outer surface of the tilting spherical part. Furthermore, the inserts of Tappex are designed with male threads to fit better with the composite hole. [61]

The cut view below shows all of the carbon fibre components. Except for the screw inserts, the difference between steel and composite solution is joining of the tilting spherical element. The glued joints are equipped with the grooves for sealing O-rings to keep the inner vacuum and avoid unrequested leaks.

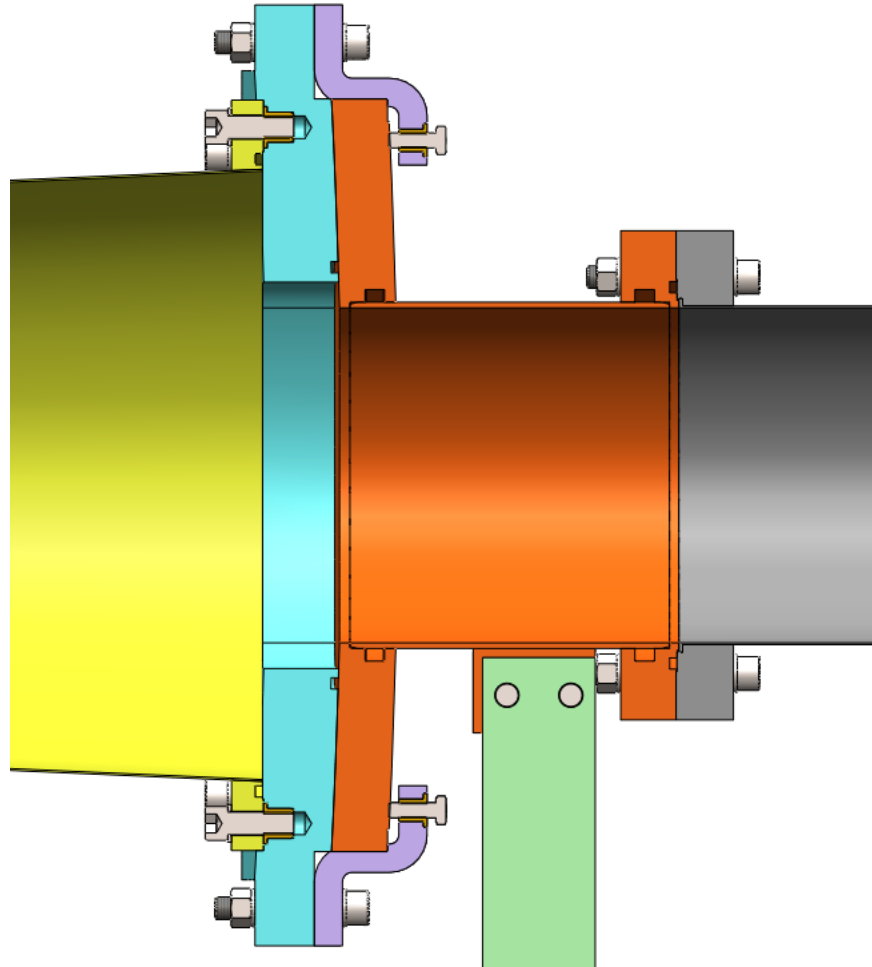


Fig. 33: Cut view of composite tilting joint

The machining of the intermediate composite spherical part consists of lamination process, milling and hole drilling as well.

Proper organisation of the laminate fabrication will impact on the final required mechanical properties of the part. The layers with the same mechanical properties are put in different angles one on each other in regular defined order. Such a method may result in elimination of some unwanted additive stresses of the material under load conditions because it is related to the overall stiffness of the part. [62]

The design of this carbon-fibre workpiece was confirmed by the CompoTech company. [63]

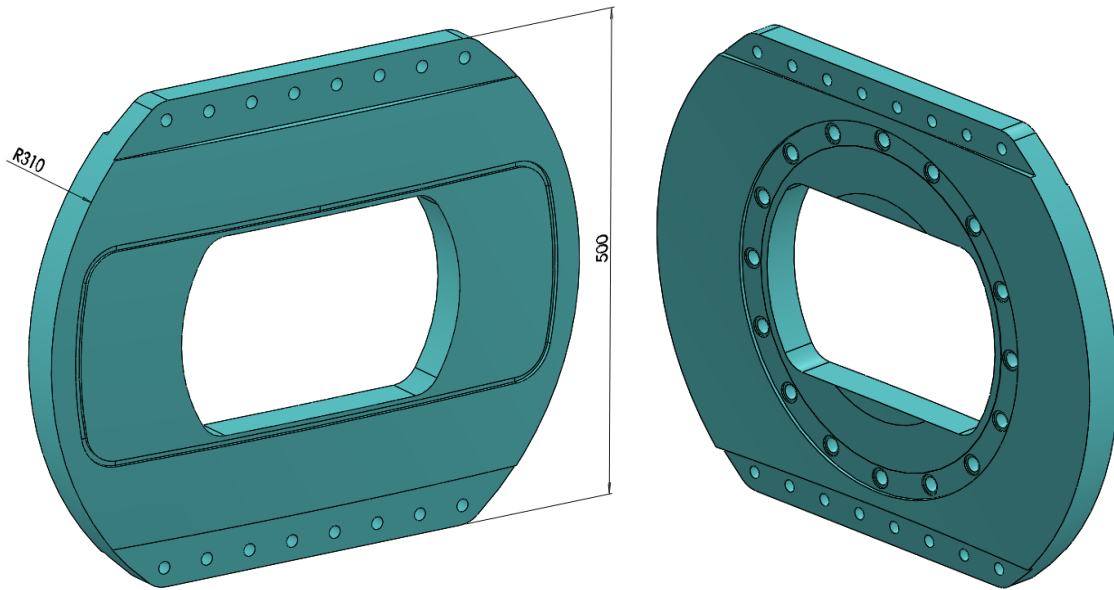


Fig. 34: Intermediate composite spherical part

3.3. Design of weldment with two bellows and intermediate tube

The recherche of the metal bellows and their comparison resulted in the choice of the most suitable type for the application within the infrastructure of the CBM experiment. Due to the wide range of advantages the edge-welded bellows have been selected for the implementation to the design of the tilting mechanism (see the chapter 2.3.2). All of the issues regarding metal bellow were discussed with the Mewasa company. The design of the bellows weldment involves two options. The main difference between these solutions is the element absorbing the axial force and, eventually, the reaction moment, if the bellow assembly is deflected from the 0° position. In case if the first design it goes around tube slender struts, that must be operated manually. The second one is adapted to passive tilting due to double rolling system, that can be driven by an electric engine. Both possibilities work with the same weldment NS-335-360-0.20-1.4404-136. The weldment comprises two bellow with the inner diameter of 335 mm, the outer diameter 360 mm and the wall-thickness of 0,2 mm. The material is the stainless steel 1.4404 (AISI 316L). The total number of convolutions of both bellows is 136. The working pressure difference is 1 bar with inner vacuum. The working temperature is 20°C .

3.3.1. Bellows weldment with slender struts

The assembly of the bellows weldment is connected through flanges to the conical part of the beam pipe. The flange in the middle is mounted radially in a metal ring, which is joined through welded fixtures and screws to a pair of carbon-fibre

composite tubes. Such tubes are expected to transmit just axial forces because the flange may be able to slide in axial direction within the surrounding ring. The tubes are connected through fixture weldments to the ground. In this section of the infrastructure, the beam pipe is situated in the height of 1 m above the ground, further behind the tilting joint it might be approximately 5 m. The bellows weldment is bended due to a kinematic mechanism, which is described in the chapter 4.3.

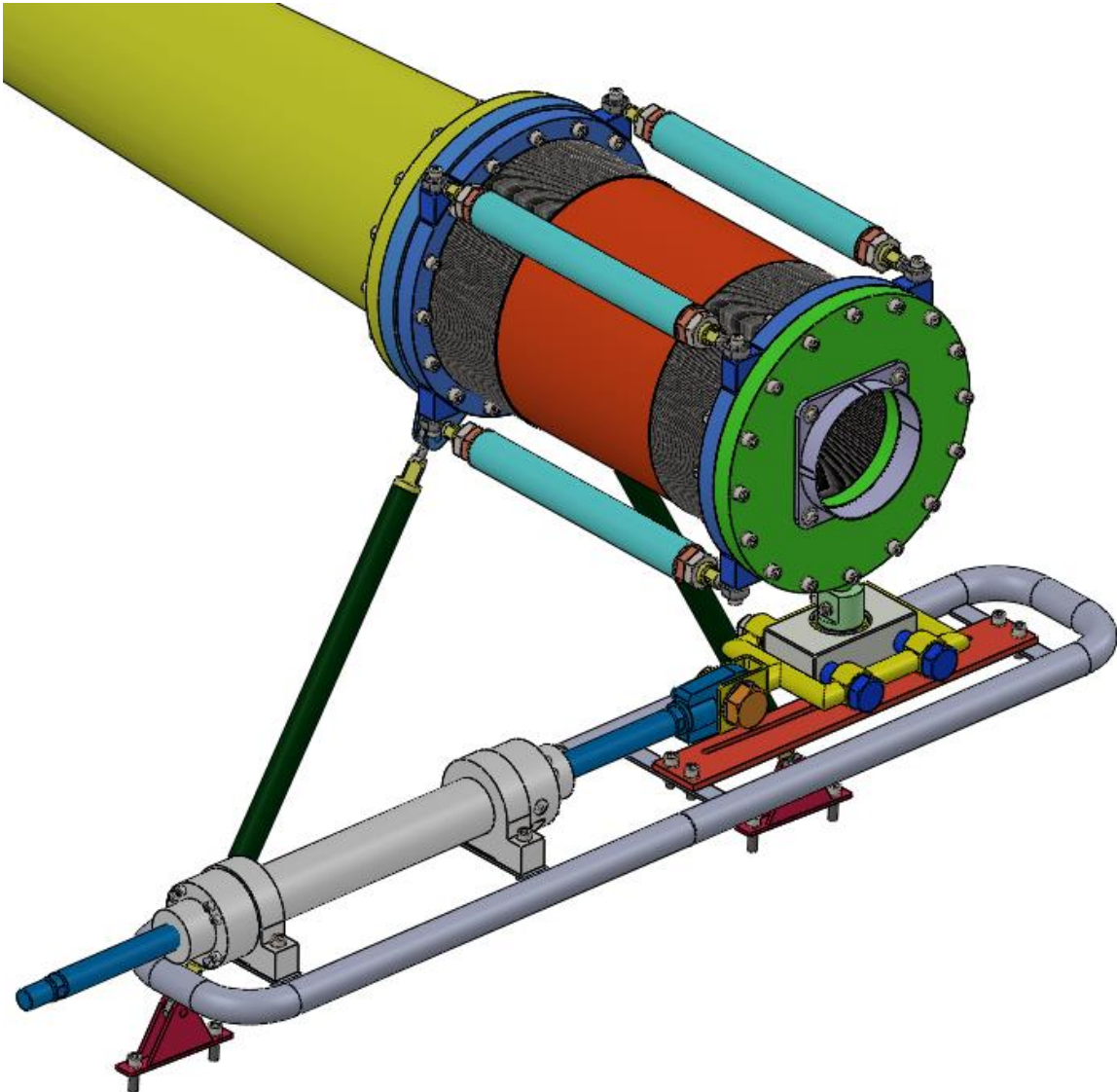


Fig. 35: Bellows weldment with slender struts

Of course, before tilting the assembly with bellow and the beam pipe may be loosened the safety hex thin nuts M30, which enables telescopic sliding of slender struts. After setting any required position of the bellow and the beam pipe in the range of $\pm 2,5^\circ$ the safety nuts are manually tightened again to prevent reverse deformation of the bellow caused by the spring rate reactions as well as vacuum reactions. The assembly and its connection to the flanges is described below.

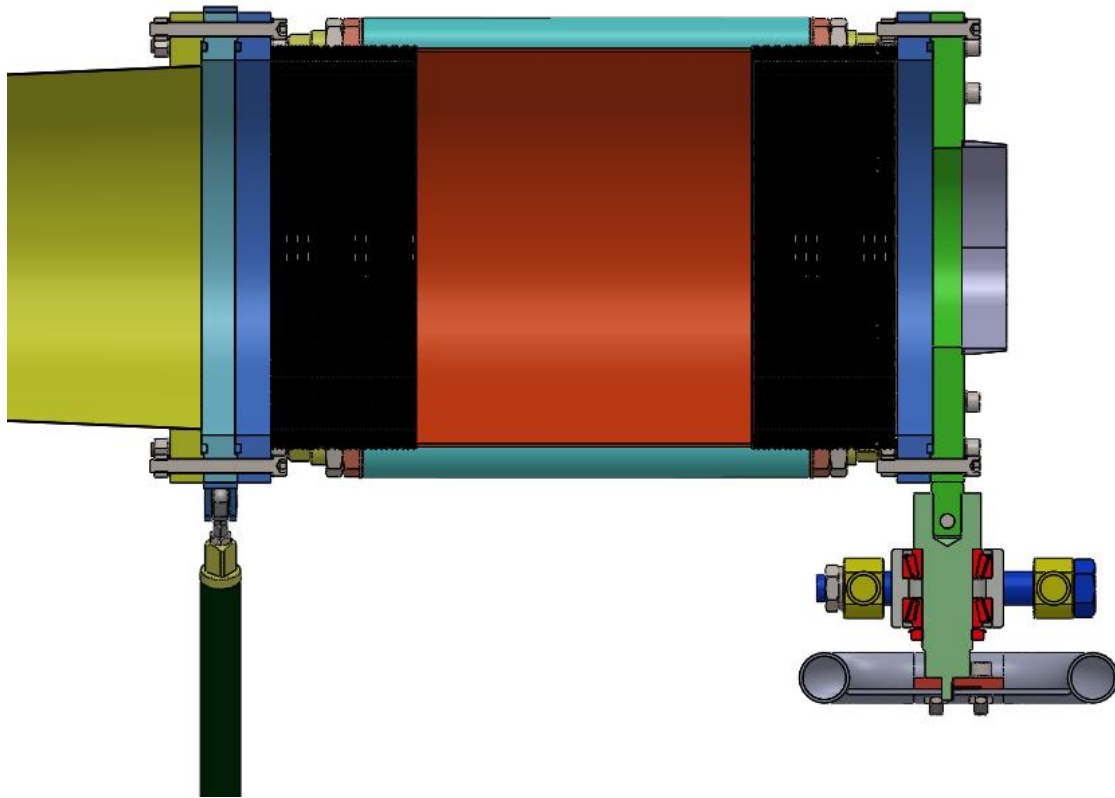


Fig. 36: Cut view through bellows weldment and kinematic mechanism

The weldment of two bellows and intermediate tube includes ring end pieces welded to the last diaphragm on both sides of bellows, that may be welded to edge flanges. The welds are performed on the inner diameter of the flange and on the same diameter of the end ring. Moreover, the weldments of flanges are equipped with triangle-shaped fixtures, which are joined through welds on the milled oblique planes of the flanges. Each of these fixtures contains bored hole with female thread for fixation of the plain bearing inserted in the rod end with a male thread SAKAC 12 M through the socket head shoulder screw. [64]

The male thread is joined to a workpiece that can slide in a tube due to a small clearance between the inner surface of this tube and outer cylindrical surface of the workpiece. If the safety nuts are tightened, the workpiece cannot move in any direction because the bellow assembly produces compressive forces that are transmitted to the slender struts. Therefore, it is not necessary to limit the movement of the workpiece in other direction, which would be caused by tensile load. The bigger safety nut determines the mutual position of the workpiece and another part with male tube thread and outer hexagon for a spanner. Such a workpiece is tightened through tube thread to the slender strut tube all the time and it serves for

the contact with the safety nut M30. The smaller safety nut M12 can set the position of the sliding workpiece in relation to the rod end with plain bearing.

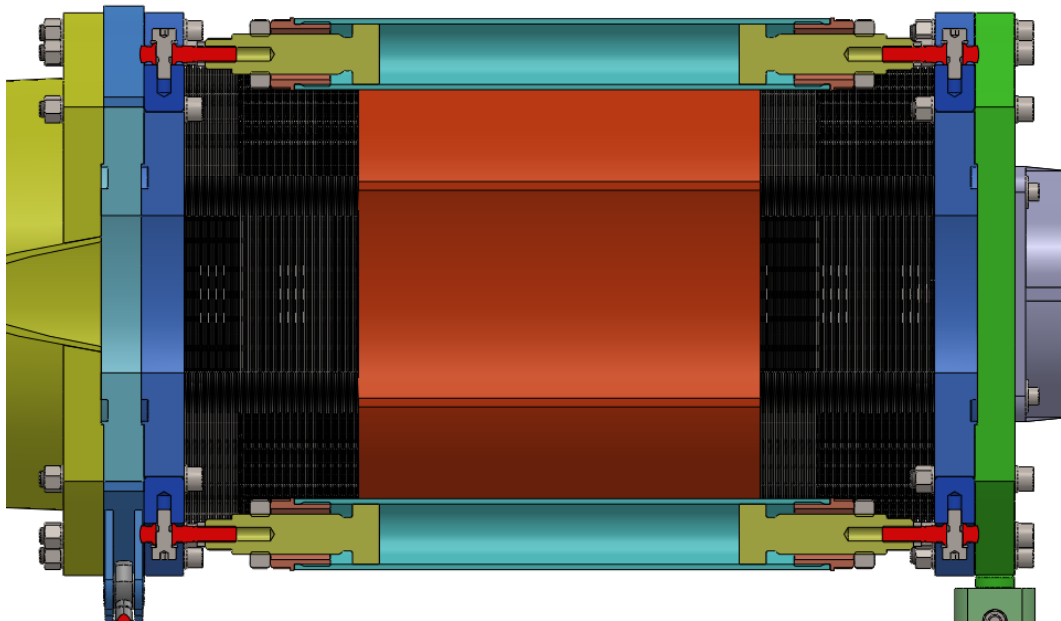


Fig. 37: Cut view through slender strut tube with telescopic workpieces

Finally, the pictures below demonstrate the deflected beam pipe position of $2,5^\circ$ with adjusted slender struts.

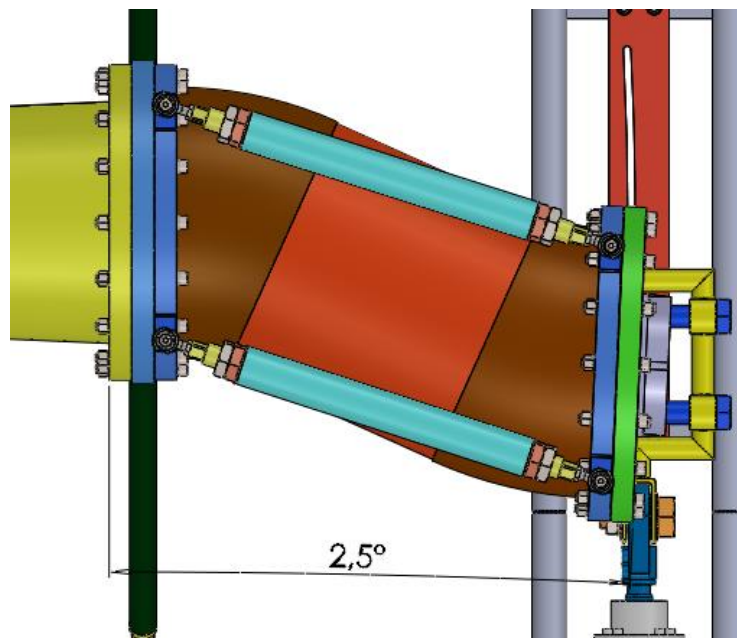


Fig. 38: Upper view of deflected bellows weldment with slender struts

The following figure highlights the limitation of the bellows weldment deflection, which is determined by the arc groove in the red bottom plate.

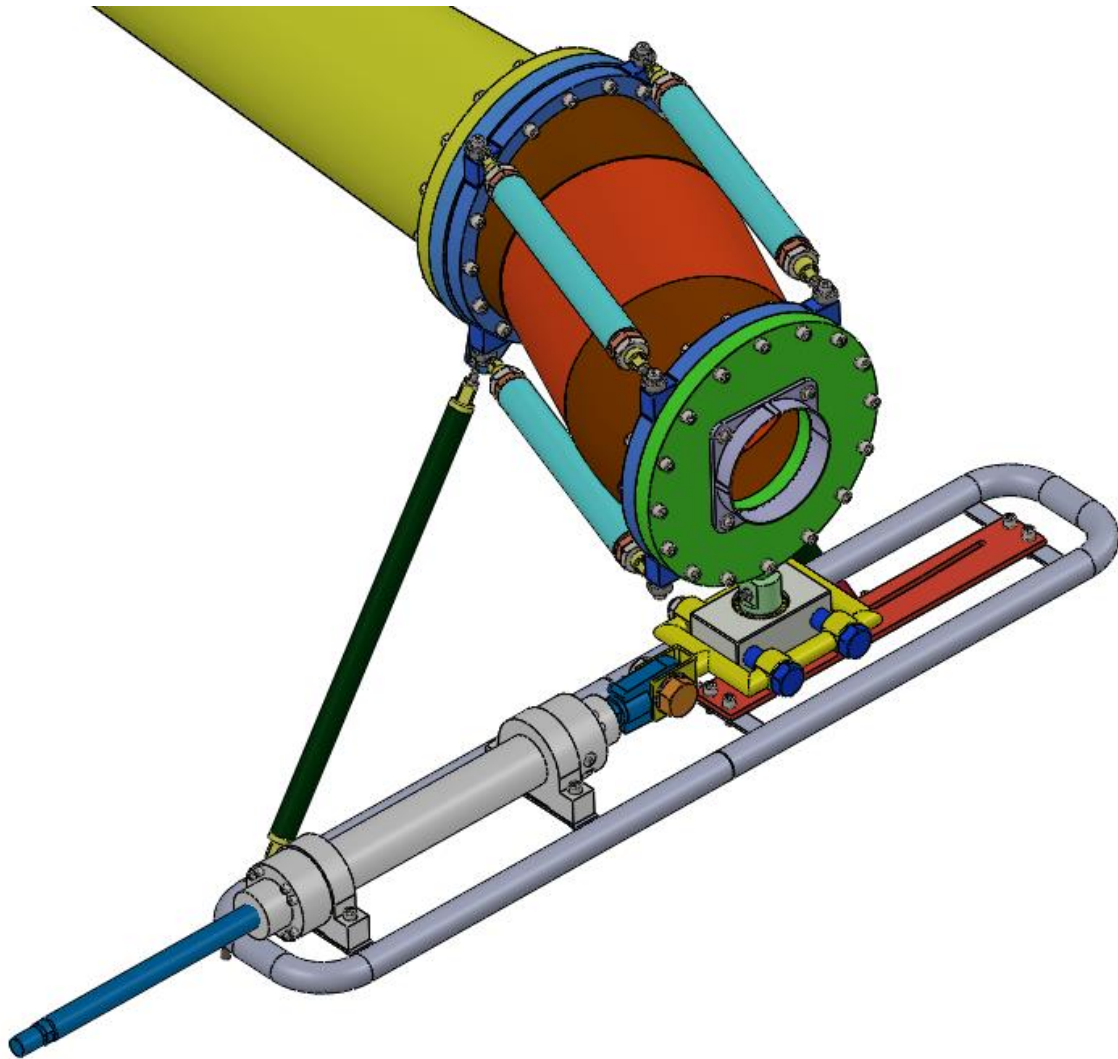


Fig. 39: Deflected bellows weldment with slender struts in extreme position

3.3.2. Bellows weldment with rolling system

The variant of bellows weldment assembly with rolling system avoids manual handling with fixation elements such as nuts etc. This represents the main advantage of such a solution. The rolling system consists of the pair of carriages, which are joined through the socket head shoulder screw to the pins welded to the metallic bellows end flange. Each of the carriages of the type AD420M comprises a board, in which are mounted 4 wheels that can roll on the specific rolling arc profile following the radius of 4 350 mm with the centre in the target of the CBM experiment. The rolling carriages were selected from the T.E.A. Technik catalogue and their provided CAD models have been modified to meet our application. The arc of the rolling profile of aluminium alloy is not offered within catalogues, and so it is expected to be manufactured independently. [65] [66]

The arc-shaped profiles are then connected to the rectangular profiles of the aluminium or stainless frame. [67] [68]

The frame is fixed to the bellow flange, which is connected to the RICH / MUCH section. There are 3 flanges and the intermediate one is supported by the radial mounting described in the previous chapters. It means, that the frame represents a rigid connection of the conical part of the beam pipe and the downstream beam pipe section. The frame absorbs certain reactions of the bellows assembly, especially those in axial direction as well as the reaction moment after deflection from 0° position.

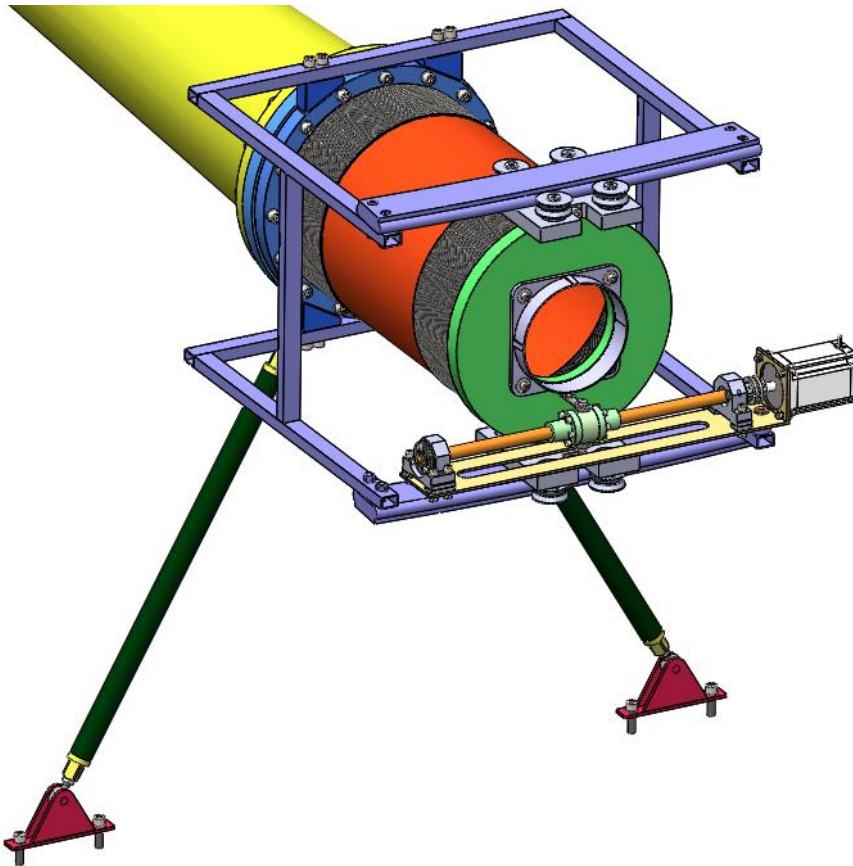


Fig. 40: Bellows weldment with rolling system in 0° position

The weldment of two edge-welded bellows and the intermediate tube is the same as in the previous chapter 3.3.1.

The figure below shows the scheme of axial dimensions and the position of the tilting mechanism as well as its length. The bellow assembly is deflected by the kinematic assembly, which is located 4 416 mm downstream the target.

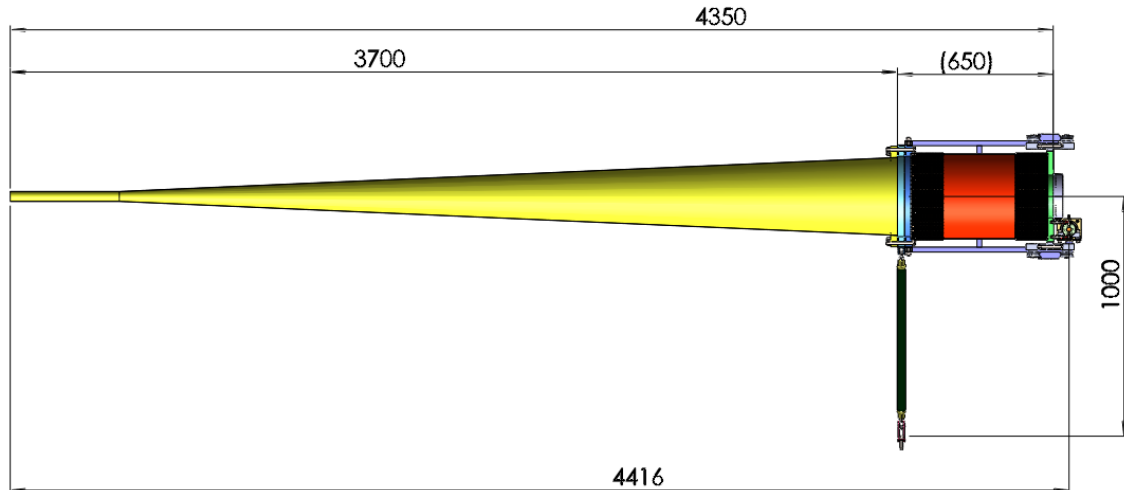


Fig. 41: Scheme of tilting joint placement and kinematic mechanism position

The kinematic assembly is joined through a pair of rod ends with female thread and clamping bolts to the holes in the end flange of the bellows weldment, which connects the downstream beam pipe. The flange involves either female threaded holes or female threaded inserts that may be glued in the holes depending on the material of the flange. If the flange is not from aluminium or stainless steel but carbon-fibre composite material, the inserts might be applied similarly as described in the chapter 3.2. The kinematic mechanism is further solved in the chapter 4.2.

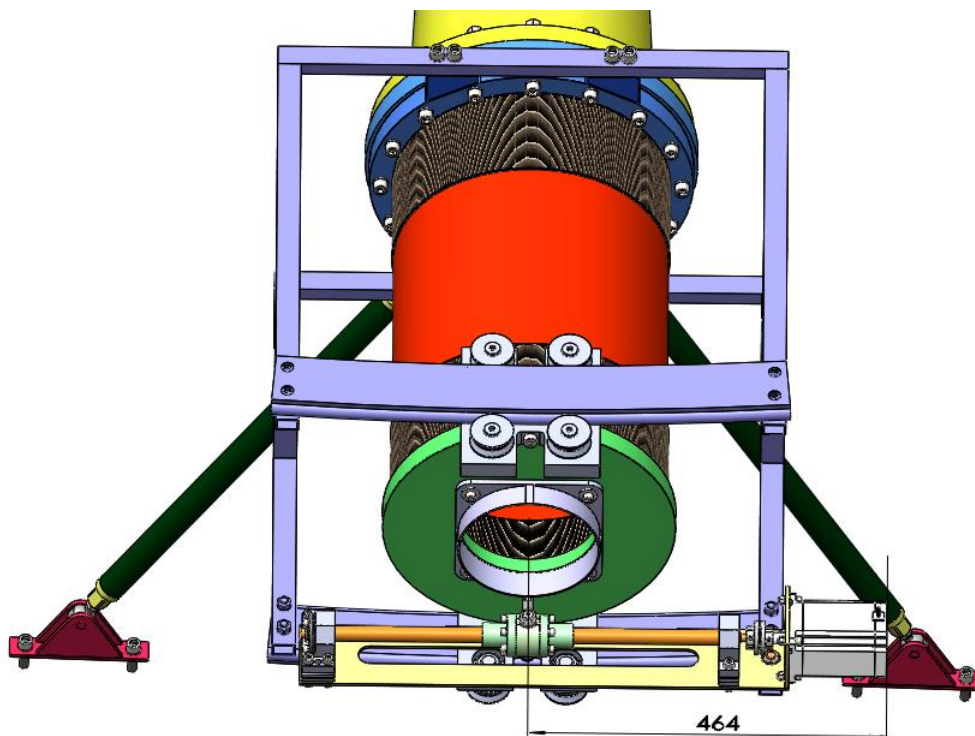


Fig. 42: Front view of bellows weldment and kinematic mechanism with highlighted dimension of maximal width occupation

The tilting joint with its frame is supposed to fit in the space that is limited by the position of surrounding detectors and absorbers. So, the maximal allowed width is 1 010 mm and the maximal height is 570 mm. Therefore, the dimension of the assembly may not exceed 505 mm. The figure above confirms this condition. The total width is then captured in the following picture. Evidently, the total height meets the requirements as well.

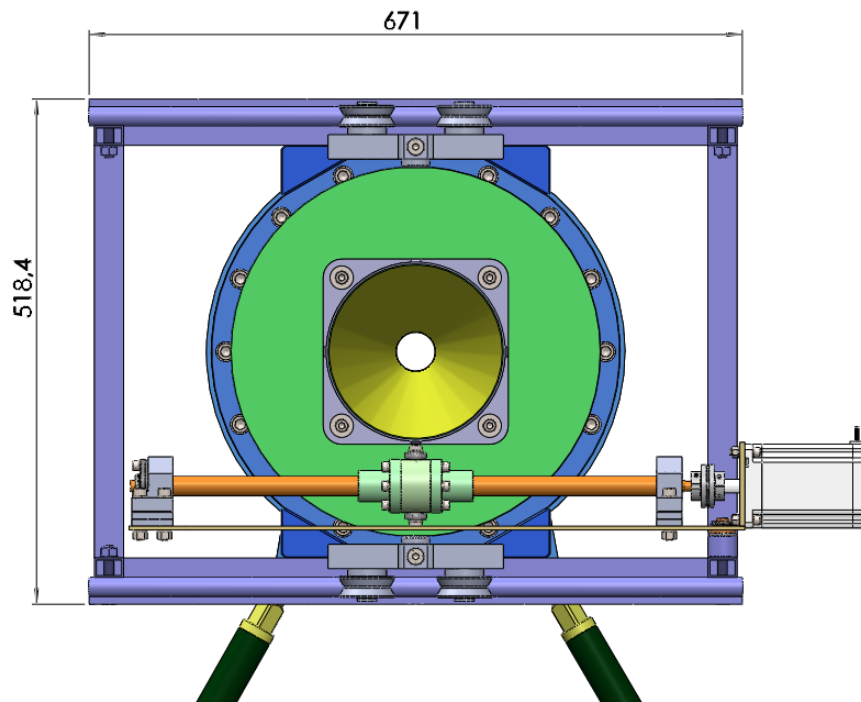


Fig. 43: Front view of bellows weldment and kinematic mechanism with highlighted dimensions of total height and width of assembly

The next figures represent the tilting joint with bellows weldment in deflected extreme position of both polarities.

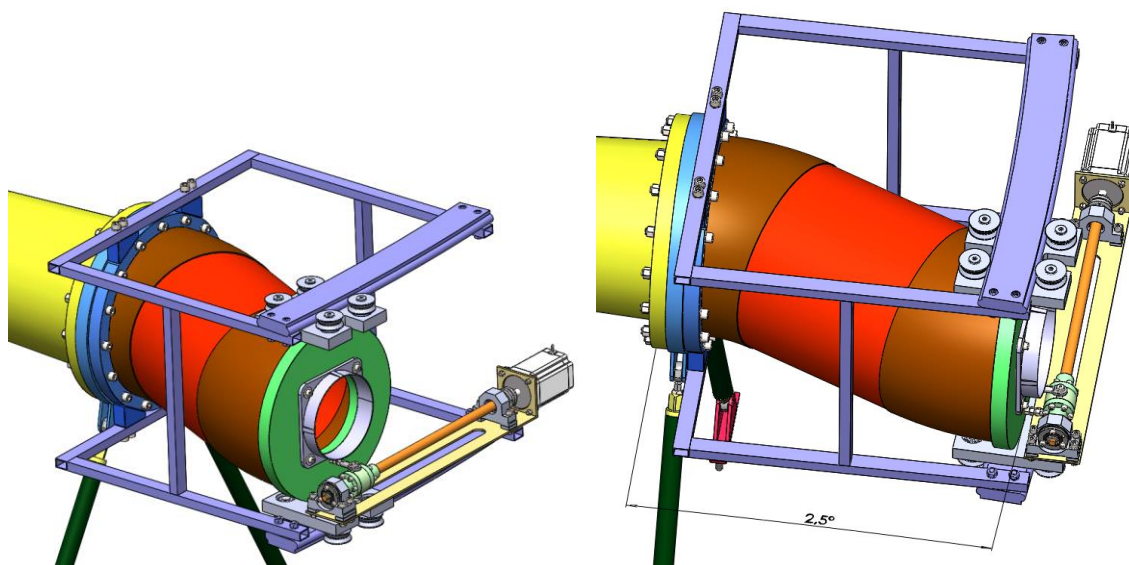


Fig. 44: Deflected bellows weldment assembly in extreme position

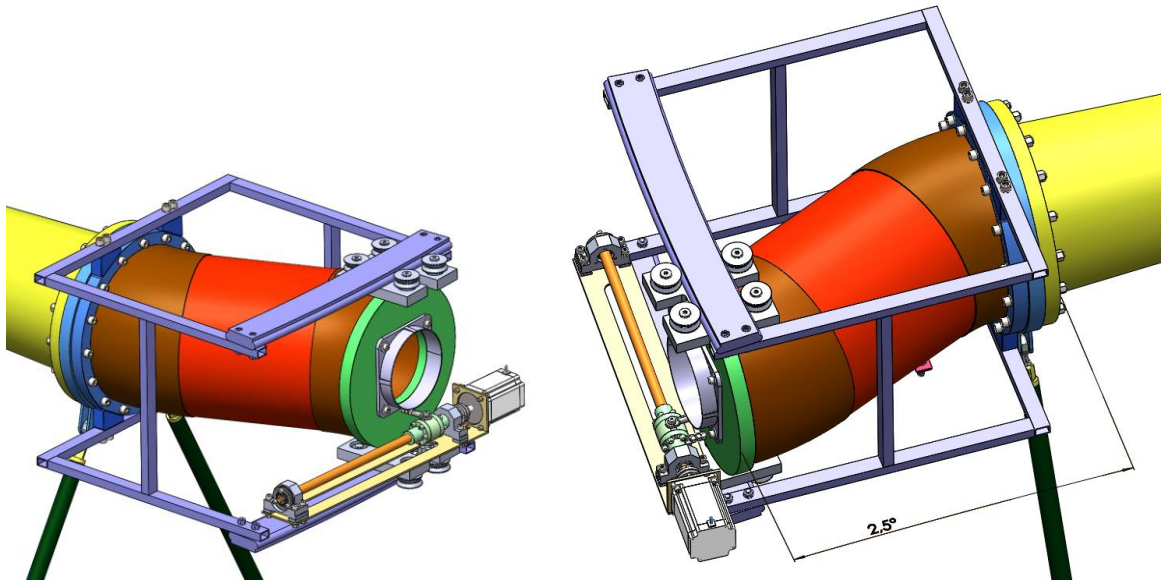


Fig. 45: Deflected bellows weldment assembly in extreme position of other polarity

Furthermore, the centre of ion beam has been sketched in both the 0° and the 2,5° position to demonstrate the functionality of the tilting joint, which is designed to keep the ion beam in the centre of the downstream beam pipe in any deflection.

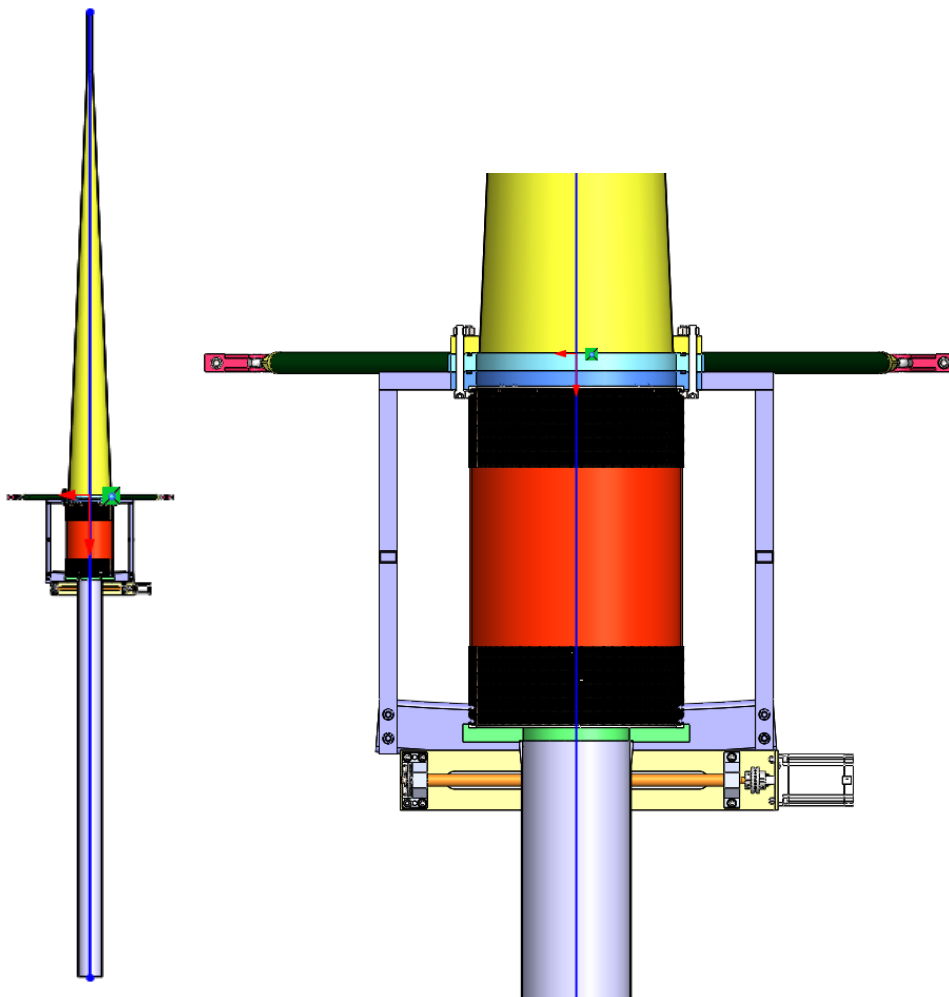


Fig. 46: Scheme of ion beam in 0° position

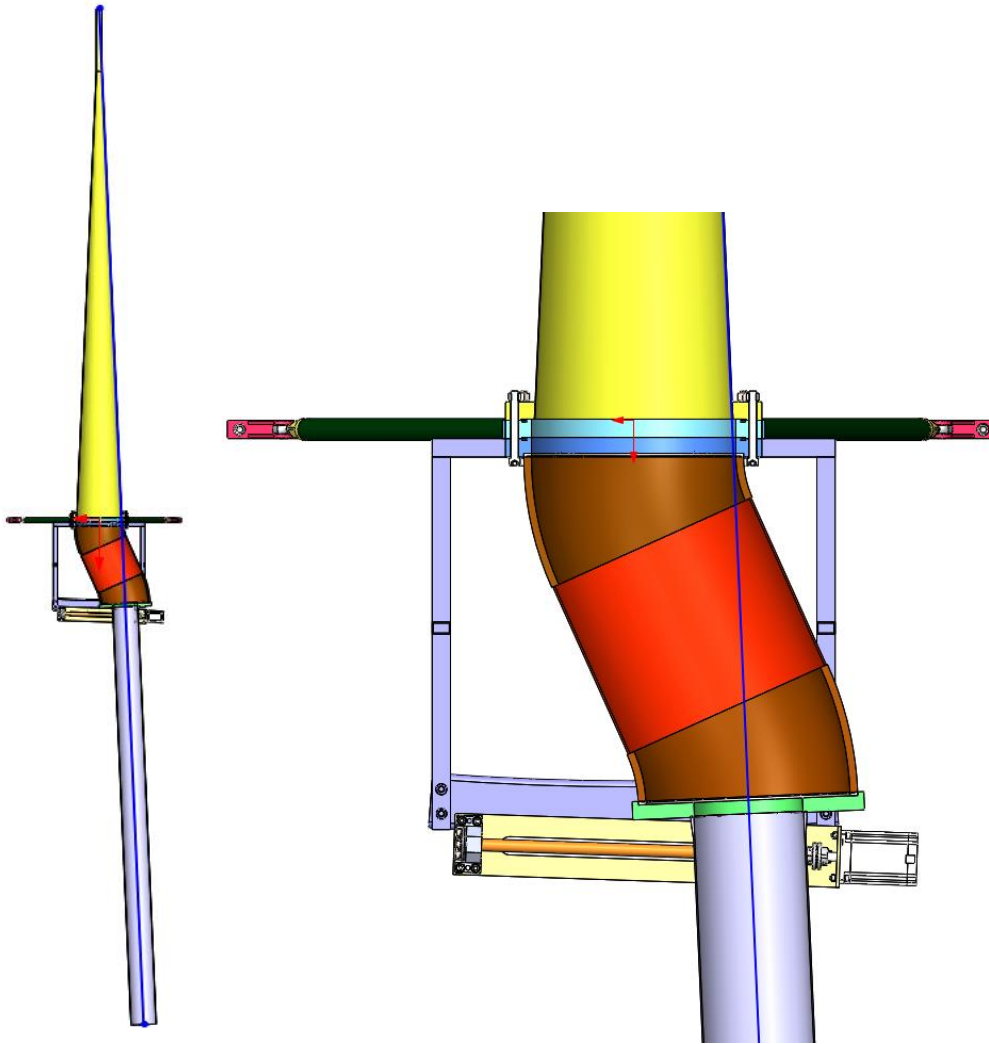


Fig. 47: Scheme of ion beam in 2,5° position

3.4. Design of the weldment with one bellow (and eccentric flange)

The design of a small eccentric mounted bellow was created primarily with the intention to tilt the mechanism passively by the movement of the hole downstream beam pipe, that would be driven by an actuator in area of the PSD detector. The passive solution of bellow assembly deformation is further solved in the chapter 4.4.

The key element is formed by a weldment again. In this case, it comprises two flanges and the bellow NS-200-235-0.20-316L-22 welded through a pair of the end rings 200/235x8 to the end flanges. The operating conditions are the same as in the previous case.

The axial reaction forces of the bellow are captured by a pair of upper and lower slender struts. Each of them consists of one stainless angled ball joint with left-handed female thread and another stainless angled ball joint with right-handed female thread. The supplier of both the left-handed type DIN 71802-16-M12L-CSN

and the right-handed type and DIN 71802-16-M12-CSN is the Elesa Ganter company. [69]

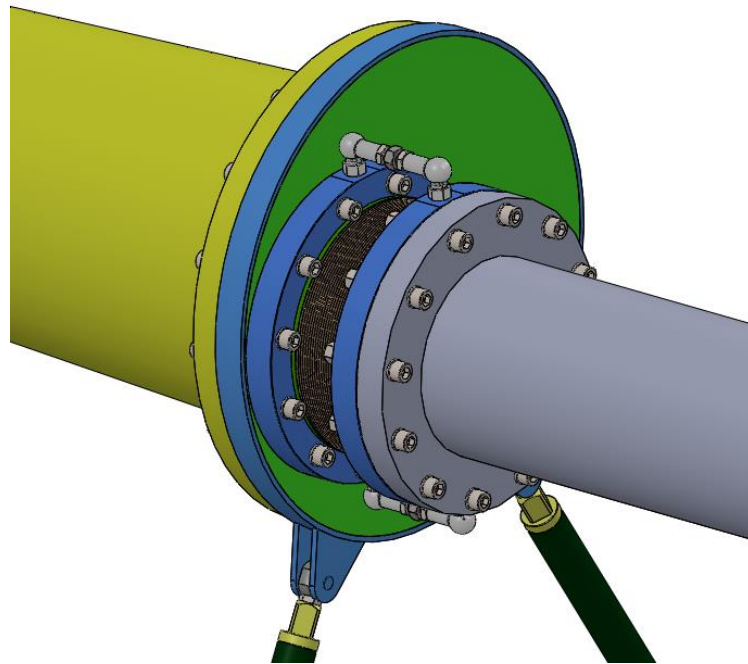


Fig. 48: Tilting joint with single eccentric bellow

The slender strut assembly serves just for angular tilting, which is such an eccentric bellow supposed to perform. Therefore, it is not necessary to handle with the clamping element formed by left-handed thread on one side and right-handed thread on the other side manually during the operation of the beam pipe positioning.

It seems like a great advantage of this solution. Nevertheless, taking into account the need to deflect the beam pipe in both directions or polarities, then it is not as practical as supposed because the huge flange with an eccentric hole that is connected to the RICH / MUCH section must be turned by 180° manually every time the polarity change is desired.

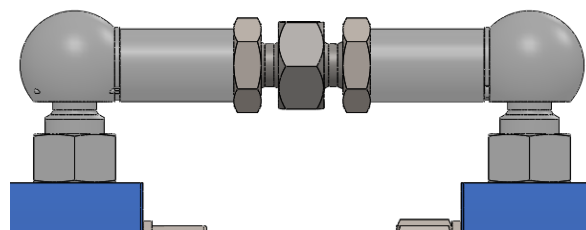


Fig. 49: Pair of angled ball joints with clamping element

The following figures depict the eccentric positioning of the bellow weldment and its location in relation to the target of the experiment, which is 3 700 mm in the upstream axial direction. The bellow design was consulted with the Mewasa company.

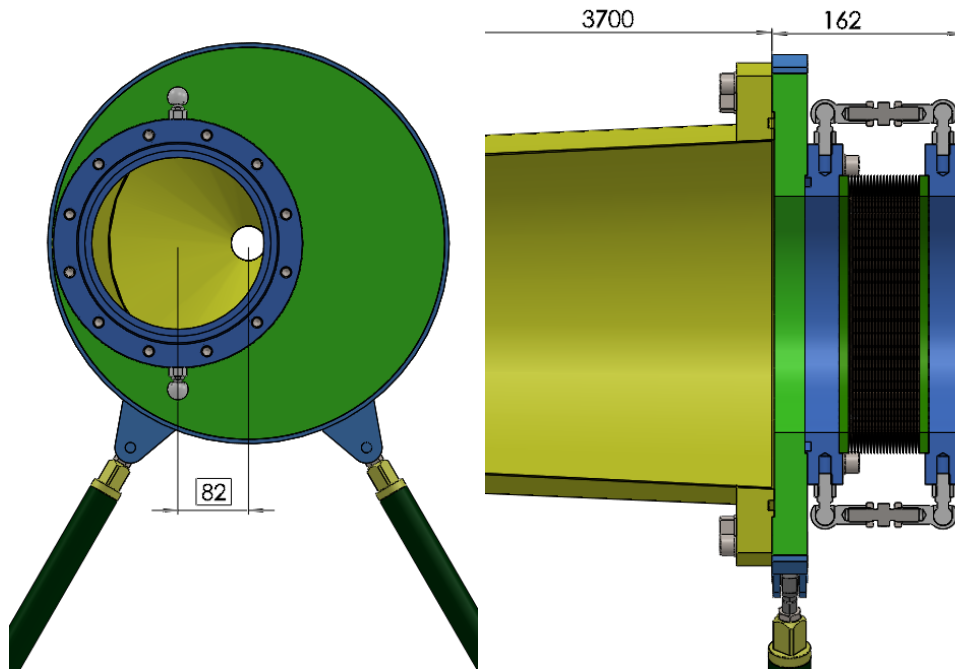


Fig. 50: Eccentric bellow weldment positioning

The next pictures just demonstrate the extreme deflection of the downstream beam pipe assembly. As the centre of the bellows rotation is situated in middle of the angled ball joint, which is near the flange with the eccentric hole, the beam of ions is not preserved in the centre of the pipe anymore. Of course, the ion beam is expected to maintain its parallel direction with the downstream beam pipe in every position.

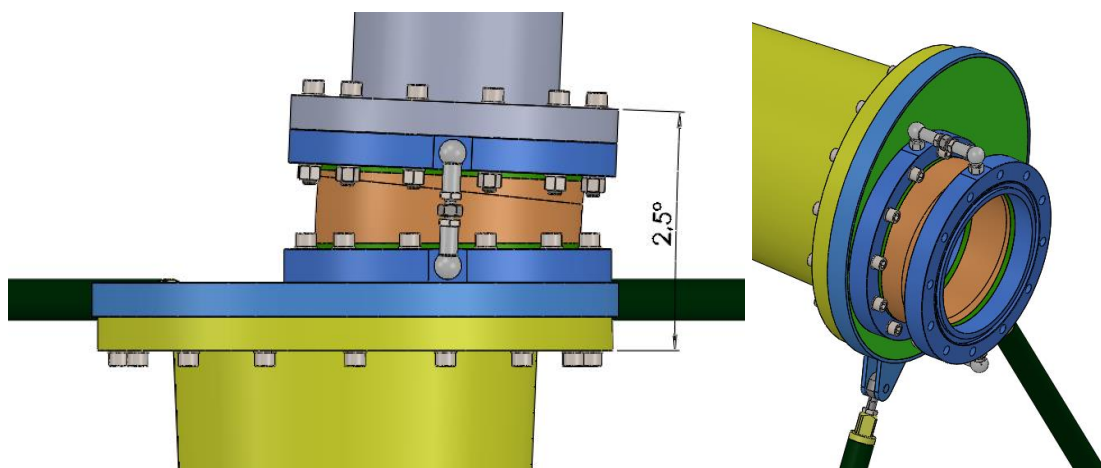


Fig. 51: Deflected tilting joint with single eccentric bellow

The following schemes demonstrate the geometry of the tilting joint with respect to the centre of the ion beam that flows through the beam pipe. In the 0° position the centre of the ion beam is just 7 mm distant from the inner surface of the beam pipe.

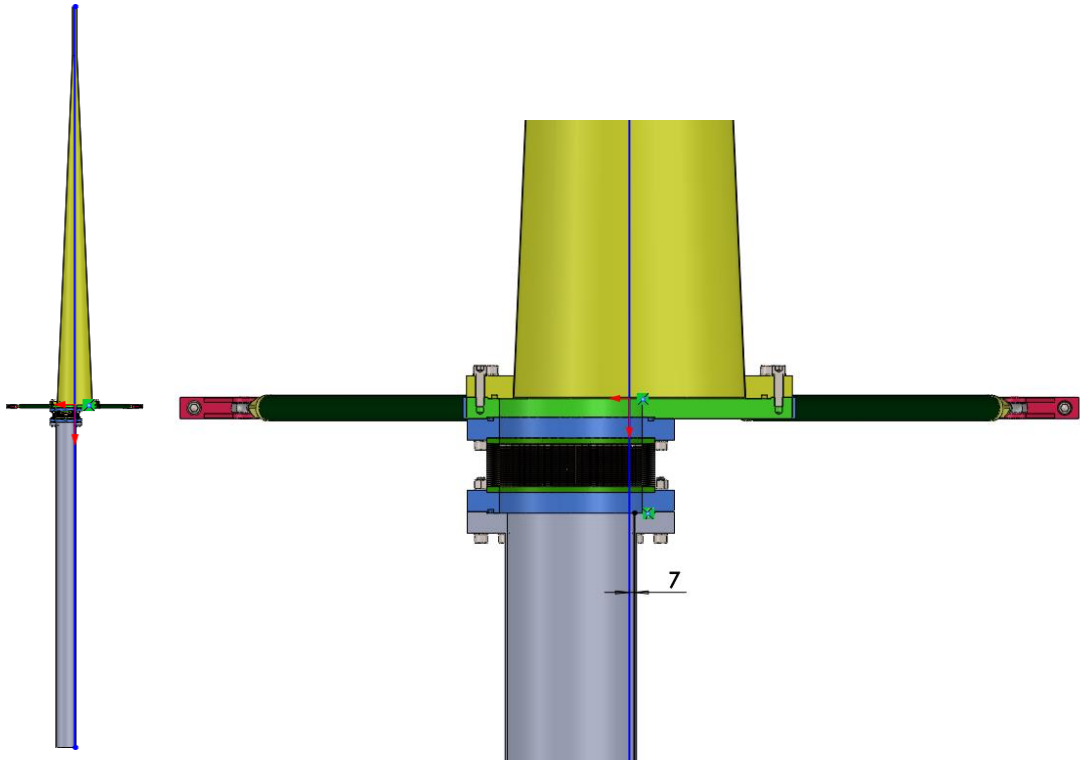


Fig. 52: Scheme of ion beam in 0° position with eccentric bellow

The distance between the centre of the ion beam and the inner surface of the beam pipe is 7,6 mm within the maximal deflected position of $2,5^\circ$. The figure below captures such an extreme case.

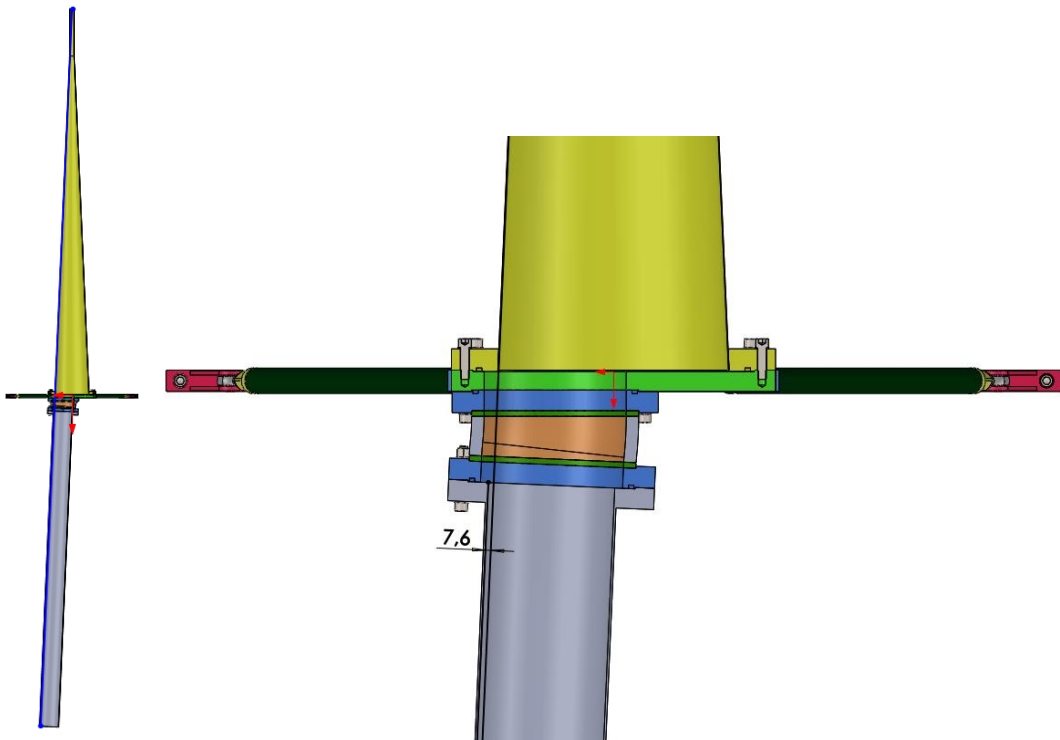


Fig. 53: Scheme of ion beam in extreme $2,5^\circ$ position with eccentric bellow

4. Design of the drive for the tilting mechanism

Actually, there occurred three attitudes of the drive design and of its kinematic mechanism. One passive solution for the bellow bending or tilting the spheric plate assembly had been considered as well, but such a way has been left because of the big deformations of the beam pipe as further described.

4.1. Handle drive (wheel)

The following system is based on the handle-operated wheel with a kinematic mechanism, that in total transforms the rotational movement of the wheel and a leadscrew into translational motion of a cuboid due to two parallel pins. The mounting of the holes for these pins are manufactured with a small clearance to enable sliding of the pins in their axial direction. The axial sliding is caused by the limited movement of the pins in their axial direction. The axial sliding is caused by the limited movement of the cube, which is set by the arc-shape of the groove in the tilting assembly above. The cut through the cube is further described in the following chapter because the electric drive handles with the same mechanism.

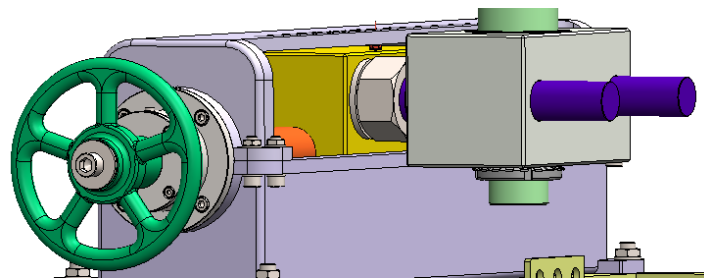


Fig. 54: Kinematic mechanism with handle-operated wheel

When focusing on the trapezoidal leadscrew, there is visible the way of its mounting within the housing in the cut view in the figure bellow. Such a mechanical mounting system with a pair of radial ball bearings [70] and a pair of axial double-row thrust ball bearings [71] represents a static indefinite system, which is commonly used for this purpose considering the movement of the lead-nut in both directions in the same speed. The mentioned lead nut holds the both sliding pins and prevent them from unwanted rotation due to the tongue and groove connection.

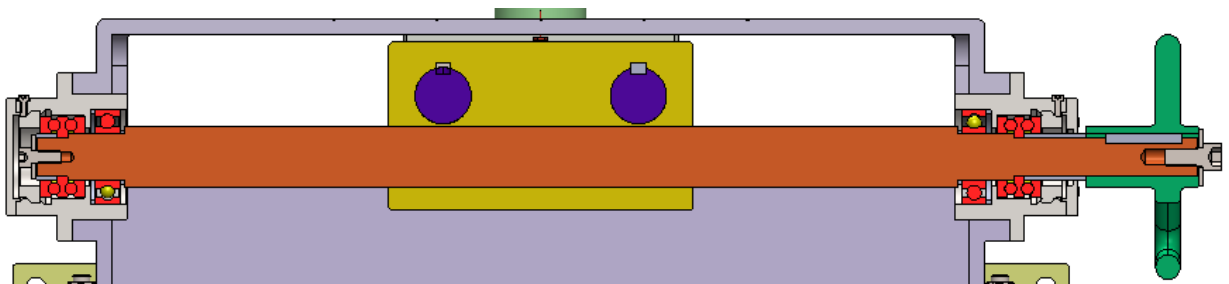


Fig. 55: Cut view through leadscrew assembly

4.2. Electric drive

The electric drive transforms the supplied electric energy into the mechanical energy in the form of a torque occurring on the output shaft. There are a few possibilities, how to design electric powered drive with a kinematic mechanism for tilting the bellow and the pipe as well in synchronous movement with the drive of PSD detector.

The first design counts with a servo engine with an implemented helical-worm gear unit. The transmission is connected to the trapezoidal leadscrew, of which nut moves with two parallel pins leading through holes in a cuboid as above described. The centre of this block is provided with holes for placement of a pair of tapered roller bearings in "O" composition. [72] These bearings ensure the rotational motion of the vertical shaft towards the shifting cuboid. Such a combination of translational as well as rotational movements provide the required displacement of the tilting mechanism e.g. with the spheric workpieces but it could serve for the tilting bellows weldment as well.

The longitudinal cut through the leadscrew looks like the same as in the previous chapter. The drive has been selected from the catalogue of the SEW Eurodrive company. The design includes a helical-worm servo gearmotor. [73]

Moreover, a scale indicating the angle of displacement has been designed on the top plate of the cast housing. The indicator is a pin screwed into the lead-nut.

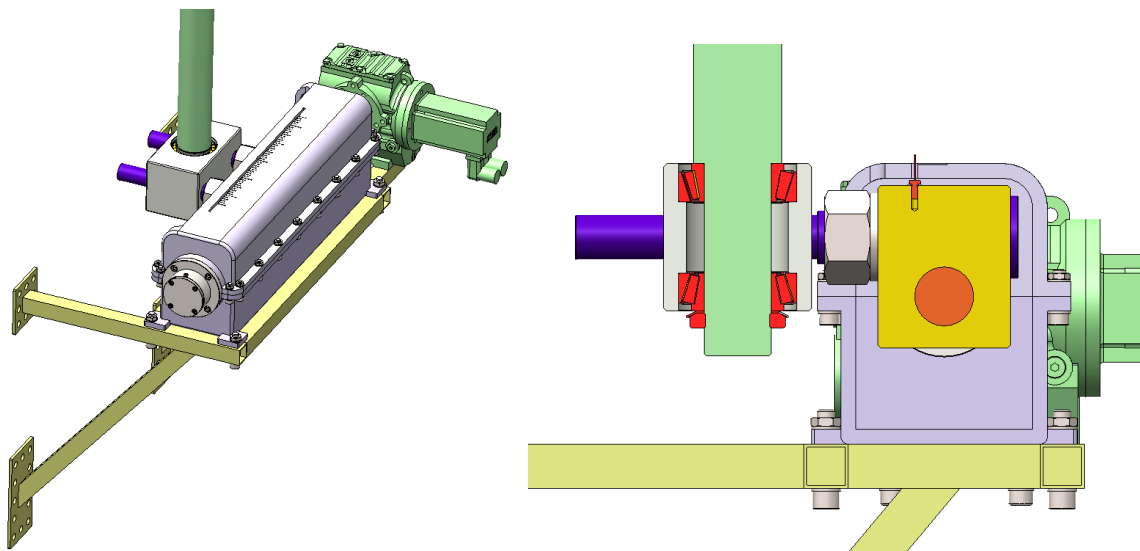


Fig. 56: Helical-worm servo gearmotor with kinematic mechanism

Above presented solutions serve just as a general design without any performance or safety calculations. With the necessity to develop the kinematic mechanism powered with a small engine unit for the bellow weldment bending has

been designed and calculated the following system with leadscrew and a stepping engine.

The position of the PSD detector ranges between 8 meters and 15 meters downstream the target. The speed of lead-nut translation is approximately 3 mm/s. The position of the leadscrew (LS) of the bellows kinematic mechanism is 4 416 mm.

$$\operatorname{tg} 2,5^{\circ} = \frac{S_{PSD}}{15\,000} \quad (6)$$

$$S_{PSD} = \operatorname{tg} 2,5^{\circ} \cdot 15\,000 \quad (7)$$

$$S_{PSD} = 654,9 \text{ mm} \quad (8)$$

$$\operatorname{tg} 2,5^{\circ} = \frac{S_{LS}}{4\,416} \quad (9)$$

$$S_{LS} = \operatorname{tg} 2,5^{\circ} \cdot 4\,416 \quad (10)$$

$$S_{LS} = 192,8 \text{ mm} \quad (11)$$

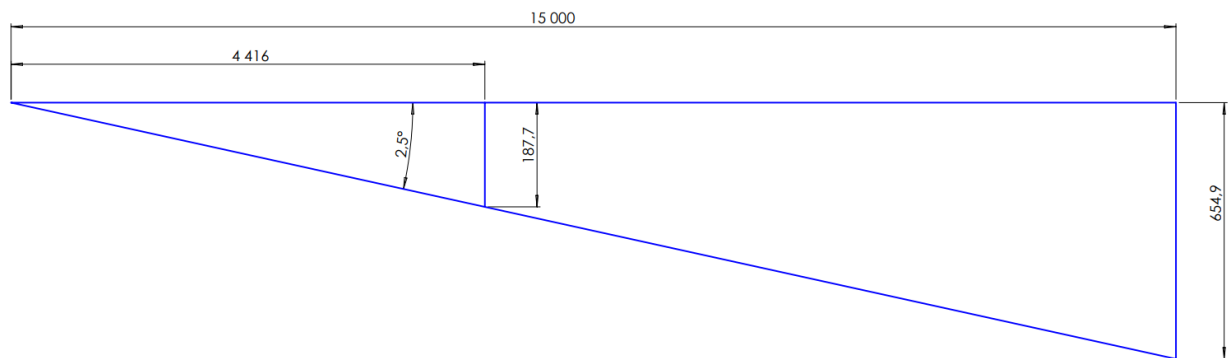


Fig. 57: Scheme of the synchronous movement of the bellows kinematic mechanism and the PSD detector

The synchronous movement of the both the bellows leadscrew and the PSD detector must fulfil the equality of the time for the tilting by certain angle, in this case it is $2,5^{\circ}$, which is the extreme position:

$$t_{LS} = t_{PSD} \quad (12)$$

$$\frac{S_{LS}}{v_{LS}} = \frac{S_{PSD}}{v_{PSD}} \quad (13)$$

$$v_{LS} = \frac{S_{LS} \cdot v_{PSD}}{S_{PSD}} \quad (14)$$

$$v_{LS} = \frac{192,8 \cdot 3}{654,9} \quad (15)$$

$$v_{LS} = 0,883 \text{ mm/s} \quad (16)$$

So, the translational velocity of the bellow lead-nut is $v_{LS} = 0,883 \text{ mm}$. Further will be calculated the torque needed for bellows bending. It was consulted with the

Mewasa company and the lateral reaction force might be $Q = 3\,500\text{ N}$ as the response to the pressure difference and bellows deformation, which causes the reaction according to the value of its spring rate. The value of the reaction force is related to the double bellows weldment with the middle tube NS-335/360.

The engine performance will be submitted to the analytical strength analysis of the slender strut load of the leadscrew. The scheme below depicts the dimensions of the leadscrew as well as the lead-nut. The maximal operating screw length is be $L = 514\text{ mm}$. The number of thread starts is $i = 1\text{ mm}$.

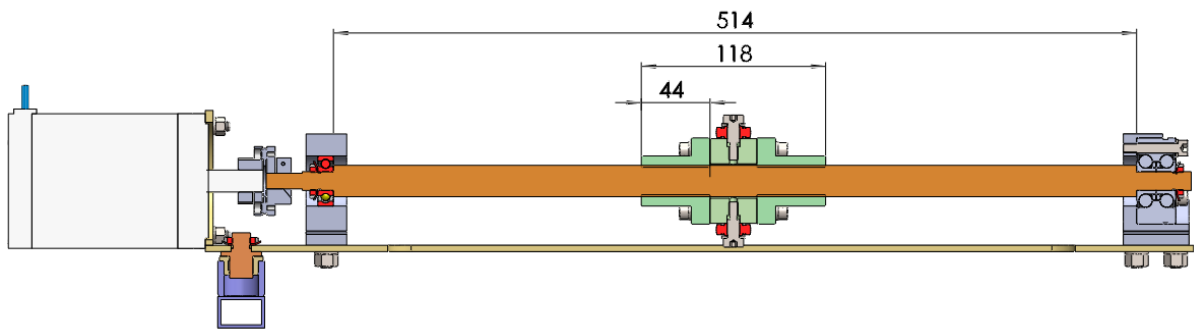


Fig. 58: Scheme of kinematic assembly with leadscrew

First of all, the preliminary middle diameter of the lead screw d_2' will be calculated on the basis of the maximal allowed stress in the threads. The mean pressure p in the threads is expected to be either equal or smaller than the allowed stress value $p_D = 7\text{ MPa}$, which is the value set by the contact of steel materials of the screw and nut threads. The coefficient of the screw height is $\Psi_H = 0,5$ for a trapezoidal screw. The coefficient of the nut height might range $\Psi_h = 1,5 - 2,5$. I choose $\Psi_h = 0,5$. [74]

$$p = \frac{Q}{\pi \cdot z \cdot d_2 \cdot H_1} \leq p_D \quad (17)$$

$$d_2' = \sqrt{\frac{Q}{\pi \cdot \Psi_H \cdot \Psi_h \cdot p_D}} \quad (18)$$

$$d_2' = \sqrt{\frac{3\,500}{\pi \cdot 0,5 \cdot 1,5 \cdot 7}} \quad (19)$$

$$d_2' = 14,57\text{ mm} \quad (20)$$

According to the Bornemann catalogue [75], I choose the pitch diameter for the first array of standardised screw dimensions:

$$d_2 = 18\text{ mm} \quad (21)$$

And the nominal diameter is $d = 20 \text{ mm}$ with the pitch $P = 4 \text{ mm}$. [75] The area of the core cross-section is $S_3 = 189 \text{ mm}^2$. The operating height is $H_1 = 2 \text{ mm}$. [74] The other parameters are presented in the Bornemann catalogue. [75]

The reason, why I missed the second array of screws is the fact, that many additional components are offered mostly for the first array of trapezoidal screws by its producers. Furthermore, there are calculated other thread parameters below.

The angle of the thread lead γ :

$$\operatorname{tg} \gamma = \frac{i \cdot P}{\pi \cdot d_2} = \frac{1 \cdot 4}{\pi \cdot 18} = 0,071 \rightarrow \gamma = 4,046^\circ \quad (22)$$

The angle of the thread side β_n :

$$\operatorname{tg} \beta_n = \operatorname{tg} \beta \cdot \cos \gamma \quad (23)$$

$$\operatorname{tg} \beta_n = \operatorname{tg} 15^\circ \cdot \cos 4,046^\circ \quad (24)$$

$$\operatorname{tg} \beta_n = 0,267 \rightarrow \beta_n = 14,963^\circ \quad (25)$$

Friction angle of the thread ϕ' :

$$\operatorname{tg} \phi' = f' = \frac{f}{\cos \beta_n} = \frac{0,13}{\cos 14,963^\circ} = 0,135 \rightarrow \phi' = 7,664^\circ \quad (26)$$

The minimal height of the lead-nut h :

$$h = \psi_h \cdot d_2 = 1,5 \cdot 18 = 27 \text{ mm} \quad (27)$$

I choose according to the Matis catalogue the nut length of 44 mm. [76] The second flange nut has got grooves instead of holes and it does not follow the catalogue standards, it has been just inspired in dimensions of the first flange nut.

The number of threads:

$$z = \frac{h}{P} = \frac{88}{4} = 22 \quad (28)$$

On the basis of high number of threads, further will be used the number of active threads $z = 8$.

The strength control of the active threads:

$$p = \frac{Q}{z \cdot \pi \cdot d_2 \cdot H_1} \leq p_D \quad (29)$$

$$p = \frac{3\,500}{8 \cdot \pi \cdot 18 \cdot 2} \leq 7 \text{ MPa} \quad (30)$$

$$p = 3,868 \text{ MPa} \leq 7 \text{ MPa} \quad (31)$$

The requirement is fulfilled.

The stress in the screw core caused by axial load:

$$\sigma_d = \frac{Q}{S_3} = \frac{Q}{\frac{\pi \cdot d_3^2}{4}} \quad (32)$$

$$\sigma_d = \frac{3\,500}{\frac{\pi \cdot 15,5^2}{4}} = 18,519 \text{ N/mm}^2 \quad (33)$$

The torsion stress calculations:

Torque on the leadscrew:

$$M_K = Q \cdot \frac{d_2}{2} \cdot \text{tg}(\gamma + \phi) \quad (34)$$

$$M_K = 3\,500 \cdot \frac{18}{2} \cdot \text{tg}(4,046^\circ + 7,664^\circ) = 6\,529,031 \text{ Nmm} \quad (35)$$

Torsion stress:

$$\tau = \frac{M_K}{W_K} = \frac{M_K}{\frac{\pi \cdot d_3^3}{16}} \quad (36)$$

$$\tau = \frac{6\,529,031}{\frac{\pi \cdot 15,5^3}{16}} = 8,929 \text{ N/mm}^2 \quad (37)$$

Reduced stress (compressive + torsion): for τ_{max} hypothesis is $\alpha = 2$

$$\sigma_{RED} = \sqrt{\sigma_d^2 + \alpha^2 \cdot \tau^2} \quad (38)$$

$$\sigma_{RED} = \sqrt{18,519^2 + 4 \cdot 8,929^2} = 25,727 \text{ N/mm}^2 \quad (39)$$

Safety factor:

The material of the leadscrew is steel ČSN 12 050 (1.0503, C45) with the yield strength in compression $\sigma_{Kd} = 345 \text{ N/mm}^2$ [77]

$$k = \frac{\sigma_{Kd}}{\sigma_{RED}} \quad (40)$$

$$k = \frac{345}{25,727} = 13,41 \quad (41)$$

$$k_{min} = 1,75 \quad (42)$$

$$k > k_{min} \quad (43)$$

The requirement is fulfilled.

Evaluation of the slender strut:

The following table includes different types of strut mountings.

Indication	Strut mounting	Coef.(theor)	Coef.(pract)
A	Clamped - Clamped	0.50	0.65
B	Clamped - Hinged	0.70	0.80
C	Clamped - Guided	1.00	1.20
D	Hinged - Hinged	1.00	1.00
E	Clamped - Free end	2.00	2.10
F	Hinged - Guided	2.00	2.00

Tab: 3 Values of reduced (effective) length coefficients [78]

All of the indications of mounting types and modes of the strut deformation are depicted in the picture below.

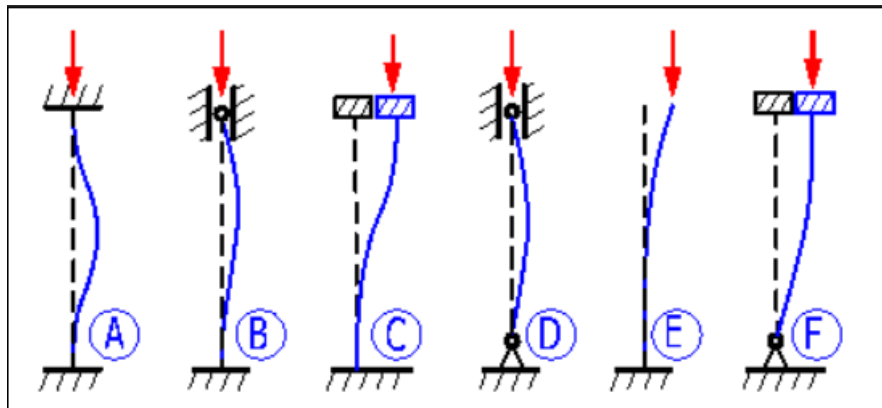


Fig. 59: Types of strut mounting [78]

In this case, it goes around the slenderness ratio for the „D“ mode of buckling

($\mu = 1$):

$$\lambda = \frac{l_V}{i_x} = \frac{\mu \cdot L}{\frac{d_3}{4}} \quad (44)$$

$$\lambda = \frac{1 \cdot 514}{\frac{15,5}{4}} = 132,645 \quad (45)$$

$$\lambda > 40 \quad (46)$$

If the slenderness ratio is bigger than 40, it is necessary to control the slender strut load. For steels of higher strength, the limit slenderness ratio is $\lambda_m = 90$. [74]

$$132,645 > 90 \quad (47)$$

$$\lambda > \lambda_m \quad (48)$$

If the slenderness ratio was lower than 90, the calculations would be made in Tetmajer's area. But the slenderness ratio is higher than 90, so there will be used the Euler's formulas. Further, the calculations will be related to the area of elastic slender strut according the Euler's formula: [74]

The critical stress according Euler σ_E :

$$\sigma_E = \frac{\pi^2 \cdot E}{\lambda^2} \quad (49)$$

$$\sigma_E = \frac{\pi^2 \cdot 2,06 \cdot 10^5}{132,645^2} = 115,554 \text{ N/mm}^2 \quad (50)$$

Safety coefficient for slender strut k_v :

$$k_v = \frac{\sigma_E}{\sigma_d} \quad (51)$$

$$k_v = \frac{115,554}{18,519} = 6,24 \quad (52)$$

The minimal safety coefficient might be $k_{vmin} = 3,5$. [74]

$$6,24 > 3,5 \quad (53)$$

$$k_v > k_{vmin} \quad (54)$$

The requirement is fulfilled.

The next step tackles some kinematic parameters.

Screw revolutions n_{LS} :

$$n_{LS} = \frac{v_{LS} \cdot 60}{i \cdot P} \quad (55)$$

$$n_{LS} = \frac{0,883 \cdot 60}{1 \cdot 4} = 13,245 \text{ min}^{-1} \quad (56)$$

Parameter of the leadscrew thread D :

$$D = \frac{v_1}{\omega_s} = \frac{i \cdot P \cdot n_s}{\frac{60}{\pi \cdot n_s}} = \frac{i \cdot P}{2\pi} \quad (57)$$

$$D = \frac{1 \cdot 4}{2\pi} = 0,637 \text{ mm} \cdot \text{rad}^{-1} \quad (58)$$

And last but not least, the energetical relations will be considered in order to get the final result, which could be the preliminary value of the minimal output torque of the engine.

Efficiency of the thread transmission of the leadscrew and lead-nut η_Z : [74]

$$\eta_Z = \frac{P_{sout}}{P_{sin}} = \frac{Q \cdot v_1}{M_K \cdot \omega_s} = \frac{Q \cdot v_1}{Q \cdot \frac{d_2}{2} \cdot \text{tg}(\gamma + \phi') \cdot \omega_s} = \frac{\text{tg}\gamma}{\text{tg}(\gamma + \phi')} \quad (59)$$

$$\eta_Z = \frac{\text{tg}(4,046^\circ)}{\text{tg}(4,046^\circ + 7,664^\circ)} = 0,341 \quad (60)$$

Efficiency of the threaded mechanism η_{Zm} : [74]

$$\eta_{Zm} = \eta_Z \cdot \eta_{lv} \quad (61)$$

$$\eta_{Zm} = 0,341 \cdot 0,97 = 0,331 \quad (62)$$

Efficiency of the shaft couplings is guessed up to $\eta_{co} = 0,96$. Total efficiency of the transmission mechanism η_C : [74]

$$\eta_C = \eta_{zm} \cdot \eta_{co} \quad (63)$$

$$\eta_C = 0,331 \cdot 0,96 = 0,318 = 31,8 \% \quad (64)$$

The output performance of the mechanism:

$$P_{out} = Q \cdot v_{LS} \quad (65)$$

$$P_{out} = 3\,500 \cdot 0,883 \cdot 10^{-3} = 3,091 \text{ W} \quad (66)$$

The minimal performance of the drive:

$$P_{min} = \frac{P_{out}}{\eta_C} \quad (67)$$

$$P_{min} = \frac{3,091}{0,318} = 9,725 \text{ W} \quad (68)$$

The revolutions of the drive:

$$n'_m = n_s \quad (69)$$

$$n'_m = 13,245 \text{ min}^{-1} \quad (70)$$

The minimal torsion torque of the drive:

$$Mk'_m = \frac{P_{min}}{\omega_M} = \frac{P_{min} \cdot 30}{\pi \cdot n'_m} \quad (71)$$

$$Mk'_m = \frac{9,725 \cdot 30}{\pi \cdot 13,245} = 7,011 \text{ Nm} \quad (72)$$

From the catalogue of the MBM Technik company was chosen the stepping engine of the type: ST8918L4508-A – NEMA 34 with the nominal operating torque 9,33 Nm. [79]



Fig. 60: Stepping engine ST8918L4508-A of the MBM Technik 79]

The transmission of the torque from the engine to the leadscrew will be ensured by the servo shaft couplings for the operating torque 10 Nm. It consists of two hubs, into which are inserted the mating shafts. The hubs serve as clamping joints, that are tightened after shaft insertion. In this case. The screws M4 are tightened by the torque of 3,4 Nm. [80]

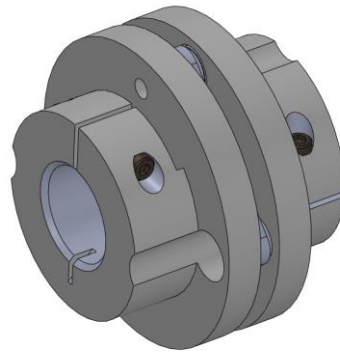


Fig. 61: ServoClass single Flex Couplings (Zero-Max) [80]

The figure below shows the final composition of the kinematic mechanism powered by the stepping engine. The rotation of the hole mechanism is performed due to the rotational mounting in the welded piece of tube on the frame profile under the support plate as depicted in the cut view above, where is situated a bronze bushing. This bushing located between the bearing housing and the engine provides a sliding mounting and enables to rotate the hole assembly with lead screw. [81]

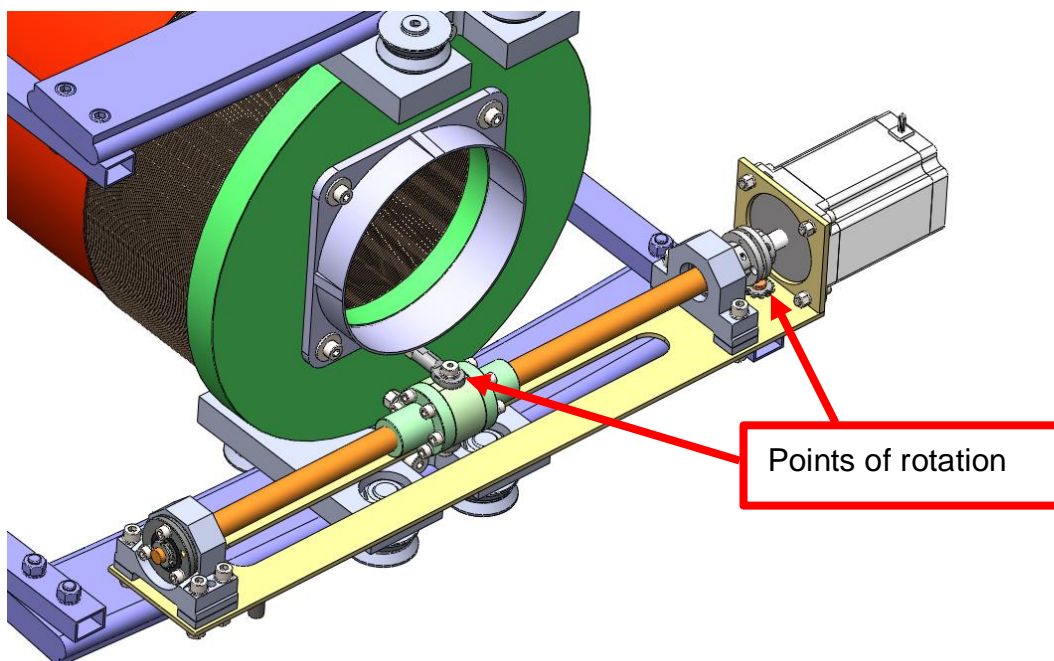


Fig. 62: Final composition of electric powered drive with leadscrew

The rotation between the lead nut and the end bellow flange is performed by a pair of rod ends with female thread and inserted plain bearing. [82]

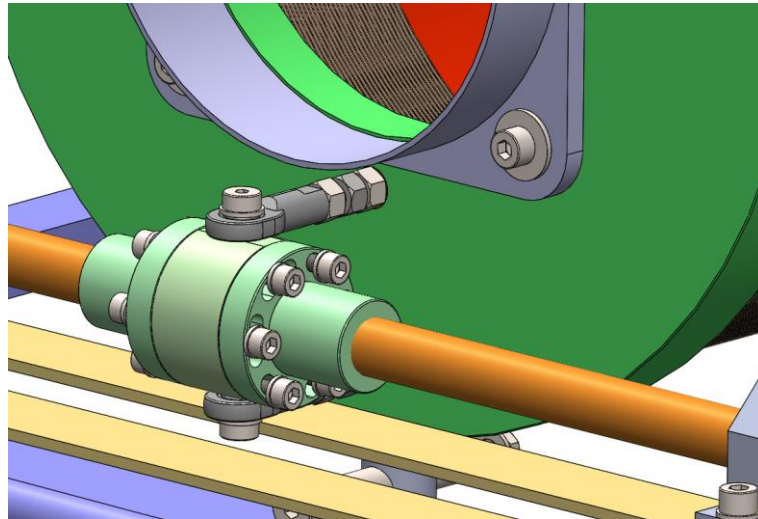


Fig. 63: Detail view of lead nuts

The picture above further shows the design of the grooves for fixing screws of the compensating nut, as described before. It contributes to disposal of the trapezoid thread clearance.

The figure 58 (Scheme of kinematic assembly with leadscrew) depicts also the mounting of the leadscrew. It consists of the radial ball bearing on the side of the engine and the opposite site is supported by the angular ball bearings, which can capture the radial as well as axial forces. The composition of this mounting follows the Matis catalogue design setup. [83]

4.3. Hydraulic cylinder

Another option, how to move with the tilting assembly, is represented by a double rod hydraulic cylinder. [84] Such a device transforms the hydraulic pressure energy into the mechanical energy. In this case, it goes around a linear movement, that could be performed in both directions at the same speed due to the adapted hydraulic circuit. The linear motion of the piston from the cylinder further transmitted within the kinematic mechanism, which is connected to the flange through a pin welded on the bottom of this flange and fixed in the hole of the vertical shaft placed in the centre of the kinematic cube.

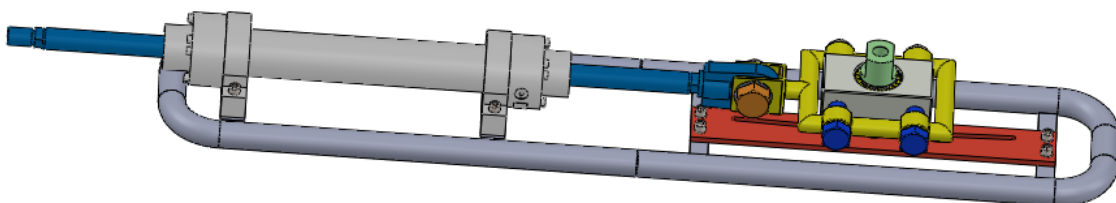


Fig. 64: Kinematic mechanism of tilting joint powered hydraulically

The cube is mounted by a pair of tapered roller bearings in “O” composition as shown in the figure below. [85]

The motion of the vertical shaft is limited by the arc-shape groove in the bottom plate fixed to the frame. The cube is provided with two parallel holes, in which can slide the pins, that connect the surrounding tube weldment of rectangular shape. The mounting of this hole is machined with a clearance to ensure smooth sliding of the pins.

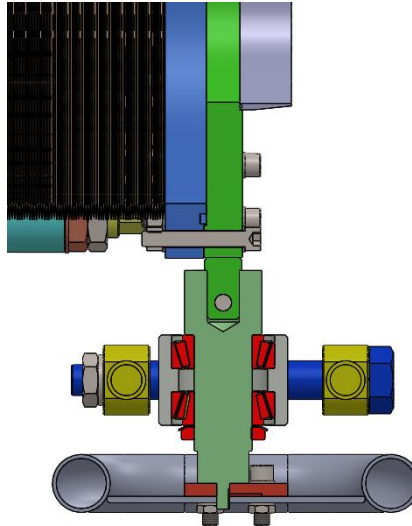


Fig. 65: Cut view of kinematic mechanism with hydraulic cylinder

The operation of the hydraulic engine (1) is maintained by attached hydraulic circuit. The schematic design is introduced in the picture below. The hydraulic fluid is pumped by a hydraulic pump (10) from an open container (8) through a suction filter (11) under pressure to the circuit. If the pressure of the fluid exceeds the limit value, the fluid is let off. It is controlled by the safety valve (7), which can draw the fluid off back to the container. In case that the switchboard (6) is found in its middle position, the flow to the cylinder is stopped and the fluid can escape through the right switch, which is controlled electromagnetically (12). The one-way valve (9) prevents from the reverse leakage of fluid from the circuit. If the switchboard (6) is set to its edge position either left or right, the one-way valve allows to pump the fluid to the hydraulic cylinder (1) through the opened hydraulic lock (5) and the branch with another one-way valve (3). Meantime, the fluid from the other chamber of the cylinder (1) on the opposite side of the piston (14) is pressed to the drain branch through the reducing valve (4). Of course, the fluid leakage is allowed in both directions, and so the left branch looks like the same as the right branch and both consist of one-way valve (3) and the reducing valve (4). The reducing valve can

regulate the flow, what impacts on the speed of the piston rod (2) movement. Taking into account the continuous type of the piston rod (2), the speed of the movement might be the same in both directions. So, the fluid escapes from the hydraulic engine (1) through opened hydraulic lock (5) and the drain branch of the circuit with a drain filter (13). When the movement of the piston (14) is stopped, the position of the switchboard (6) is set in its middle position again and the hydraulic lock (5) is automatically activated. [86]

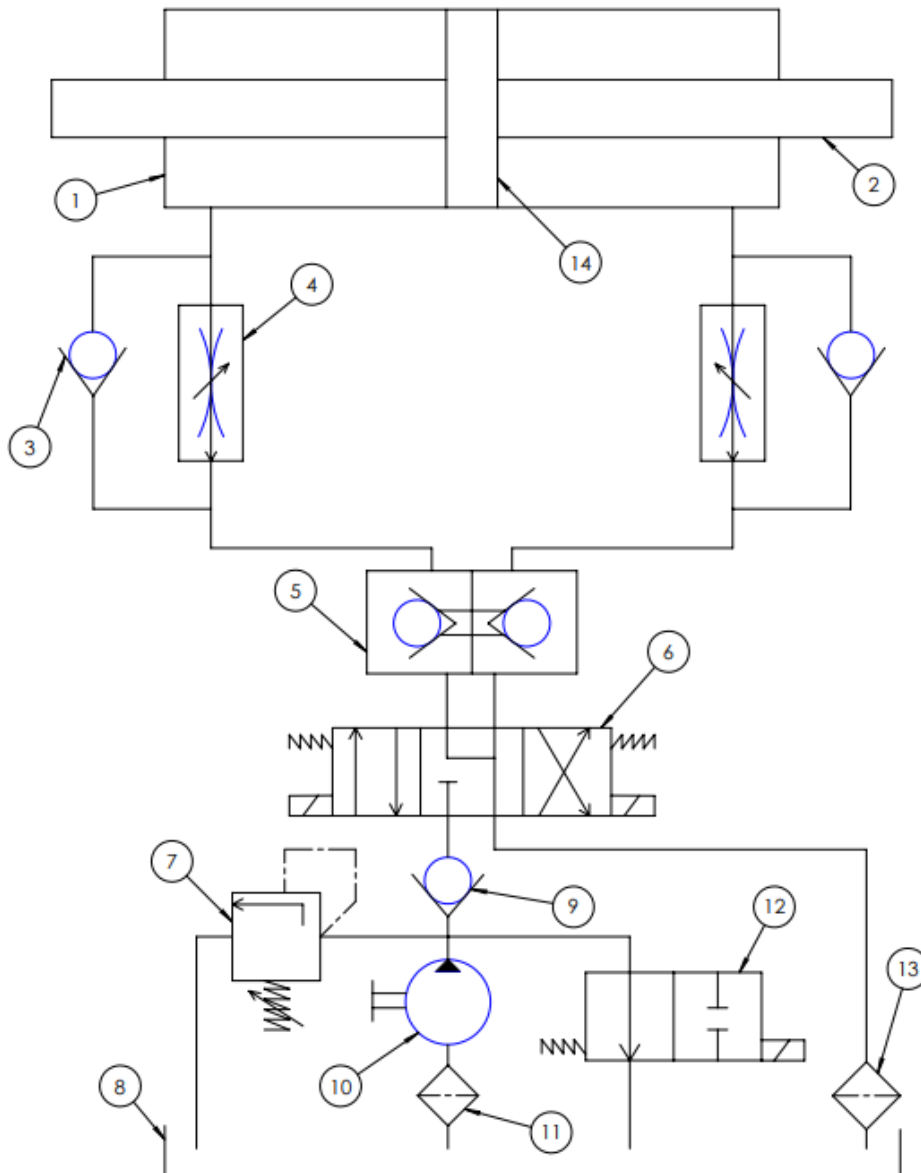


Fig. 66: Scheme of hydraulic circuit

4.4. Passive tilting of bellow joint

Within the technical development of the infrastructure of the CBM experiment had been considered the solution of passive bending of the bellow joint. The analysis was performed for the design with the bellow weldment, that consist of two

pieces of bellow and the middle tube, under atmosphere conditions. Such a solution deals with capturing axial reactions as well as reaction moment. It means, that the actuator in the PSD detector would move with the hole downstream beam pipe and, moreover, absorb the lateral reaction force of the bellow. In case of the atmosphere conditions, the reaction force is caused just by the spring rate of the bellow. Nevertheless, under the vacuum conditions the reaction force of the bellow evoked by the pressure difference must be added to the total value. The following table compares the solutions of the design of the tilting joint with the bellow 335/360 and the smaller bellow 200/235 with their lateral reaction forces. The data were discussed with the Mewasa company.

Type of bellow	Vacuum conditions	Atmosphere conditions
NS-335-360-0.20-1.4404-136	3 500 N	163 N
NS-200-235-0.20-1.4404-22	230 N	66 N

Tab: 4 The values of lateral forces of two solutions with bellow in Newton

The value of lateral reaction of 163 N for the bellow 335/360 had been found out from the FEM analysis of the bellow deformation without vacuum. The procedure is described in the chapter 7. The total reaction force of 3 500 N was calculated on the base reaction force from the spring rate, which is 163 N, and from the vacuum in lateral direction. To be sure, the total value has been finally enlarged. The angle of the bellow deflection is in this case approximately 18,5°. The lateral vacuum reaction force of the whole bellow weldment is 9 500 N. The lateral force might be corresponding to the axial force due to the tangent of 18,5°:

$$F = \operatorname{tg} 18,5^\circ \cdot F_{\text{vacuum}_{\text{axial}}} = \operatorname{tg} 18,5^\circ \cdot 9\,500 = 3\,179\text{ N} \quad (73)$$

In the case of the bellow 200/235 under atmosphere conditions is possible to calculate the reaction force based on the spring rate properties of the bellow analytically. The axial spring rate is $\text{SRCz} = 120\text{ N/mm}$. The number of convolutions is $\text{NC} = 22$. [87] The axial spring rate $\text{SRCz}(\text{one})$ for one convolution is:

$$\text{SRCz}(\text{one}_{\text{axial}}) = \frac{\text{SRCz}}{\text{NC}} = \frac{120}{22} = 5,5\text{ N/mm} \quad (74)$$

The lateral spring rate is by this type of bellow approximately three times bigger than the axial spring rate:

$$\text{SRCz}(\text{one}_{\text{lateral}}) = 3 \cdot \text{SRCz}(\text{one}_{\text{axial}}) = 3 \cdot 5,5 = 16,5\text{ N/mm} \quad (75)$$

The lateral displacement of the bellow 200/235 in its extreme position is 4 mm, which means that the force from spring rate lateral for this bellow is:

$$F_{spring_rate} = 4 \cdot SRCz(one_lateral) = 4 \cdot 16,5 = 66 \text{ N} \quad (76)$$

The lateral vacuum reaction force of the bellow 200/235 corresponds with the tangent of $2,5^\circ$, what is of the deflected angle of this small bellow, of the total axial vacuum reaction force of 3723 N.

$$F_{vacuum} = tg 2,5^\circ \cdot 3723 = 164 \text{ N} \quad (77)$$

So, the total lateral reaction force of the bellow 200/235 under vacuum conditions is:

$$F = F_{spring_rate} + F_{vacuum} = 66 + 164 = 230 \text{ N} \quad (78)$$

The FEM calculations of the carbon beam pipe deformations were made in terms of another diploma thesis (Martin Smetana: *Design of a Composite Beam Pipe for CBM experiment*) for the case of the bellow NS-335-360-0.20-1.4404-136 under the atmosphere conditions and the results have been unacceptable because of the huge beam pipe deformations. The discovery led to the decision to use a small separate actuator for bellow bending as described in the previous chapters, especially focusing on the solution with the stepping engine.

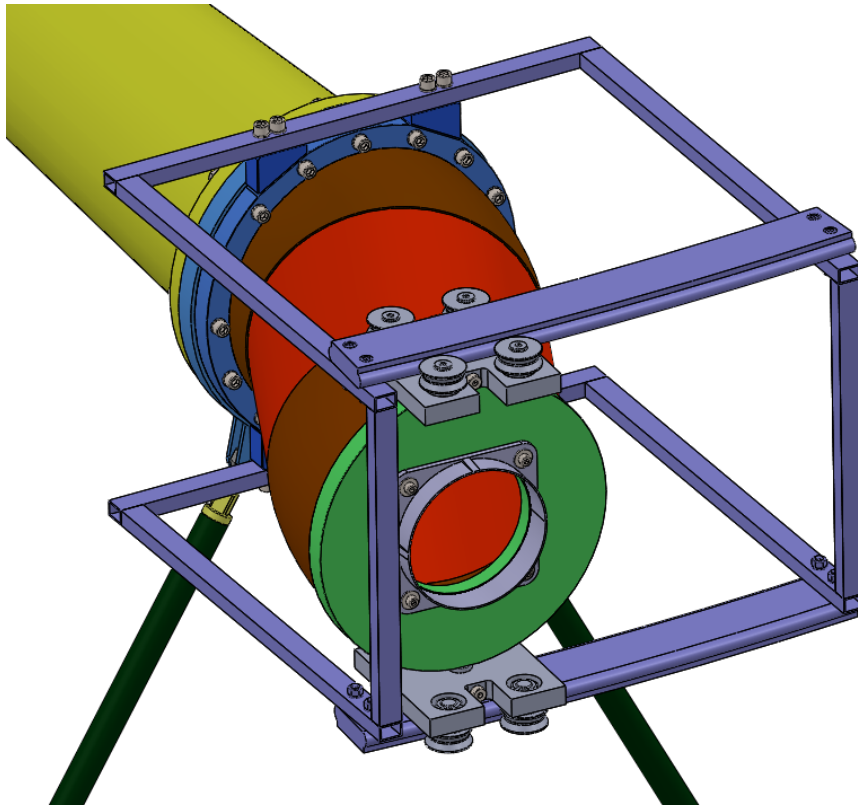


Fig. 67: Design of the passive bended bellow weldment

5. FEM analysis of bellows deformation

The tilting joint designed with the bellows weldment requires a geometrical description and shape simulation in its limit position. Realization of the bellow shape deformation is supposed to be performed in the RFEM static program.

The RFEM software serves for construction stability analysis via finite element method. It is possible to use it for civil as well as mechanical engineering. RFEM meets the task requirements, because the program can easily simulate huge non-linear displacements in relatively short time. [88]

The extreme position is characterised by the deflection of $2,5^\circ$ and by the combination of huge axial and lateral displacements of the upper flange. The general attributes of the bellow limit position are introduced in the chapter 3.3. “*Deflected bellows weldment assembly in extreme position*” (fig. 44).

The result of the simulation is expected to draw a deformed shape of the weldment with bellows in its specified extreme position.

First of all, the bellow weldment has been sketched. The model for the FEM analysis fits the real design of the bellow 335/360 in the chapter 3.1, which consists of two welded bellows with end flanges and intermediate tube. The shape of convolutions strongly influences the analysis results. Therefore, the splines have been drawn properly in order to describe the real shape as precise as possible. Some simplifications of the spline-shape led to the easier program processing, especially considering the neglect of the rounded weld seams between the edge-welded rings.

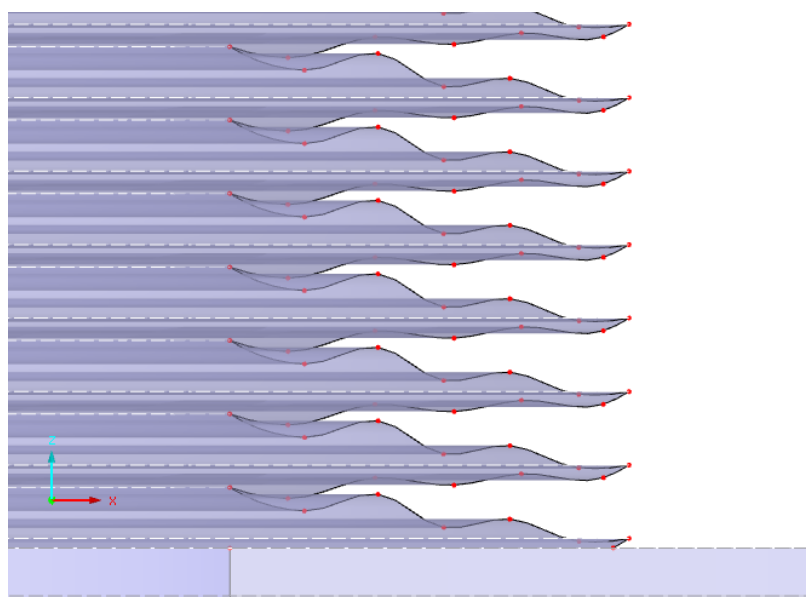


Fig. 68: Sketch of the bellow for FEM analysis

The flanges have been assigned with the standard material type for bodies and the 1.4404 material has been selected from the database for these endpieces. The boundary planes of the body are assigned with the zero type, which means that they have got no thickness and they just form the boundary elements for body inserting.

The convolutions are created from the pressed thin-wall rings, so the splines have been assigned with the standard type for planes of the thickness 0,2 mm and with the stainless material 1.4404. After forming the first convolution from the pair of rotational planes defined by the first and the second spline-shape curves, the other convolutions have been copied in a linear field.

The tube in the middle has been sketched in the same way as the flanges. Its boundary surfaces are formed by the zero type planes and the inner volume has been assigned with the standard type of body with the material 1.4404.

In the next step, the whole weldment has been meshed by the finite elements with the allowed shape of square and triangle. The length of these elements has been set on 10 mm. Smaller lengths have not been allowed by the program because of its number.

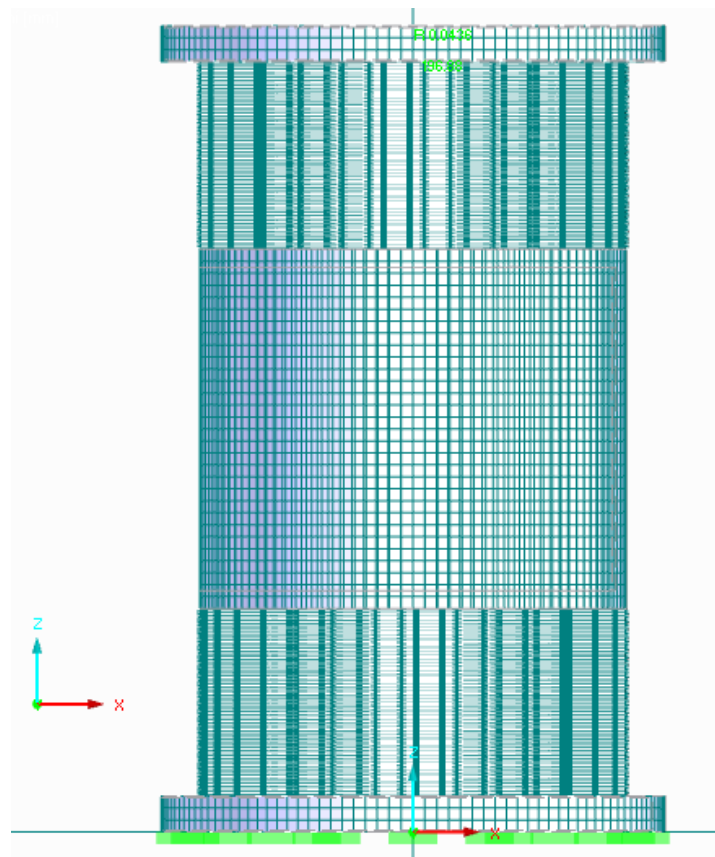


Fig. 69: Bellows weldment with the meshed elements

As shown in the picture above, the boundary conditions have been set for the bottom flange. The edges of the front site of the flange have been encastered, so that the movement of the bottom body is restricted in all directions.

The RFEM program is specific for the way of enforced displacements setting. The requirements for deflection determining are based on the direction restrictions. Such boundary conditions should limit the movement of the supported nodes or lines in the same directions as an intended displacement. In this case, the movement of the geometrical middle node of the front surface of the upper flange is restricted by the imaginary support in all „x, y, z“ axis in terms of the shift. The tilting motion of this node is ,restricted around the „y“ axis, because the intended displacement consists, except for the combination of lateral deflection of the value 187,13 mm („y“ axis) and axial compressive deflection of the value -56,58 mm („z“ axis), of the tilting motion of the upper flange, which reaches up to 2,5°. The motion of the reference node in the „x“ axis has been also restricted for any displacement in order to prevent the deflection from unwanted unsymmetric deformation.

The given deformation is represented by the red line in the picture below. Its origin is situated in the middle, supported reference node. The reference point lies on the intersection of the geometrical lines with absolute rigid properties (2 black dashed lines), that are connecting the reference node with the inner edge of the front surface of the upper flange.

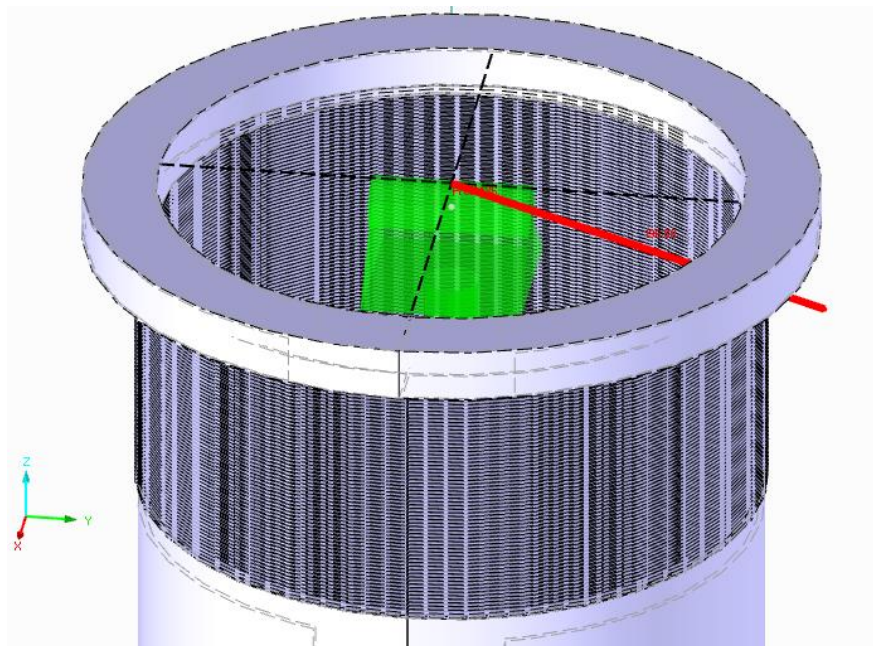


Fig. 70: Upper mounted reference point for enforced deformation

The analysis setting for the bellow weldment includes direct method for the equation system or the Mindlins theory for the plate bending, which take into consideration the sliding deformation influence. [89] The limit number of iterations has been set on 100. Another important parameter introduces the number of increments of the load per a load state. Its value of 10 meets the expectations of the smooth analysis procedure.

After the job submitting, the analysis took approximately 15 minutes under this program setting. The results are aimed at the stress distribution on surfaces and on bodies separately. The figures regarding the stress analysis are in the attachment 1. But the most important outcome of the analysis represents the deformed shape of the bellow weldment as well as the force reactions that are introduced below.

Going to the final shape of the bellow weldment after its deflection, we can compare both, the original state of the undeformed component and the geometrical shape after its deformation. According to the picture below, there is fairly well recognizable the combined axial, lateral and angular displacement.

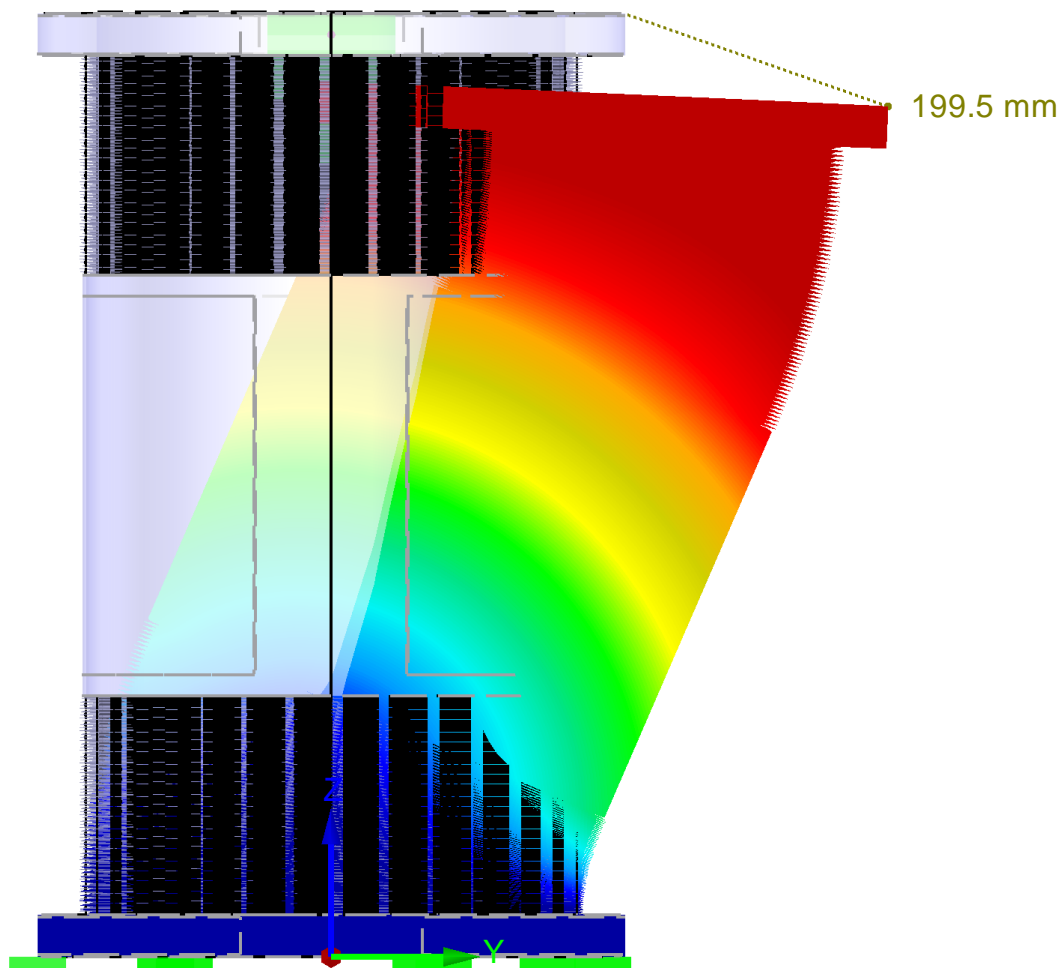


Fig. 71: Shape differences between undeformed and deformed bellow

The following figure depicts the deformed shape of the deflected bellow weldment apart from the starting position. This figure shows better drawn convolutions, which have been stretched on the one side and compressed on the other side of the upper or lower bellow. The intermediate steel tube helps to define the final shape of the bellows. The value chart informs about the total space displacement in millimetres.

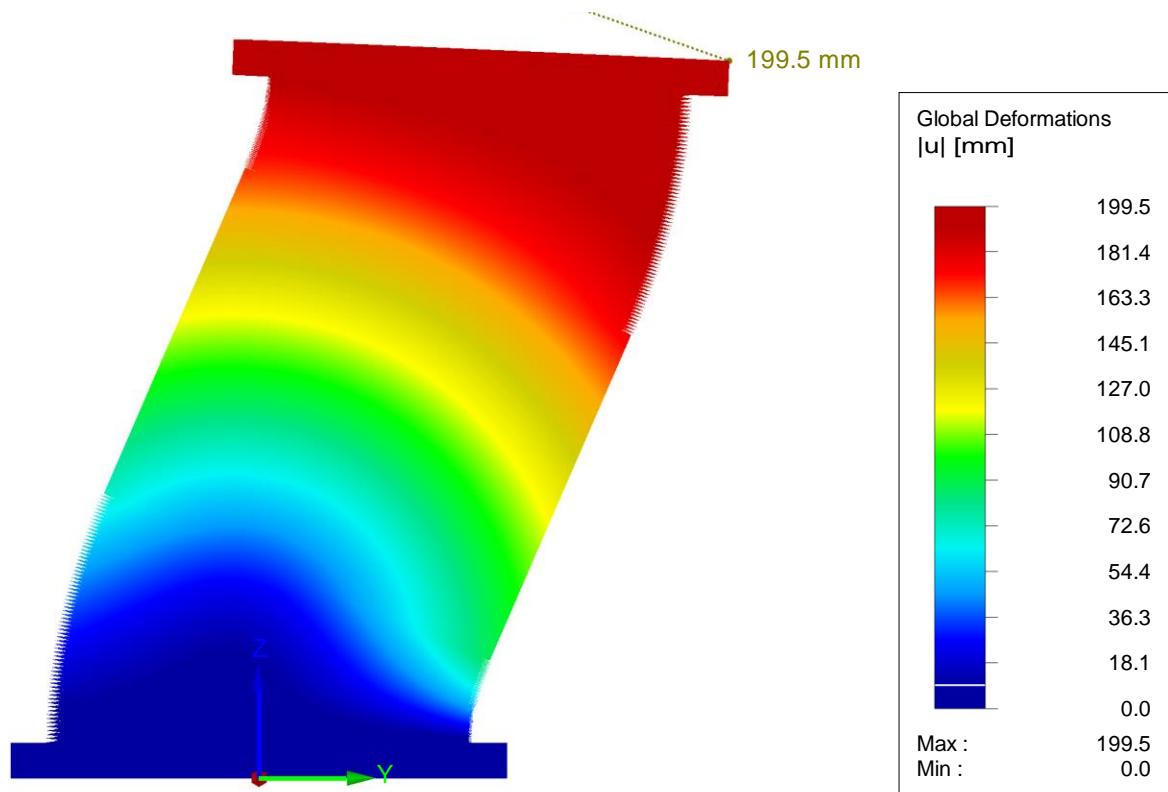


Fig. 72: Shape of bellow in its limit position

Because of the need to calculate the power of the kinematic mechanism or to solve the case of passive bending of the bellow it is necessary to know the force reactions of the bellows assembly caused by the spring rate in its limit position of 2,5°. The analysis took place under atmosphere conditions without any vacuum. The vacuum reaction forces were discussed with the producer of bellows the Mewasa company. So, the picture below captures the values of reactions in every direction at the end of the bellows weldment, where is the connection to the carbon-fibre beam pipe. The force 1,2 N is caused by the inaccuracy of the model in RFEM for the simulation. The lateral force of 163,4 N in “y” direction is expected to be absorbed by a kinematic mechanism a by passive tilting of the beam pipe. The axial force in “Z” direction may be absorbed by the bellows frame.

Support Reactions

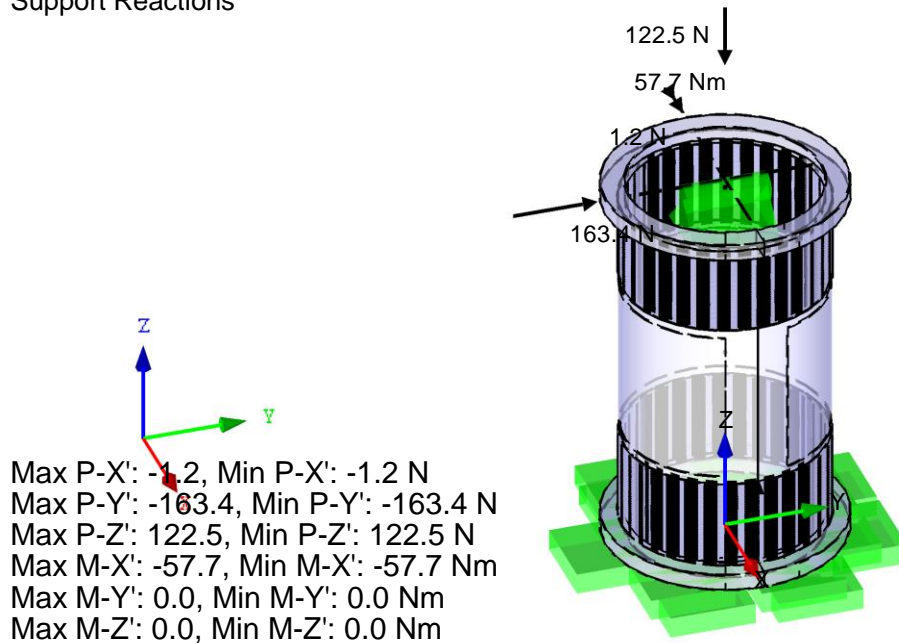


Fig. 73: Reaction forces of the bellow after its deflection by 2,5°

Furthermore, a smaller bellow weldment might be analysed via RFEM to get the results for a comparison with a real experimental bellow. Such an experiment is expected to prove the program setting for bellow analysis in RFEM software. The following chapter is dedicated to the design of the experiment with bellow.

6. Experiment with bellow

During the project an experiment for bellow testing have been designed. The aim of this experiment is to prove mechanical properties of a metal bellow. The experiment should serve for simulation of the bellow deformation in its required limit position and so the output will be the bellows shape after its deflection. Furthermore, there will be created an under-pressure inside of the assembly in order to check the vacuum connection and behaviour of all components under high vacuum.

All of the attachments related to this experiment are marked with the prefix as “EX” within the list of attachments.

6.1. Design of experiment

The construction model for the deformation experiment seems to be quite similar to the real concept of the design of the weldment with two bellows. Nevertheless, there occur several significant differences in its design. The first one is related to the bellows size, which is much smaller in all dimensions. The construction of the slender struts has been also simplified to ensure easier fabrication.

The choice of the bellow weldment was consulted with the Mewasa company and the types of NS-180-215-0.20-316L-26 on one side as well as NS-180-215-0.20-316L-23 on the other side with an intermediate tube of the length 150 mm and flanges welded to the bellow end ring endpieces have been selected in order to connect the bellow weldment to the blind flange on the left side and to the composite tube on the right side. The dimension of the bellow is corresponding to the composite tube 180x1-300. The composite assembly including the tube, vacuum connection and flanges will be produced by the Compotech company and the design is being solved in another diploma thesis (Martin Smetana: *Design of a Composite Beam Pipe for CBM experiment*). The composite assembly may be joined directly behind the bellow through the flanges.

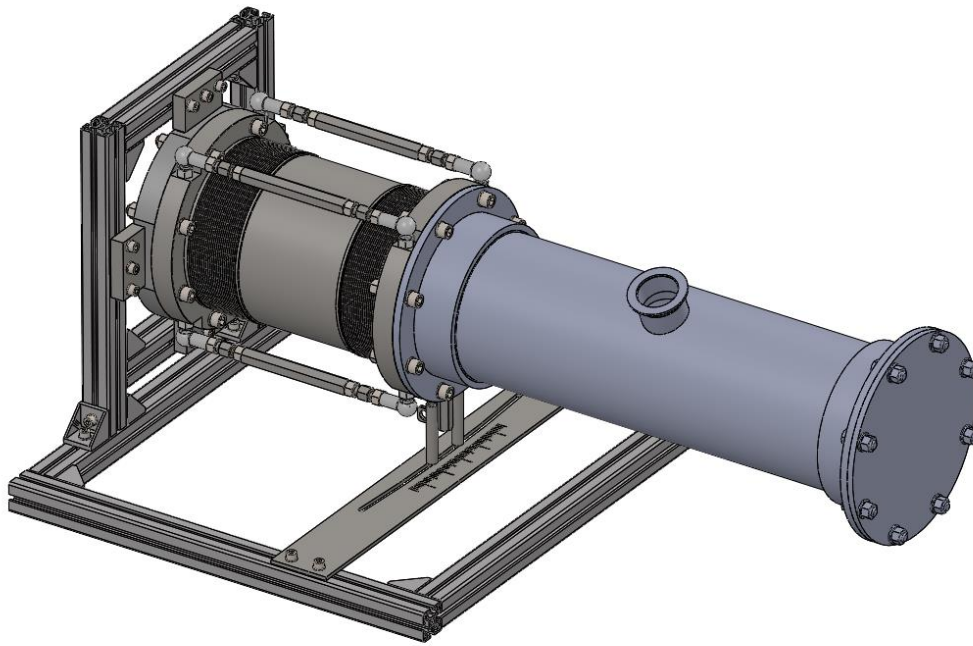


Fig. 74: Experiment with bellow - assembly design

The bellow assembly contains 4 hexagonal slender struts, that absorb the force reactions in the corner flanges of the weldment caused by the bellow deformation and vacuum forces. The slender struts are mounted through clamping bolts with right-handed thread on one side and with left-handed thread on the other side to the angled ball joints.

Stainless angled ball joints of the type DIN 71802-16-M12L-CSN supplied by the Elessa Ganter company in the number of 8 allow the position setting of the slender struts. [69]

Angled ball joints are mounted to the bellow flanges through thread connections after the deflection of the assembly and the tightened slender struts can assure the properly fixed position of the assembly.

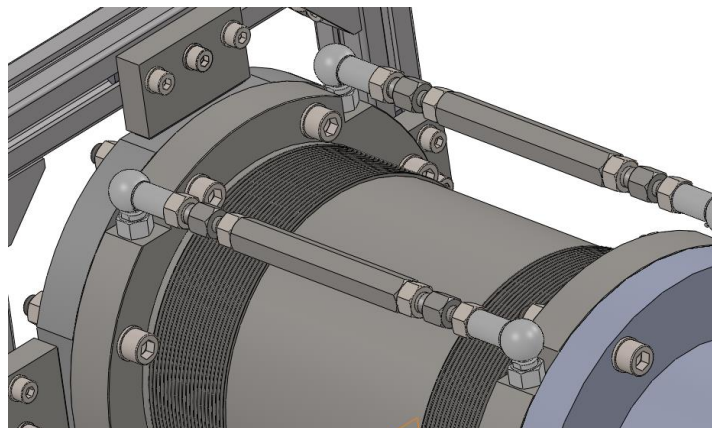


Fig. 75: Slender struts for bellow

The weldment of the left blind flange (Attachment 23) contains a milled round shape part with drilled threaded holes and 4 blocks with holes for screws to fix the assembly to the frame.

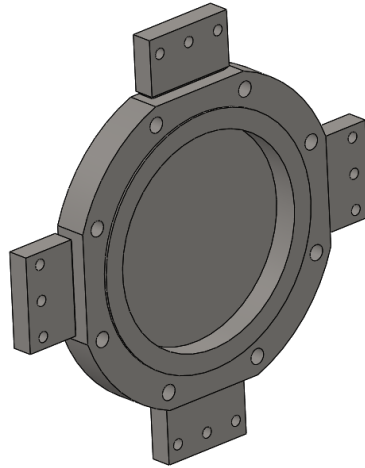


Fig. 76: Weldment of left blind flange

The inside space might be sealed to preserve a vacuum, therefore has been chosen O-ring sealing, which is mounted on both flanges of the bellow weldment. There are the same O-rings on both sides placed in milled sealing grooves. According to the DIMER catalogue has been selected the O-ring OK FPM 90 192x7 made from viton material. [58]

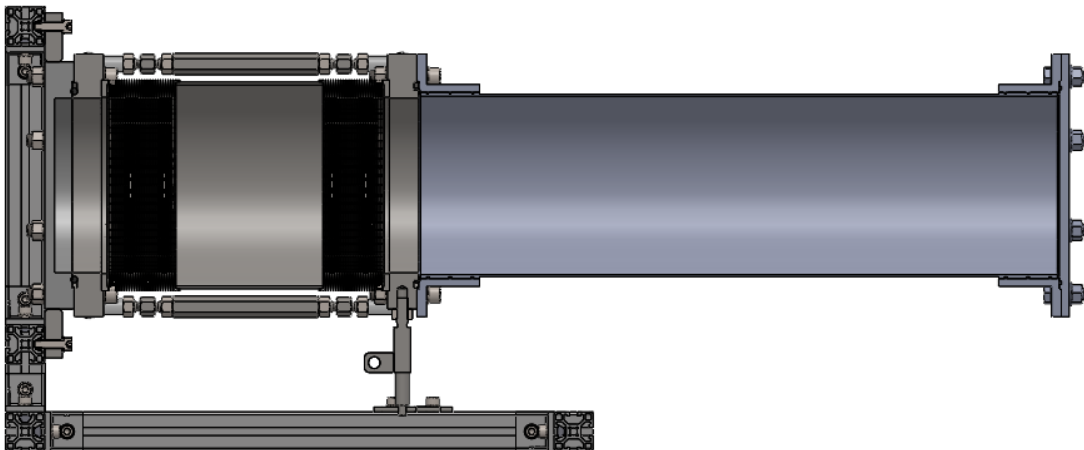


Fig. 77: Longitudinal cut view of the experimental assembly

There are drilled 3 threaded holes on the bottom side of the right flange of the bellow weldment. The middle one is intended for connection of a welded element that includes a hole for a string, which transmit tensile force of the hydraulic cylinder. The other 2 threaded holes serve for the fixation of a pair of round bars, that determine the track of bellow deflection through the arc groove in the bottom plate

mounted to the frame. The bottom plate with an angular scale is manufactured by laser cutting technology. [90]

Frame will be assembled from the aluminium structural system of the company Alutec kk involving specific profiles enabling screw mounting due to adapted nuts. The profiles are fixed with polytopes together [67]

6.2. Bellow struts

Bellow slender struts should be fabricated from hexagonal semi-manufactured product of the stainless steel material 1.4301, which is commonly spread and available for example by the Matezex distribution company [68] It is convenient for the processing, because the semi-product must be just cut into the required length on a band-saw and right-hand threaded holes might be drilled on both front sides of the bar on a lathe.

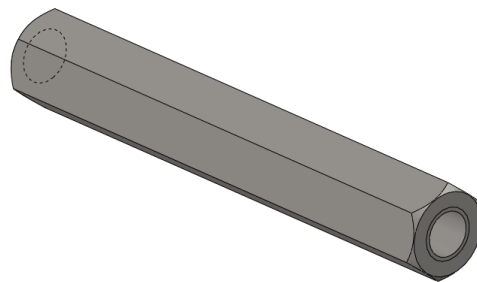


Fig. 78: Hexagonal slender strut of bellow

6.2.1. Analytical calculations

It is necessary to set characteristic dimension of the slender struts on the basis of strength calculation and stability analysis.

Material characteristics of stainless steel and the geometrical attributes of the struts are presented in the following table: [91] [92]

quantity	sign	value	unit
Poison's ratio	P	0,27	-
Young's modulus	E	200	MPa
Elastic limit	σ_u	190	MPa
Yield strength	σ_k	205	MPa
Compressive strength	σ_{pd}	210	MPa
Tensile strength	σ_t	510	MPa

Tab: 5 Material characteristics of 1.4301

The value of the compressive axial vacuum force $F = 9\,500\text{ kN}$ was calculated and provided by the Mewasa company. This force directly effects the strut construction in the way of its spreading to all of the hexagonal bars. The possibility of an uneven force distribution should be taken into account and compensated by a higher safety factor $k = 2$.

The following calculations are related to the stress analysis of the slender struts. The single steps of the calculations are inspired by the study material (J. Řezníček: *Pružnost a pevnost II příklady*). [93]

First will be set the second moment of area J_y (area moment of inertia) of a regular hexagon with a characteristic dimension of „ a “:

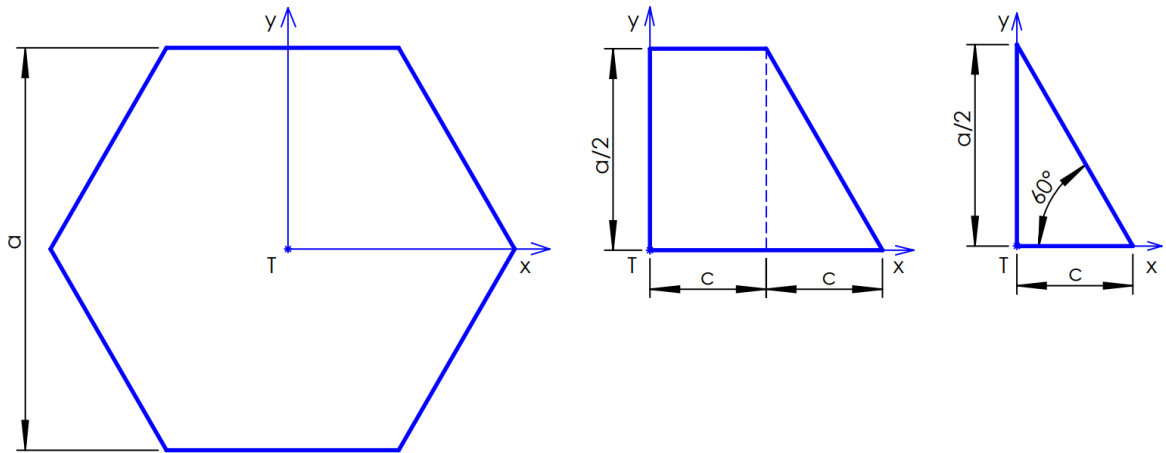


Fig. 79: Scheme of regular hexagon

The second moments of area are of the same value in both axis directions:

$$J_y = J_x \quad (79)$$

The definition of the second moment of area related to the „ y “ axis:

$$J_y = \iint_M x^2 dydx \quad (80)$$

Formulation of needed geometrical relations:

$$\operatorname{tg}30^\circ = \frac{c}{\frac{a}{2}} = \frac{\sqrt{3}}{3} \quad (81)$$

$$c = \frac{a \cdot \sqrt{3}}{6} \quad (82)$$

Formulation of „ y “ of the triangle hypotenuse line related to „ x “ axis:

$$\frac{\frac{a}{2}}{c} = \frac{y}{2c - x} \quad (83)$$

$$y = a - \frac{a \cdot x}{2c} \quad (84)$$

Substitution to the formula of the second moment of area:

$$J_y = 4 \cdot \left(\int_0^c \int_0^{\frac{a}{2}} x^2 dy dx + \int_c^{2c} \int_0^{a - \frac{a \cdot x}{2c}} x^2 dy dx \right) \quad (85)$$

$$J_y = 4 \cdot \left(\int_0^c x^2 \cdot [y]_0^{\frac{a}{2}} dx + \int_c^{2c} x^2 \cdot [y]_0^{a - \frac{a \cdot x}{2c}} dx \right) \quad (86)$$

$$J_y = 4 \cdot \left(\frac{a}{2} \cdot \int_0^c x^2 dx + \int_c^{2c} x^2 \cdot \left(a - \frac{a \cdot x}{2c} \right) dx \right) \quad (87)$$

$$J_y = 4 \cdot \left(\frac{a}{2} \cdot \left[\frac{x^3}{3} \right]_0^c + \left[\frac{a \cdot x^3}{3} - \frac{a \cdot x^4}{4 \cdot 2 \cdot c} \right]_c^{2c} \right) \quad (88)$$

$$J_y = 4 \cdot \left(\frac{a}{2} \cdot \frac{c^3}{3} + \frac{a \cdot 8 \cdot c^3}{3} - \frac{a \cdot 16 \cdot c^4}{4 \cdot 2 \cdot c} - \left(\frac{a \cdot c^3}{3} - \frac{a \cdot c^4}{4 \cdot 2 \cdot c} \right) \right) \quad (89)$$

$$J_y = 4 \cdot \left(\frac{ac^3}{6} + \frac{8ac^3}{3} - \frac{16ac^3}{8} - \frac{ac^3}{3} + \frac{ac^3}{8} \right) \quad (90)$$

$$J_y = 4 \cdot \left(\frac{ac^3}{6} + \frac{7ac^3}{3} - \frac{15ac^3}{8} \right) \quad (91)$$

$$J_y = \frac{15ac^3}{6} = \frac{15a \cdot 3\sqrt{3} \cdot a^3}{6 \cdot 216} \quad (92)$$

$$J_y = \frac{5\sqrt{3} \cdot a^4}{144} \quad (93)$$

Area of a hexagonal cross-section A:

$$A_{triangle} = \frac{a}{2} \cdot c = \frac{a}{2} \cdot \frac{a \cdot \sqrt{3}}{6} \quad (94)$$

$$A = 6 \cdot A_{triangle} = 6 \cdot \frac{a^2 \cdot \sqrt{3}}{12} \quad (95)$$

$$A = \frac{a^2 \cdot \sqrt{3}}{2} \quad (96)$$

Quadratic radius of the cross-section: i_{min}

$$J_y = J_z = J_{min} \quad (97)$$

$$i_{min} = \sqrt{\frac{J_{min}}{A}} = \sqrt{\frac{\frac{5\sqrt{3} \cdot a^4}{144}}{\frac{a^2 \cdot \sqrt{3}}{2}}} = \sqrt{\frac{5 \cdot a^2}{72}} = \frac{1}{6} \cdot \sqrt{\frac{5}{2}} \cdot a \quad (98)$$

$$i_{min} = \frac{\sqrt{10} \cdot a}{12} \quad (99)$$

Slenderness ratio of a bar:

$$\lambda = \frac{l}{i_{min}} \quad (100)$$

$$\lambda = \frac{400}{\frac{\sqrt{10} \cdot a}{12}} = \frac{480 \cdot \sqrt{10}}{a} \quad (101)$$

Furthermore, the limit slenderness ratio λ_{lim} for any mode of strut mounting will be expressed through the critical slender strut force:

$$F_{kr} = n \cdot \frac{\pi^2 \cdot E \cdot J_{min}}{l^2} \quad (102)$$

$$\sigma_{kr} = \frac{F_{kr}}{A} = \mu \cdot \frac{\pi^2 \cdot E \cdot J_{min}}{l^2 \cdot A} \quad (103)$$

$$i_{min}^2 = \frac{J_{min}}{A} = \frac{l^2}{\lambda_{lim}^2} \quad (104)$$

$$\sigma_{kr} = \frac{F_{kr}}{A} = \mu \cdot \frac{\pi^2 \cdot E \cdot l^2}{l^2 \cdot \lambda_{lim}^2} \quad (105)$$

$$\sigma_{kr} = \frac{F_{kr}}{A} = \mu \cdot \frac{\pi^2 \cdot E}{\lambda_{lim}^2} \quad (106)$$

For guaranteed elastic behaviour of the material must be the critical inertial stress of the bar σ_{kr} smaller or equal then its elastic stress limit σ_u . For calculation of the limit slenderness ratio will be used the equation:

$$\sigma_{kr} = \sigma_u \quad (107)$$

$$\lambda_{lim} = \sqrt{\mu \cdot \frac{\pi^2 \cdot E}{\sigma_u}} \quad (108)$$

Where „ μ “ is the reduced length coefficient, which values are given in the table 3 in the chapter 4.2.

All of the indications of mounting types and modes of the strut deformation are depicted in the picture below.

Limit slenderness ratio for the „A“ mode of buckling ($\mu = 0,65$) according to the figure 59 in the chapter 4.2 set by the equation (108):

$$\lambda_{lim}^A = \sqrt{0,65 \cdot \frac{\pi^2 \cdot 2 \cdot 10^5}{190}} = 82.18 \quad (109)$$

1. Step – calculation of the characteristic dimension a of the hexagonal bar according to Euler's formula for the „A“ mode of buckling:

$$F_{kr}^{II} = \mu \cdot \frac{\pi^2 \cdot E \cdot J_{min}}{l^2} = k \cdot F \quad (110)$$

$$J_{min} = \frac{k \cdot F \cdot l^2}{\mu \cdot \pi^2 \cdot E} = \frac{5\sqrt{3} \cdot a_E^4}{144} \quad (111)$$

$$a_E = \sqrt[4]{\frac{144 \cdot k \cdot F \cdot l^2}{5\sqrt{3} \cdot \mu \cdot \pi^2 \cdot E}} \quad (112)$$

$$a_E = \sqrt[4]{\frac{144 \cdot 2 \cdot 2375 \cdot 150^2}{5\sqrt{3} \cdot 1 \cdot \pi^2 \cdot 2 \cdot 10^5}} \quad (113)$$

$$a_E = 6,1 \text{ mm} \quad (114)$$

2. Step – verifying of validity of the Euler's formula:

a) Primary check of applicability of Euler's formula according to stress:

$$\sigma_{kr1}^E = \frac{k \cdot F}{A_E} = \frac{k \cdot F}{\frac{a_E^2 \cdot \sqrt{3}}{2}} \quad (115)$$

$$\sigma_{kr1}^E = \frac{2 \cdot 2375}{\frac{6,1^2 \cdot \sqrt{3}}{2}} \quad (116)$$

$$\sigma_{kr1}^E = 147,38 \text{ N/mm}^2 \quad (117)$$

$$\sigma_{kr1}^E \leq \sigma_u \quad (118)$$

$$147,38 \text{ N/mm}^2 \leq 190 \text{ N/mm}^2 \quad (119)$$

b) Secondary check of applicability of Euler's formula according to the slenderness ratio:

$$\lambda_E = \frac{l}{i_{minE}} = \frac{190}{\frac{\sqrt{10} \cdot a_E}{12}} = \frac{480 \cdot \sqrt{10}}{a_E} \quad (120)$$

$$\lambda_E = \frac{480 \cdot \sqrt{10}}{12,65} \quad (121)$$

$$\lambda_E = 248,81 \quad (122)$$

$$\lambda_E \geq \lambda_{lim}^A \quad (123)$$

$$248,81 \geq 82,18 \quad (124)$$

The minimal dimension a is 6,1 mm. I have chosen 19 mm as the characteristic parameter 19 mm of the hexagonal strut for the experiment. According to the script in Matlab, the maximal permitted load on one slender strut was calculated. The maximal value of the load on the single slender strut is 16 kN with the total safety factor $k=4$. (attachment 2)

6.2.2. Finite element method

The slender strut has been checked via the finite element method in the Abaqus software. The analysis might give the information about the progress of

inner stress in the hexagonal bar caused by the compressive forces. The force, the material and geometry properties are of the same values as in the previous chapter.

First of all, several cutting planes has been defined in order to enable precious meshing. The cutting planes have divided the bar into symmetric sections. The threaded holes have been simplified and just simple holes have been drawn. It is possible to neglect thread, because the force transmission is realized via the contact of the front planes of the bar with the tightening nuts.

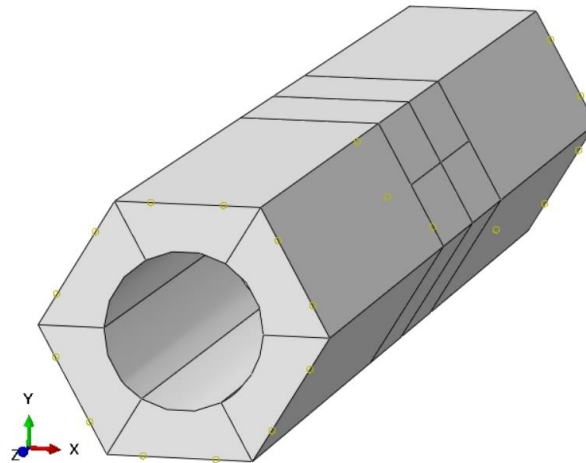


Fig. 80: Hexagonal bar divided into sections with cutting planes

After assigning material characteristics, the mesh was created. Each of the sections has been assigned with the standard elements from 3D stress family with a linear geometric order. The „hex“ element shape has been applied for the meshing operation.

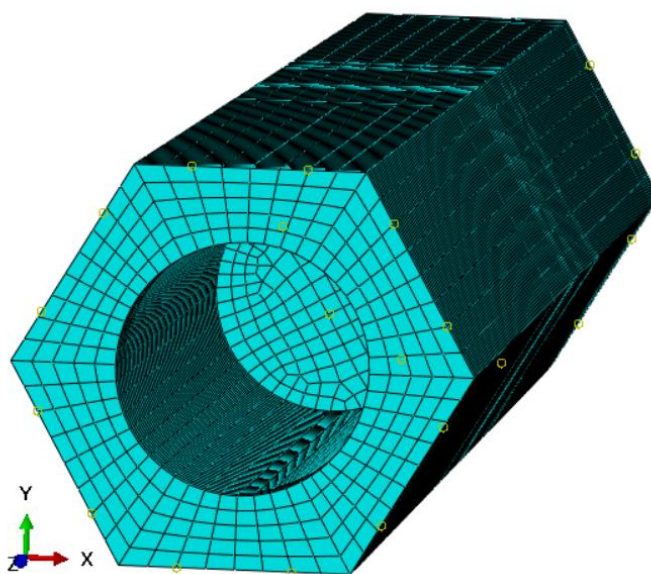


Fig. 81: Mesh of hexagonal strut

The one front plane has been encastered to fix the position and to define the boundary conditions. The other front side is represented by the reference point in the middle of the round cross-section of the hole, which is being referred to the front plane divided into 6 sections. This reference point has been appointed as the point of application of the load, in which operates the axial force specified above.

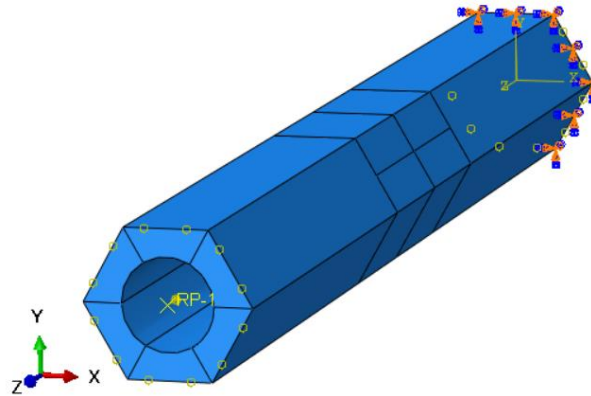


Fig. 82: Mounting and load simulation of slender strut

The results of the linear analysis are shown in the picture below. The common value of the inner compressive stress fluctuates around 10 MPa. The peak of the stress 15 MPa occurs in the area of the cross-section change, which is actually the bottom of the hole.

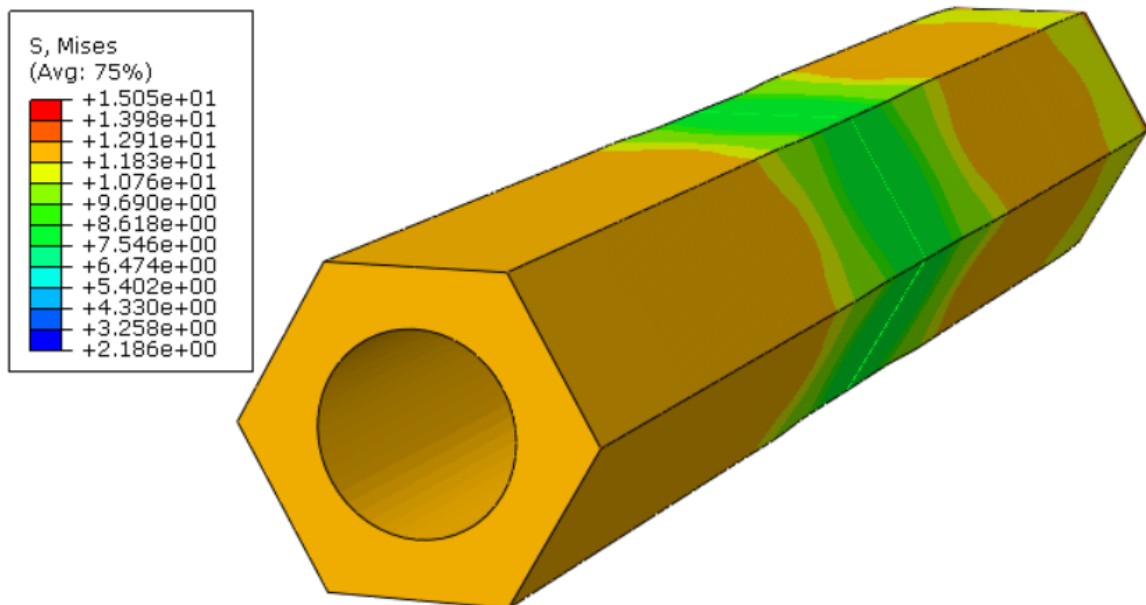


Fig. 83: FEM results of hexagonal strut for experiment assembly

The analysis results confirm the stability of the slender struts because the value of the elastic limit 190 MPa of the material 1.4301 in terms of inner stress is much higher than the evaluated peak 15 MPa.

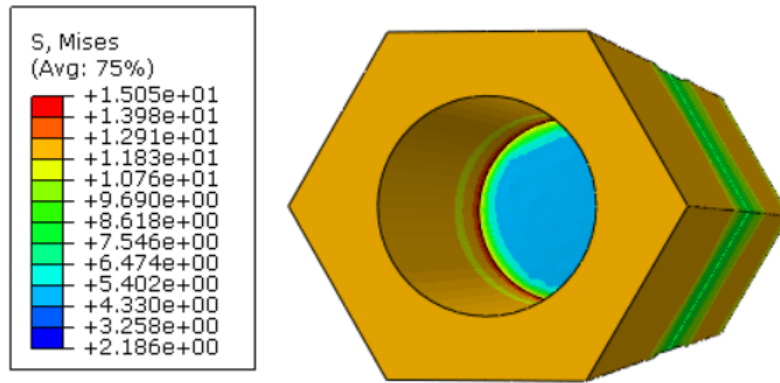


Fig. 84: FEM results of hexagonal struts with highlighted stress peaks

6.2.3. RFEM analysis

The real experimental bellow weldment can be compared with the RFEM simulation. The simulation setting and the sketch attributes are corresponding to the first bellow 335/360 upper described. This smaller bellow weldment 180/215 serves just for the confirmation of the functionality of the RFEM simulations. As the bellows behave non-linear and there are many factors influencing its mechanical properties, there are no characteristic numbers between the different types and sizes of metal bellows. The stress results are included in the attachment 1.

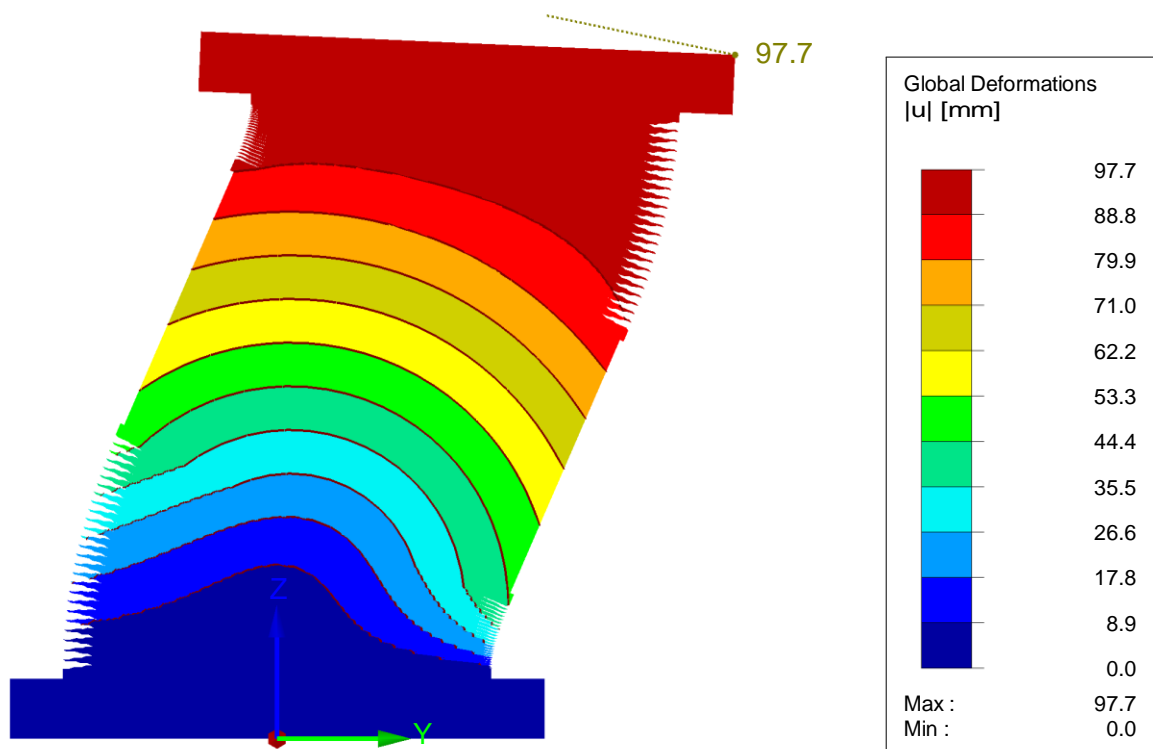


Fig. 85: Shape of experimental bellow in its limit position

7. Conclusion

The main goal of this diploma thesis was to provide a few mechanical concepts of the tilting joint for the infrastructure of the beam pipe within the CBM experiment. The secondary tasks have been fulfilled such as the recherche concerning the metal bellows, the simulation of deformed shape of the whole bellows weldment or the experiment with a similar bellows assembly for the verification of the software setting of such a finite element method analysis. The choice of a proper drive has been accomplished. The attached technical documentation was created with the help of some support materials for the rules of technical drawing. [94] [95] [96]

Due to the discussions with technical deputies of the GSI institute, the design could be developed to meet the experimental requirements as much as possible. Hopefully, the results of this thesis may contribute to the future development and fabrication of the tilting joint and the beam pipe constructure. The favourite solution seems to be represented by the stainless bellows weldment of 2 edge-welded bellows and an intermediate tube with the aluminium rolling system. The movement might be performed by the kinematic mechanism with a leadscrew powered by a stepping engine.

In the present time, the geometrical optimization of the tilting joint with the bellow setup is being solved. The design of the bellow weldment must be actualized after resolving the final geometrical conditions and this issue is necessary to consult with the producer of metal bellows the Mewasa company. Last but not least, the surrounding frame could be improved and transformed into the carbon-fibre composite material. After clarifying the material budget, the connecting end flanges might be finalized with regard to its manufacturing.

Furthermore, within the university research may be tested an experimental piece of bellow weldment. The experimental assembly should be adapted to the actual needs and design changes of the CBM experiment infrastructure. Eventually, the experiment could be performed on the final bellows weldment of the tilting joint in the real form. In fact, the size would exactly correspond with the applied design of the tilting joint to the infrastructure of the CBM experiment.

The future outlines and steps may lead through modifications to the final design of the tilting joint. Because of the persisting development of the CBM experiment, the design might be able to accept some dimensional changes as well as to adapt to the actual technical requirements.

LITERATURE

- [1] B. Friman, C. Höhne, J. Knoll, S. Leupold, J. Randrup, R. Rapp, P. Senger, and others: *The CBM Physics Book, Compressed Baryonic Matter in Laboratory Experiments*, 27. 1. 2011, Springer Verlag, ISBN 978-3-642-13293-3
- [2] L. Eidam, O. Boine-Frankenheim, and D.F.A. Winters, “*Simulation Studies on Intensity Limitations of Laser Cooling at High Energy*”, [online], 2016 cit. [23. 4. 2021], pdf, in Proc. Int. Workshop on Beam Cooling and Related Topics (COOL'15), Newport News, VA, USA, Sep. -, paper TUZAUD03, pp. 93-96, ISBN: 978-3-95450-174-8, doi:10.18429/JACoW-COOL2015-TUZAUD03, available on: <<https://spms.fnal.gov/pls/cool15/papers/tuzaud03>>
- [3] GSI Helmholtzzentrum für Schwerionenforschung GmbH: *Über uns* [online], 2021 cit. [23. 4. 2021], GSI website, available on: <https://www.gsi.de/ueber_uns>
- [4] A. Dolinskii, P. Beller, K. Beckert and others.: *Layout of the storage ring complex of the international accelerator facility for research with ions and antiprotons at GSI* [online], January 2004 cit. [24. 4. 2021], article, available on: <https://www.researchgate.net/publication/239600714_Layout_of_the_storage_ring_complex_of_the_international_accelerator_facility_for_research_with_ions_and_antiprotons_at_GSI>
- [5] FAIR: The PANDA Collaboration: *Technical Design Report for the: PANDA Straw Tube Tracker, Strong Interaction Studies with Antiprotons* [online], February 2013 cit. [23. 4. 2021], article, editors: Paola Gianotti, Peter Wintz, available on: <https://www.researchgate.net/publication/225044921_Technical_Design_Report_for_the_PANDA_Straw_Tube_Tracker/figures?lo=1>
- [6] FAIR: Compressed Baryonic Matter experiment at FAIR: *The detector and data processing system* [online], 2021 cit. [23. 4. 2021], FAIR website, available on: <<https://www.cbm.gsi.de/detectors>>
- [7] BENDAROUACH Jordan: *Conception and design of a mirror alignment and control system for the Ring Imaging Cherenkov detector of the CBM experiment* [online], Mai 2019 cit. [6. 4. 2021], Inaugural-Dissertation, Justus-Liebig-Universität Gießen, fair-center.eu – users -experiments – nuclear matter physics – cbm – documents - Bachelor, Master, Diploma and PhD Thesis – 2019, available on: <<https://indico.gsi.de/event/8803/contributions/38270/attachments/27560/>>
- [8] SENGER Peter: *Astrophysics in the Laboratory—The CBM Experiment at FAIR* [online], 2. 4. 2020 cit. [19. 4. 2021], article, available on: <<https://www.mdpi.com/2571-712X/3/2/24>>
- [9] FAIR: *The Compressed Baryonic Matter Experiment* [online], 2021 cit. [6. 4. 2021], fair-center.eu – users -experiments – nuclear matter physics – cbm – introduction, available on: <<https://fair-center.eu/en/for-users/experiments/nuclear-matter-physics/cbm/introduction.html>>
- [10] GSI: *Exploring Cosmic Matter in the Laboratory* [online], 2021 cit. [17. 4. 2021], website of CBM experiment at FAIR, available on: <<https://www.cbm.gsi.de/>>



- [11] FAIR: The CBM Collaboration: *Technical Design Report for the CBM, Muon Chambers (MuCh)* [online], November 2014 cit. [24. 4. 2021], editors: S. Chattopadhyay, Y. P. Vijoyi, P. Senger, W.F.J. Müller, C.J. Schmidt, available on: <<http://repository.gsi.de/record/161297/files/>>
- [12] CBM Collaboration, GSI Helmholtzzentrum für Schwerionenforschung GmbH, Darmstadt, Germany: *Compressed Baryonic Matter experiment at FAIR, CBM Progress Report 2018* [online], October 2019 cit. [24. 4. 2021], editors: Ilya Selyuzhenkov, Ilya Selyuzhenkov, ISBN 978-3-9815227-6-1, DOI:10.15120/GSI-2019-01018, Printed in Darmstadt by GSI, available on: <<http://repository.gsi.de/record/220128>>
- [13] FAIR: The CBM Collaboration: *Technical Design Report for the CBM, Projectile spectator detector (PSD)* [online], 21. 7. 2015 cit. [25. 4. 2021], editors: Guber F., Selyuzhenkov I., available on: <<http://repository.gsi.de/record/109059/files/>>
- [14] CBM Collaboration, GSI Helmholtzzentrum für Schwerionenforschung GmbH, Darmstadt, Germany: *Compressed Baryonic Matter experiment at FAIR, CBM Progress Report 2019* [online], June 2020 cit. [26. 4. 2021], editors: CBM Collaboration. Peter Senger, ISBN 978-3-9815227-8-5, DOI: 10.15120/GSI-2020-00904, Printed in Darmstadt by GSI, available on: <<https://dx.doi.org/10.15120/GSI-2020-00904>>
- [15] Witzenmann GmbH: *Metal bellows manual* [online], May 2019 cit. [19. 2. 2021], www.witzenmann.de – Produkte – Metallbäge – Membranbälge - downloads, available on: <<https://www.witzenmann.de/de/download/download-center/>>
- [16] MW Components: *Metal Bellows* [online], 2021 cit. [7. 5. 2021], website, available on: <<https://www.mwcomponents.com/metal-bellows>>
- [17] MW Components: *Metal Bellows - Key Enabling Technology for a Wide Range of Engineering Applications* [online], 2021 cit. [8. 5. 2021], catalogue / white paper, available on: <<https://f.hubspotusercontent20.net/hubfs/8642978/PDFs/MW-COMPONENTS-Metal-Bellows-Key-Enabling-Technology-for-a-Wide-Range-of-Engineering-Applications-SVM.pdf>>
- [18] Sigma-Netics, Inc.: *Designing With Metal Bellows* [online], 2015 cit. [29. 4. 2021], catalogue, www.sigmanetics.com – white papers - Designing with Metal Bellows, available on: <https://www.sigmanetics.com/pdfs/white-papers/SN_WP_MetalBellows.pdf>
- [19] John Crane company: *7 things to know before selecting welded metal bellows seals for your application* [online], 25. 2. 2020 cit. [25. 5. 2021], website, available on: <<https://www.johncrane.com/Resources/Blog/2020/7-things-to-know-before-selecting-welded-metal-bellows-seals-for-your-application>>
- [20] Bellowstech, MW Industries, Inc.: *Edge Welded Bellows Technology* [online], 2021 cit. [21. 5. 2021], website, available on: <<https://bellowstech.com/edge-welded-tech/>>
- [21] Vacuum Engineering: *Leak Rate Definition* [online], 2020 cit. [1. 6. 2021], website - pdf, vac-eng.com – resources – Leak Rate Definition pdf download, available on: <<https://www.vac-eng.com/wp-content/uploads/2020/03/leak-rate-definition.pdf>>



- [22] Mera Bellows Sp. z o.o.: *Katalog für Metallbälge* [online], 11. 10. 2018 cit. [6. 5. 2021], online catalogue, available on: <https://www.merabellows.com/pdf/katalog_p.pdf>
- [23] Beijing Bellowman Technology Co.,Ltd: *Precision metal bellows* [online], 2021 cit. [8. 5. 2021], website, available on: <<http://www.bellowman.com/en/products/precision-metal-bellows.html>>
- [24] AutoForm: *Deep Drawing* [online], 2021 cit. [7. 5. 2021], website, available on: <<https://www.autoform.com/en/glossary/deep-drawing/>>
- [25] Mera Bellows Sp. z o.o.: *From a metal-strip to a seamless metal bellow* [online], 2021 cit. [6. 5. 2021], website, available on: <<https://www.merabellows.com/products/metal-bellows>>
- [26] AutoForm: *Hydroforming* [online], 2021 cit. [7. 5. 2021], website, available on: <<https://www.autoform.com/en/glossary/hydroforming/>>
- [27] H&T ProduktionsTechnologie GmbH.: *Metal Bellow Machines* [online], 2021 cit. [18. 5. 2021], website, available on: <<https://www.ht-pt.com/en/press-manufacture/metal-bellow-machines/>>
- [28] Fulton Bellows: *Precision Formed Bellows* [online], 2021 cit. [11. 5. 2021], website, available on: <<https://fultonbellows.com/precision-bellows/>>
- [29] Triad Bellows: *Understanding the Manufacturing Methods for Metal Bellows* [online], 2017 cit. [8. 5. 2021], website, available on: <<https://www.triadbellows.com/understanding-the-manufacturing-methods-for-metal-bellows/>>
- [30] MW Components: *Metal Bellows Comparison* [online], 2021 cit. [8. 5. 2021], catalogue, available on: <<https://f.hubspotusercontent20.net/hubfs/8642978/PDFs/MW-Components-Metal-Bellows-Comparison.pdf>>
- [31] Sigma-Netics, Inc.: *Metal bellows, Material technology* [online], 2021 cit. [11. 5. 2021], website, available on: <<https://www.sigmanetics.com/technical-resources/metal-bellows-technology/bellows-materials/>>
- [32] Mera Bellows Sp. z o.o.: *Open-ended metal bellows – Closed-ended metal bellows – Double-Ply Bellows* [online], 2021 cit. [11. 5. 2021], website, available on: <<https://www.merabellows.com/products/metal-bellows>>
- [33] Lenntech: *Monel* [online], 2021 cit. [11. 5. 2021], website, available on: <<https://www.lenntech.com/monel.htm>>
- [34] Bibus Metals s.r.o.: *INCONEL® Alloy 600* [online], 2021 cit. [19. 5. 2021], website, available on: <<https://www.bibusmetals.cz/materialy/nikl-niklove-slitiny/inconelr-alloys/inconelr-alloy-600/>>
- [35] NeoNickel: *Alloy C276* [online], 2021 cit. [19. 5. 2021], website, available on: <<https://www.neonickel.com/cs/alloys/slitiny-niklu/alloy-c276/>>
- [36] Fulton Bellows: *Markets an Applications* [online], 2021 cit. [31. 5. 2021], website, available on: <<https://fultonbellows.com/markets-and-applications/>>
- [37] Spiroflex: *Bellows forming* [online], 2021 cit. [13. 5. 2021], website, available on: <<http://www.spiroflex.hr/bellows-forming>>
- [38] Nutberry Limited: *Metal bellows* [online], 2021 cit. [13. 5. 2021], website, available on: <<https://www.nutberry.co.uk/en/bellows/>>
- [39] Inventor: James W. Banks, Bozman, Md, assignee: Chemetron Corporation, Chicago: *Bellows forming method and apparatus* [online], 30. 3. 1976 cit. [18.



5. 2021], United States Patent, available on: <<https://patents.google.com/patent/US3937051>>
- [40] Belman: *Pressure balanced expansion joints* [online], 2017 cit. [20. 5. 2021], website, available on: <<https://www.belman.com/pressure-balanced-expansion-joints/>>
- [41] Technics Group: *Edge-Welded Bellows* [online], 2021 cit. [22. 5. 2021], EnPro Industries companies, catalogue, available on: <https://technetics.com/wp-content/uploads/2020/11/Bellows_low-res.pdf>
- [42] COMVAT AG: *Leading in Welded Bellow* [online], 2021 cit. [21. 5. 2021], catalogue on the website comvat.com – Welded-Bellows – Downloads – General Bellows Brochure, available on: <https://www.comvat.com/en/welded-bellows/downloads/?preview=1%29%20AND%20%28SELECT%206766%20FROM%28SELECT%20COUNT%28%2A%29%2C CONCAT%280x7176786a71%2C%28SELECT%20%28ELT%286766%3D6766%2C1%29%29%29%2C0x716b6a7671%2CFLOOR%28RAND%280%29%2A2%29%29x%20FROM%20INFORMATION_SCHEMA.PLUGINS%20GROUP%20BY%20x%29a%29%20AND%20%288030%3D8030>
- [43] Mewasa AG: Membranbalg / Metallbalg / Faltenbalg Herstellung / manufacturing process of an edge welded bellows [online], 16. 5. 2013 cit. [22. 5. 2021], online video on Youtube, available on: <<https://www.youtube.com/watch?v=ArTXGU-oED4&t=11s>>
- [44] ABSACC: *Edge Welded Bellows* [online], 2021 cit. [22. 5. 2021], website, available on: <<https://www.abssac.co.uk/p/Edge+Welded+Bellows/40/>>
- [45] Mewasa AG: *Edge welded bellows* [online], 4. 1. 2021 cit. [23. 5. 2021], website, mewasa.ch - Downloads English – Standard end pieces, available on: <<http://www.mewasa.ch/>>
- [46] Mewasa AG: *Bildergalerie* [online], 4. 1. 2021 cit. [19. 2. 2021], www.mewasa.ch – bildergalerie, available on: <http://www.mewasa.ch/bildergalerie_de.htm>
- [47] Vacom: *Edge Welded Bellows* [online], 2020 cit. [26. 5. 2021], website, available on: <<https://www.vacom.de/en/products/edge-welded-bellows>>
- [48] Ferrovac GmbH: *Port Aligner DN40CF* [online], 2021 cit. [22. 5. 2021], ultra high vacuum technology, website, available on: <<https://www.ferrovac.com/?tool=ProductDescription&product=PA40>>
- [49] Servometer, MW Industries Inc.: *Electroforming Process* [online], 2021 cit. [28. 5. 2021], website, available on: <<https://servometer.com/electroforming-process/>>
- [50] Servometer, MW Industries Inc.: *Electroforming Basics for Miniature and Specialized Components* [online], 2021 cit. [29. 5. 2021], white paper, servometer.com – electroforming process – learn more about the process of electroformed bellows – download the white paper, available on: <<https://servometer.com/electroforming-process/>>
- [51] NiCoForm: *Mandrel* [online], 2021 cit. [29. 5. 2021], website, available on: <<https://www.nicoform.com/index.cfm?Page=Mandrel>>
- [52] NiCoForm: *NiColoy® Bellows & Contacts* [online], 2021 cit. [31. 5. 2021], website, available on:



- <<https://www.nicoform.com/index.cfm?Page=Seamless-Bellows-and-Bellows-Contacts>>
- [53] Parkinson Ron: *Electroforming — a unique metal fabrication process* [online], October 1998 cit. [29. 5. 2021], Nickel Development Institute, available on: <https://nickelinstitute.org/media/1674/electroforming_auniquemetalfabricationprocess_10084_.pdf>
- [54] Engineeringclicks: *What is Electroforming and where is it used?* [online], 31. October 2019 cit. [29. 5. 2021], engineeringclicks.com – electroforming process, available on: <<https://www.engineeringclicks.com/electroforming-process/>>
- [55] Sigma-Netics, Inc.: *Electroformed Nickel Bellows Assemblies* [online], 2021 cit. [31. 5. 2021], website, available on: <<https://www.sigmanetics.com/metal-bellows/electroformed-nickel-bellows-assemblies>>
- [56] ArcFlex: *Single hinged expansion joint* [online], 2021 cit. [2. 6. 2021], website, available on: <<https://www.arcflex.com/single-hinged-expansion-joint/>>
- [57] ArcFlex: *Gimbal expansion joint* [online], 2021 cit. [2. 6. 2021], website, available on: <<https://www.arcflex.com/gimbal-expansion-joint/>>
- [58] DIMER: *O-kroužky* [online], leden 2012 cit. [19. 3. 2021], dimer.cz – těsnění – katalogy ke stažení, (O-ring sealing catalogue) available on: <https://www.dimer.cz/tesneni/files/5072/cz/oring_cz.pdf>
- [59] Eriks nv.: *Viton material properties* [online], 2021 cit. [18. 6. 2021], website, RubberTechnology.info - Rubber products - Seals - Viton seal properties - Viton material properties, available on: <<https://rubbertechnology.info/en/rubber-products/seals/viton-seal-properties/viton-material-properties/>>
- [60] Henkel ČR s.r.o.: *LOCTITE®* [online], 2021 cit. [19. 6. 2021], website, available on: <<https://www.henkel-adhesives.com/cz/en/about/our-brands/loctite.html>>
- [61] Tappex Thread Inserts Ltd: *Trisert-3®* [online], 2021 cit. [18. 6. 2021], website, catalogue, Home - Our Products - Self-Tapping Threaded Inserts - Trisert-3®, available on: <<https://www.tappex.co.uk/products/self-tapping-threaded-inserts/trisert-3>>
- [62] LAŠ Vladislav: *Mechanika kompozitních materiálů*, Plzeň 2008, Západočeská Univerzita v Plzni, Fakulta aplikovaných věd, ISBN 978-80-7043-698-9
- [63] Compo Tech PLUS, spol. s r.o.: *About CompoTech* [online], 2021 cit. [18. 6. 2021], website, available on: <<https://compotech.com/about-us/about-compotech/>>
- [64] SKF: *SAKAC 12 M, Rod ends with a male thread* [online], 2021 cit. [20. 6. 2021], website, 3D CAD model, available on: <<https://www.skf.com/group/products/plain-bearings/spherical-plain-bearings-rod-ends/rod-ends/productid-SAKAC%2012%20M>>
- [65] T.E.A. TECHNIK s.r.o.: *ALUROL* [online], 2021 cit. [22. 6. 2021], website, catalogue, 3D CAD model, available on: <<https://www.teatechnik.cz/obloukova-alurol/>>
- [66] T.E.A. TECHNIK s.r.o.: *Lineární vedení ALUROL* [online], 2015 cit. [22. 6. 2021], catalogue, teatechnik.cz – katalogy – Lineární vedení Alurol, available on: <<https://www.teatechnik.cz/katalogy/>>



- [67] ALUTEC KK: Hliníkový konstrukční systém a příslušenství [online], 2021 cit. [2. 4. 2021], aluteckk.cz – produkty – hliníkový konstrukční systém, available on: <<https://www.aluteckk.cz/hlinikovy-konstrukcni-system>>
- [68] MATEZEX: Nerezové tyče šestihřanné [online], 2021 cit. [3. 4. 2021], metezex.cz – tyče a profily – tyče šestihřanné, available on: <<https://www.matezex.cz/tyce-sestihranne.html>>
- [69] Elesa S.p.A, Otto Ganter GmbH & Co. KG: *DIN 71802 Angled ball joints* [online], 2021 cit. [1. 4. 2021], elesa-ganter.com – home – products – joints, couplings – angled ball joints, available on: <<https://www.elesa-ganter.com/en/www/products/joints-couplings--1/Joints--Angled-ball-joints--DIN71802#sortBy=0&facetvalue=>>>
- [70] SKF: *W 6206, Deep groove ball bearings* [online], 2021 cit. [9. 6. 2021], website, 3D CAD model, available on: <<https://www.skf.com/group/products/rolling-bearings/ball-bearings/deep-groove-ball-bearings/productid-W%206206>>
- [71] SKF: *52206, Thrust ball bearings, double direction* [online], 2021 cit. [9. 6. 2021], website, 3D CAD model, available on: <<https://www.skf.com/group/products/rolling-bearings/ball-bearings/thrust-ball-bearings/productid-52206>>
- [72] SKF: *33109, Tapered roller bearings, single row* [online], 2021 cit. [9. 6. 2021], website, 3D CAD model, available on: <<https://www.skf.com/group/products/rolling-bearings/roller-bearings/tapered-roller-bearings/single-row-tapered-roller-bearings/productid-33109>>
- [73] SEW Eurodrive: *Helical-worm servo gearmotors* [online], 2021 cit. [9. 6. 2021], website, 3D CAD model, available on: <https://www.sew-eurodrive.cz/products/gearmotors/servo_gearmotors/helical-worm_servo_gearmotors_scmp/helical-worm_servo_gearmotors_scmp.html>
- [74] Department of Designing and Machine Elements, Czech Technical University in Prague: *Části a mechanismy strojů I. ČMS1, Převodový mechanismus se závitovou dvojicí (pohybový šroub)*, 9. 9. 2014 cit. [10. 6. 2021], presentation, internal study materials for the subject „Machine parts and mechanisms“
- [75] Bornemann Gewindetechnik GmbH & Co. KG: *Trapezoidal thread according to DIN 103* [online], 2021 cit. [10. 6. 2021], catalogue, bornemann-gewindetechnik.de/ - home – products – trapezoidal threads – download pdf, available on: <<https://www.bornemann-gewindetechnik.de/wordpress/wp-content/uploads/2016/04/Trapezoidal-thread-EN.pdf>>
- [76] Matis s.r.o.: *CQA - ocelová čtyřhranná matice* [online], 2021 cit. [10. 6. 2021], website, catalogue, available on: <<https://www.matis.cz/cs/produkt/cqa-ocelova-ctyrhranna-matice>>
- [77] Matis s.r.o.: *KUE - jednochodé, ocel C45, class 100* [online], 2021 cit. [10. 6. 2021], website, catalogue, available on: <<https://www.matis.cz/cs/produkt/kue-jednochode-ocel-c45-class-100>>
- [78] MITCalc: *Slender strut (column) buckling* [online], 2021 cit. [31. 3. 2021], mitcalc.com – documentation – list of calculations and programmes – slender



- astrut (column) buckling – available on:
<<https://www.mitcalc.com/doc/buckling/help/en/buckling.htm>>
- [79] MBM Technik: *ST8918 - NEMA 34* [online], 2021 cit. [8. 6. 2021], website, catalogue, 3D CAD model, available on:
<<https://www.mbmtechnik.cz/elektromotory/krokove-motory/krokove-motory-36/st8918-nema-34#3d-modely>>
- [80] Zero-Max, Inc.: *ServoClass Single Flex Couplings* [online], 2021 cit. [8. 6. 2021], website, catalogue, 3D CAD model, available on: <<https://www.zero-max.com/servoclass-single-flex-couplings-p-131.html>>
- [81] SKF: *PBMF 1522 12 M1G1, Bushings* [online], 2021 cit. [15. 6. 2021], website, 3D CAD model, available on: <<https://www.skf.com/group/products/plain-bearings/bushings-thrust-washers-strips/bushings/productid-PBMF%20152212%20M1G1>>
- [82] SKF: *SI 8 C, Rod ends with a female thread* [online], 2021 cit. [15. 6. 2021], website, 3D CAD model, available on:
<<https://www.skf.com/group/products/plain-bearings/spherical-plain-bearings-rod-ends/rod-ends/productid-SI%208%20C>>
- [83] Matis s.r.o.: *Standardní typy opracování konců kuličkových šroubů pro uložení SFA a SLA.* [online], 2021 cit. [15. 6. 2021], website, catalogue, available on:
<https://www.matis.cz/data/pdf/kulickove_srouby/KONCE_KS_SFA_SLA.pdf>
- [84] Bosch Rexroth Corporation: *Mill type cylinder* [online], 2021 cit. [15. 6. 2021], website, 3D CAD model, available on:
<<https://www.boschrexroth.com/en/us/products/product-groups/industrial-hydraulics/cylinders/mill-type-cylinder>>
- [85] SKF: *33109, Tapered roller bearings, single row* [online], 2021 cit. [15. 6. 2021], website, 3D CAD model, available on:
<<https://www.skf.com/group/products/rolling-bearings/roller-bearings/tapered-roller-bearings/single-row-tapered-roller-bearings/productid-33109>>
- [86] Doc. Ing. Miroslav Škopán, CSc. *Hydraulické pohony strojů* [online], November 2009 cit. [15. 6. 2021], study material – syllabus, Technical University in Brno, Faculty of Mechanical Engineering, Department of Transport Technique, available on:
<<http://www.iae.fme.vutbr.cz/userfiles/uadi/files/Hydraulick%C3%A9%20pohony%20stroj%C5%AF.pdf>>
- [87] Mewasa AG: *Datentabelle neu* [online], 4. 1. 2021 cit. [25. 5. 2021], catalogue, mewasa.ch – Downloads Deutsch – Membrantabelle, available on: <<http://www.mewasa.ch/>>
- [88] Dlubal Software: *Uživatelský manuál* [online], March 2020 cit. [11. 4. 2021], dlubal.com – stahování a informace – dokumenty – manuály, available on:
<<https://www.dlubal.com/-/media/Files/website/documents/manuals/rfem-fea-software/rfem-5/rfem-5-manual-cs.pdf?la=cs&mlid=40621BBE737344C1AD800822BCB17F29&hash=8302CB77D6D7E325A50941953FABC0C46C9BB05E>>



- [89] VOŘECHOVSKÝ Miroslav: *Pružnost a plasticita* [online], 2005 cit. [13. 4. 2021], available on: <<http://lences.cz/domains/lences.cz/skola/subory/Skripta/CD03-Pruznost%20a%20plasticita/CD03-Pruznost%20a%20plasticita%20%20P01-Pruznost%20a%20plasticita%20-%20pruvodce%20predmetem.pdf>>
- [90] Feron: *vypalování plechů* [online], 2021 cit. [31. 3. 2021], ferona.cz – služby – vypalování plechů, available on: <<https://www.ferona.cz/sluzby-vypalovani-plechu>>
- [91] NEONALLOYS: *304 stainless steel – the most commonly used steel* [online], 2016 cit. [3. 4. 2021], neonalloys.com – blog – 304 stainless steel – the most commonly used steel, available on: <<https://www.neonalloys.com/304-stainless-steel>>
- [92] Bohdan Bolzano s.r.o.: *X5CrNi18-10* [online], 2016 cit. [3. 4. 2021], Bolzano - Technická podpora - Technická příručka - Výrobky z korozivzdorných a žáruvzdorných ocelí - Výrobky z ocelí korozivzdorných - Materiálové listy - X6CrNi18-10 (1.4301) austenitické, available on: <<https://bbolzano.cz/cz/technicka-podpora/technicka-priucka/vyrobky-z-korozivzdornych-a-zaruvzdornych-oceli/vyrobky-z-oceli-korozivzdornych/materialove-listy/x6crni18-10-austeniticke>>
- [93] ŘEZNÍČEK Jan: *Pružnost a pevnost II příklady* [online], 15. 10. 2018 cit. [25. 6. 2021], study support materials for the lectures of the subject Elasticity and Strength of material; CTU in Prague, Faculty of Mechanical Engineering, Department of Mechanics, Biomechanics and Mechatronics; division of Elasticity and Strength of material; available on: <http://drone.fsid.cvut.cz/pp2/resene_priklady/PP_II_priklady.pdf>
- [94] POSPÍCHAL, Jaroslav. *Technické kreslení*. 4., přeprac. vyd. V Praze: ČVUT, 2014. 94 s. (Technical Drawing) ISBN 978-80-01-05595-3.
- [95] DRASTÍK, František a Pavel VÁVRA. *Strojnické tabulky pro konstrukci i dílnu.*: pomocná učebnice pro školy technického zaměření. (Mechanical engineering tables) 2. vyd. Ostrava: Montanex, 1999, 722 s. ISBN 80-857-8095-X.
- [96] PETR, Karel: Support material for the lectures of the subject “Moderní technická dokumentace” (Modern technical drawing), 2021, Department of designing and machine elements U12113 at the Faculty of Mechanical Engineering at CTU in Prague

LIST OF FIGURES

Fig. 1: Scheme of accelerator facilities in Darmstadt (FAIR, The PANDA Collaboration: Technical Design Report) [5]	2
Fig. 2: The HADES detector (left) with the assembly for CBM experiment (right) (Peter Senger) [8]	3
Fig. 3: Scheme of the CBM experiment	4
Fig. 4: Beam pipe versions (CBM progress report 2018, Design simulations of beam pipe and radiation studies for the CBM experiment, A. Senger and the CBM collaboration) [12]	7
Fig. 5: Horizontal profiles of Au beams in the beam pipe deflected by a magnetic field (Design simulations of beam pipe and radiation studies for the CBM experiment, A. Senger and the CBM collaboration) [12]	8
Fig. 6: The diagram of relation between force and deflection of bellow (Sigma-Netics catalogue) [18]	12
Fig. 7: From left: sinus and omega convolution profiles of formed bellows (Witzenmann catalogue) [15]	13
Fig. 8: Seamless hydroformed bellows of (from left) brass, beryllium-copper and bronze (Mera Bellows) [32]	15
Fig. 9: Seamless hydroformed bellows of Monel (Sigma-Netics) [31]	16
Fig. 10: Seamless hydroformed bellows of stainless steel (Mera Bellows) [32]	16
Fig. 11: From left: packless valve, expansion joint, expansion chamber (Fulton Bellows company) [36]	18
Fig. 12: Roll forming tool (Spiroflex) [37]	19
Fig. 13: Application of pressure balanced expansion joints at turbine pipeline (left) and as an axial in-line compensator (right) (Spiroflex) [37]	21
Fig. 14: Diaphragm profile of an edge-welded bellow (Witzenmann catalogue) [15]	21
Fig. 15: Edge welded bellow with end flanges, detail of welded joints (Bellowstech) [20]	22
Fig. 16: Stamping tools mounted on the machine (Comvat AG) [42]	22
Fig. 17: Stamped metal diaphragm on a stand prepared for welding (Mewasa AG) [43]	23
Fig. 18: Edge-welding of inner diameter of two diaphragms (Mewasa AG) [43]	24
Fig. 19: Standard end pieces for bellows (Mewasa AG) [45]	24
Fig. 20: Edge-welded bellow with flanges in deflected position (Mewasa AG) [46]	26
Fig. 21: Edge welded bellow with pivot mounts as an aligner [48]	27
Fig. 22: Metallic mandrels for electroforming (NiCoForm) [51]	28
Fig. 23: Scheme of electroforming [54]	29
Fig. 24: From left: Single hinged and gimbal expansion joints (ArcFlex) [56].	31
Fig. 25: Design of tilting mechanism with spheric-shaped workpieces	32
Fig. 26: Different views of the design of spheric connection	33
Fig. 27: Cut view of spheric tilting joint with highlighted clearance	34
Fig. 28: Example of drawing views of spheric workpiece (attachment 14)	34
Fig. 29: Views of drawing with welds (attachment 13)	35
Fig. 30: Characteristic diameters of O-ring and groove dimensions (Dimer catalogue) [58]	36
Fig. 31: Position of 2,5° of the tilting weldment	36
Fig. 32: Composite version of the tilting mechanism with spherical parts	37
Fig. 33: Cut view of composite tilting joint	38
Fig. 34: Intermediate composite spherical part	39
Fig. 35: Bellows weldment with slender struts	40
Fig. 36: Cut view through bellows weldment and kinematic mechanism	41
Fig. 37: Cut view through slender strut tube with telescopic workpieces	42
Fig. 38: Upper view of deflected bellows weldment with slender struts	42
Fig. 39: Deflected bellows weldment with slender struts in extreme position	43
Fig. 40: Bellows weldment with rolling system in 0° position	44
Fig. 41: Scheme of tilting joint placement and kinematic mechanism position	45
Fig. 42: Front view of bellows weldment and kinematic mechanism with highlighted dimension of maximal width occupation	45
Fig. 43: Front view of bellows weldment and kinematic mechanism with highlighted dimensions of total hight and width of assembly	46



Fig. 44: Deflected bellows weldment assembly in extreme position	46
Fig. 45: Deflected bellows weldment assembly in extreme position of other polarity	47
Fig. 46: Scheme of ion beam in 0° position	47
Fig. 47: Scheme of ion beam in 2,5° position	48
Fig. 48: Tilting joint with single eccentric bellow	49
Fig. 49: Pair of angled ball joints with clamping element	49
Fig. 50: Eccentric bellow weldment positioning	50
Fig. 51: Deflected tilting joint with single eccentric bellow	50
Fig. 52: Scheme of ion beam in 0° position with eccentric bellow	51
Fig. 53: Scheme of ion beam in extreme 2,5° position with eccentric bellow	51
Fig. 54: Kinematic mechanism with handle-operated wheel	52
Fig. 55: Cut view through leadscrew assembly	52
Fig. 56: Helical-worm servo gearmotor with kinematic mechanism	53
Fig. 57: Scheme of the synchronous movement of the bellows kinematic mechanism and the PSD detector	54
Fig. 58: Scheme of kinematic assembly with leadscrew	55
Fig. 59: Types of strut mounting [78]	58
Fig. 60: Stepping engine ST8918L4508-A of the MBM Technik 79]	60
Fig. 61: ServoClass single Flex Couplings (Zero-Max) [80]	61
Fig. 62: Final composition of electric powered drive with leadscrew	61
Fig. 63: Detail view of lead nuts	62
Fig. 64: Kinematic mechanism of tilting joint powered hydraulically	62
Fig. 65: Cut view of kinematic mechanism with hydraulic cylinder	63
Fig. 66: Scheme of hydraulic circuit	64
Fig. 67: Design of the passive bended bellow weldment	66
Fig. 68: Sketch of the bellow for FEM analysis	67
Fig. 69: Bellows weldment with the meshed elements	68
Fig. 70: Upper mounted reference point for enforced deformation	69
Fig. 71: Shape differences between undeformed and deformed bellow	70
Fig. 72: Shape of bellow in its limit position	71
Fig. 73: Reaction forces of the bellow after its deflection by 2,5°	72
Fig. 74: Experiment with bellow - assembly design	74
Fig. 75: Slender struts for bellow	74
Fig. 76: Weldment of left blind flange	75
Fig. 77: Longitudinal cut view of the experimental assembly	75
Fig. 78: Hexagonal slender strut of bellow	76
Fig. 79: Scheme of regular hexagon	77
Fig. 80: Hexagonal bar divided into sections with cutting planes	81
Fig. 81: Mesh of hexagonal strut	81
Fig. 82: Mounting and load simulation of slender strut	82
Fig. 83: FEM results of hexagonal strut for experiment assembly	82
Fig. 84: FEM results of hexagonal struts with highlighted stress peaks	83
Fig. 85: Shape of experimental bellow in its limit position	83



LIST OF TABLES

Tab: 1 Dimensional attributes of bellows (MW Components catalogue) [17].....	10
Tab: 2 Performance attributes of bellows (MW Components catalogue) [17]	11
Tab: 3 Values of reduced (effective) length coefficients [78].....	58
Tab: 4 The values of lateral forces of two solutions with bellow in Newton	65
Tab: 5 Material characteristics of 1.4301	76

LIST OF ATTACHMENTS

- (Attachment 1) RFEM_stress_analysis.pdf
- (Attachment 2) Matlab script "slender Strut_calculation.m"
- (Attachment 3) CAD model "assembly_bellow_360_+2.5.STEP"
- (Attachment 4) CAD model "assembly_bellow_360_0.STEP"
- (Attachment 5) CAD model "assembly_bellow_360_-2.5.STEP"
- (Attachment 6) CAD model "assembly_eccentric_bellow_0.STEP"
- (Attachment 7) CAD model "assembly_eccentric_bellow_2.5.STEP"
- (Attachment 8) CAD model "composite_version.STEP"
- (Attachment 9) CAD model "steel_or_aluminum_version.STEP"
- (Attachment 10) CAD model "two_bellows_with_tube_struts_0.STEP"
- (Attachment 11) CAD model "two_bellows_with_tube_struts_2.5.STEP"
- (Attachment 12) Drawing TJ-01-01.PDF
- (Attachment 13) Drawing TJ-02-01.PDF
- (Attachment 14) Drawing TJ-03-01.PDF
- (Attachment 15) Drawing MA-01-01.PDF
- (Attachment 16) Drawing BP-01-01.PDF
- (Attachment 17) Drawing BP-02-01.PDF
- (Attachment 18) Drawing BP-01-02.PDF
- (Attachment 19) Drawing BP-02-02.PDF
- (Attachment 20) Drawing EX-01-01.PDF
- (Attachment 21) Drawing EX-01-02.PDF
- (Attachment 22) Drawing EX-01-03.PDF
- (Attachment 23) Drawing EX-02-01.PDF
- (Attachment 24) Drawing EX-02-02.PDF
- (Attachment 25) Drawing EX-02-03.PDF
- (Attachment 26) Drawing EX-03-01.PDF
- (Attachment 27) Drawing EX-03-02.PDF
- (Attachment 28) Drawing EX-03-03.PDF
- (Attachment 29) Drawing EX-03-04.PDF
- (Attachment 30) Drawing EX-03-05.PDF
- (Attachment 31) Drawing EX-03-06.PDF
- (Attachment 32) Drawing EX-03-07.PDF
- (Attachment 33) Drawing EX-03-08.PDF
- (Attachment 34) Drawing EX-03-09.PDF
- (Attachment 35) Drawing EX-03-10.PDF

LIST OF ABBREVIATIONS AND SYMBOLS

CBM	Compressed Baryonic Matter
CAD	Computer-Aided Design
FAIR	Facility for Antiproton and Ion Research
GSI	Gesellschaft für Schwerionenforschung (Institute for heavy ion research)
QCD	Quantum Chromo Dynamics
SIS	SchwerlonenSynchrotron (Heavy ion synchrotron)
UNILAC	UNIversal LINEar ACcelerator
APPA	Atomic, Plasma Physics and Applications
NUSTAR	NUclear STructure, Astrophysics, and Reactions
PANDA	antiProton ANnihilation in Darmstadt
Super-FRS	Superconducting FRagment Separator
HESR	High Energy Storage Ring
CR	Collector Ring
RESR	accumulator / decelerator Storage Ring
NESR	New Experimental Storage Ring
HADES	High Acceptance DiElectron Spectrometer
Au	Aurum (gold)
Ag	Argentum (silver)
Ni	Niccolum (nickel)
Cu	Cuprum (copper)
Zn	Zincum (zinc)
Sn	Stannum (tin)
Be	Beryllium (beryllium)
Fe	Ferrum (iron)
Co	Cobaltum (cobalt)
MVD	Micro-Vertex Detector
STS	Silicon Tracking System
RICH	Ring-Imaging Cherenkov Detector
MuCH	Muon Chambers
TRD	Transition Radiation Detector
TOF	Time-of-Flight Detector
ECAL	Electromagnetic calorimeter

PSD	Projectile Spectator Detector
MEA	Mean Effective Area
ID	Inner Diameter
OD	Outer Diameter
SR	Spring Rate
LR	leak rate
V	Volume
Δp	pressure difference
Δt	time difference
AISI	American Iron and Steel Institute
ISO	International Organization for Standardization
DIN	Deutsches Institut für Normung (German institute for standardization)
CNC	Computer Numerical Control
TIG	Tungsten Inert Gas (welding method)
MIG	Metal Inert Gas (welding method)
MAG	Metal Active Gas (welding method)
FPM	fluoroelastomer according to DIN/ISO
LS	leadscrew
s	track (physical)
t	time
v	velocity
Q	Lateral reaction force
L	length
i	number of thread starts
p	pressure
p_D	maximal allowed pressure
d_2'	preliminary middle diameter of leadscrew
d_2	middle diameter of leadscrew
d_3	core diameter of screw
Ψ_H	coefficient of screw height
Ψ_h	coefficient of the nut height
d	nominal diameter
P	pitch

S_3	area of the core cross-section
H_1	operating hight
z	number of threads
γ	angle of the thread lead
β_n	angle of thread side normal
β	angle of thread sidel
ϕ'	friction angle of the thread
f	friction coefficient
h	hight of lead-nut
σ_d	stress in the screw core caused by axial load
M_K	torsion
τ	torsion stress
W_K	cross-section characteristics – modulus in torsion
σ_{RED}	reduced stress
α	coefficient of stress hypothesis
τ_{max}	stress hypothesis
σ_{Kd}	yield strength in compression
k	safety factor
k_{min}	minimal safety coefficient
μ	coefficient of buckling mode (reduced effective length)
λ	slenderness ratio
l_V	calculation length for slenderness ratio of screw
i_X	quadratic radius of cross-section
λ_m	limit slenderness ratio
σ_E	critical stress according Euler
E	Young's modulus (elasticity modulus)
k_v	safety coefficient for slender strut
n	revolutions
D	parameter of leadscrew thread
η_Z	Efficiency of thread transmission of leadscrew and lead-nut
P_{Sout}	Output Performance of leadscrew mechanism
P_{Sin}	Input Performance of leadscrew mechanism
ω_s	angular voelocity

η_{Zm}	Efficiency of threaded mechanism
η_{lv}	Efficiency of bearings of leadscrew
η_{co}	Efficiency of couplings
P_{out}	Output Performance of mechanism
P_{min}	Minimal Performance
η_C	Total Efficiency
ω_M	engine angular velocity
FEM	Finite Element Method
F	Force
SRCz	axial spring rate
NC	Number of Convolutions
P	Poisson's ratio
σ_u	elastic limit
σ_k	yield strength
σ_{pd}	compressive strength
σ_t	tensile strength
J_y	area moment of inertia in "y" axis direction
J_x	area moment of inertia in "x" axis direction
a	characteristic dimension
c	geometrical parameter of regular hexagon
A	Area of a hexagonal cross-section
i_{min}	minimal quadratic radius of cross-section
l	length of bar
F_{kr}	critical force
σ_{kr}	critical stress
J_{min}	minimal area moment of inertia
GG	Last squares association criterion
GN	Minimum circumscribed association criterion
GX	Maximum inscribed association criterion
ACS	Any cross section
ALS	Any longitudinal section
CZ	Common zone
CT	Common toleranced feature of size
LS	Local size defined by a sphere



- P Projected tolerance zone
- M Maximum material requirement